Title
Reorganization of neural dynamics during motor recovery after stroke

Author
Guo, Ling

Publication Date
2020

Peer reviewed|Thesis/dissertation

Reorganization of neural dynamics during motor recovery after stroke

by
Ling Guo

DISSERTATION
Submitted in partial satisfaction of the requirements for degree of
DOCTOR OF PHILOSOPHY

in

Neuroscience

in the

GRADUATE DIVISION
of the
UNIVERSITY OF CALIFORNIA, SAN FRANCISCO

Approved:

DocuSigned by:
Michael Brainard
7ED6AD87FF16412...

Michael Brainard
Chair

DocuSigned by:
Karunesh Ganguly

Karunesh Ganguly

DocuSigned by:
Alexandra Nelson

Alexandra Nelson

DocuSigned by:
Jeanne Paz
129DDCD87B64445...

Jeanne Paz

Committee Members

ACKNOWLEDGEMENTS

I am incredibly grateful for the many people who supported me, academically, socially and emotionally, throughout my PhD journey, without whom this work would not have been possible. Firstly, I would like to thank my thesis advisor, Karunesh Ganguly, who guided me throughout my PhD and taught me valuable lessons both in life and at work. Karunesh was not just supportive of my academic work, but also my personal and career development goals. He was always available whenever I needed help, even when he was really busy with clinical duties, grants and numerous other projects in the lab. His enthusiasm and optimism also spurred me on at times of difficulty and was a good balance for my skepticism and criticism.

Next, I would like to thank my thesis committee members, Michael Brainard (thesis chair), Alexandra Nelson and Jeanne Paz, for their attention and time during and beyond my thesis meetings. Michael encouraged me to think critically about the interpretations of my experiments and results, and gave me many helpful ideas and viewpoints. Alexandra taught me how to scope my research questions and communicate my research effectively, and helped me jump over the many hurdles I encountered during my PhD. Jeanne provided valuable perspectives and suggestions for experiments, especially from the stroke and disease point of view. Flip Sabes and Phil Starr, who were in my qualifying exam but not thesis committee, helped conceptualize my project when I was starting out.

Thank you to past and present members of the Ganguly lab, who helped me with my research and shared this journey with me. Special thanks go out to Dhakshin Ramanathan and Tanuj Gulati, who mentored me at the beginning of my PhD and taught me how to do surgery, conduct electrophysiology experiments and analyze the data. Thank you to the graduate students in my batch, Tess Veuthey, Stefan Lemke and Kate Derosier, with whom I shared much time debugging experiments, exchanging ideas and navigating the ups and downs of graduate school life. I am also really grateful to Sravani Kondapavulur,

who helped me with a lot of the experiments, especially at a time when I was pushing ahead to finish up my paper and PhD. Thank you to Preeya Khanna, Nikhilesh Natraj and Jaekyung Kim, who provided valuable feedback and suggestions for this work. Thank you to Seok-Joon Won, who taught me a lot of the histological and molecular techniques and helped with stroke surgeries. Finally, thank you to the rats that participated in the experiments.

This work would also be impossible without the UCSF neuroscience program, which trusted in my abilities and provided the resources for my research and education, and my classmates in the program who supported me emotionally, morally and socially along the way. I would also like to thank the program administrators of the neuroscience program, Pat Veitch and Lucita Nacionales, who tended to my numerous questions and worries during graduate school and made sure that the program is always running smoothly.

My friends both within and outside of UCSF were essential in keeping me sane and ensured that I spent a healthy amount of time outside of lab. Thank you to the friends who shared my various hobbies through the years: my boardgame, cookout, dance, pottery and woodworking buddies. Thank you also to my Singaporeans friends in the US who shared food and holidays from home with me, and my friends from overseas who still keep in touch with me.

Last but not least, thank you to my family, my mum and my sister, who continuously supported me during my numerous years overseas away from home. Thank you to my partner in life, Jermyn. Words cannot express my appreciation and gratitude to you.

This work was conducted with funding from the Agency for Science, Technology and Research (A*STAR), Singapore.

CONTRIBUTIONS

Chapter 2 was reprinted largely as it appears in: Ramanathan, D. S.*, Guo, L.*, Gulati, T.*, Davison, G., Hishinuma, A. K., Won, S.-J., Knight, R. T., Chang, E. F., Swanson, R. A. & Ganguly, K. Low-frequency cortical activity is a neuromodulatory target that tracks recovery after stroke. *Nature Medicine* **24**, 1257-1267 (2018).

*Equal contribution.

For the rodent experiments, D.S.R., L.G., T.G., S.-J.W. and K.G. conceived and designed the experiments. R.A.S. provided input on the design of the stroke models. D.S.R., L.G., T.G., G.D., A.K.H. and S.-J.W. performed the experiments. D.S.R., L.G., G.D. and T.G. analyzed the data. For the human experiments, T.G., K.G., E.F.C. and R.T.K. were involved in data collection. D.S.R. analyzed the data. D.S.R., L.G., T.G. and K.G. wrote the manuscript. All authors contributed to editing and revising the manuscript.

Chapter 3 was written by Ling Guo. Work in this chapter is currently under review at a peer-reviewed journal. The work presented was done with help from Sravani Kondapavulur, Stefan M. Lemke and Seok-Joon Won from the Ganguly lab.

L.G. and KG conceived and designed the experiments. L.G. conducted the experiments and analyzed the data. S.K. assisted with the infusion experiments. S.M.L. performed striatal recordings in intact animals. S.-J.W. performed the stroke induction and conducted the histological analysis. L.G. and K.G. wrote and edited the manuscript. All read and edited the manuscript.

REORGANIZATION OF NEURAL DYNAMICS DURING MOTOR RECOVERY AFTER STROKE

Ling Guo

ABSTRACT

Chronic impairment of upper limb motor function is a common and debilitating consequence of stroke with limited treatment options. While past research has identified neuroplastic changes that are crucial for recovery, most studies focused on changes that are not directly related to movement and in single brain areas. A better understanding of how neural dynamics during movement, across multiple motor areas, are altered throughout recovery is necessary to develop targeted neuromodulatory treatments.

In both chapters 2 and 3, spiking and local field potential (LFP) activity were measured from motor areas of rodents undergoing upper limb rehabilitation after a motor cortical stroke. Chapter 2 studied the movement-related neural dynamics in the perilesional cortex (PLC), the primary site of plasticity post-stroke. Movement-related low frequency oscillations (LFOs), present in both spiking and LFP, in PLC was diminished after stroke and was associated with motor recovery. The amplitude of LFOs was also reduced in a human stroke patient compared to intact subjects. Epidural direct current stimulation applied during movement increased the amplitude of LFOs and improved motor function in rodents, even in the chronic phase post-stroke. These findings demonstrate that LFOs can be a stable and translatable biomarker for tracking of post-stroke motor function and a target for neuromodulation. Chapter 3 investigated the role of the dorsolateral striatum (DLS), a motor area one synapse downstream of cortex and crucial for both motor execution and learning, and the interaction between PLC and DLS during recovery. With recovery, neural activity in both PLC and DLS became more movement modulated, more reliable and contained more information about motor behavior. PLC and DLS reorganized simultaneously throughout rehabilitation and

their spiking activity also became more coordinated. These results show that motor recovery involve concerted reorganization of neural activity patterns in both cortical and subcortical motor areas.

Overall, this thesis showed that synchronous and reliable neural patterns during movement, coordinated across motor areas, are important for motor recovery. Neuromodulatory methods, such as electrical stimulation, that increase the reliability and coordination of neural activity could be promising treatments to enhance motor function post-stroke.

TABLE OF CONTENTS

LIST OF FIGURES

LIST OF TABLES

CHAPTER 1 : INTRODUCTION

Stroke is a leading cause of permanent disability worldwide and is predicted to affect an increasing number of people in the future[1]. Impairment of dexterous upper limb function, in particular, is one of the most common and debilitating consequences of stroke[2]. There are limited treatment options, especially in the chronic phase – several weeks to years after the initial stroke, and patients often never regain full motor function even with extensive rehabilitation[3,4]. Hence, there is an urgent need to better understand the neurophysiological mechanisms behind stroke recovery to develop novel strategies to improve motor function post-stroke.

Past research has identified cellular and molecular events, as well as structural, anatomical and functional connectivity changes that take place after stroke and are crucial for recovery[3,5–8]. After a cortical stroke, a key brain area where these events and changes take place is the perilesional cortex (PLC), the uninjured cortex adjacent of stroke site. Significant synaptogenesis, axonal sprouting and motor map reorganization occurs in the PLC and are associated with functional recovery [7,9–11]. After a lesion to the distal forelimb area of motor cortex, new forelimb representations emerged in the PLC after rehabilitation training of the affected limb[11–13]. Lesioning the PLC after an initial motor cortical stroke also causes further impairments and diminishes any gains during recovery[14,15], showing that the PLC has a causal role in recovery.

Nevertheless, it is still not well understood how these neuroplastic changes relate to motor function and how movement related neural activity in the PLC change during rehabilitation. One reason for this is because previous studies mostly measured neural changes during spontaneous periods away from movement and at static time points after stroke. To understand how dynamic neural changes post-stroke relate to ongoing movement, we need to measure neural activity with high temporal resolution during the performance of motor actions throughout rehabilitation. An understanding of the movement-related neural

dynamics over the course of recovery will enable us to identify biomarkers and targets for neuromodulation, for example the identification of pathological beta oscillations and development of deep brain stimulation in the case of Parkinson's Disease[16].

Besides the PLC, reorganization also occurs in other brain areas that were previously connected to the stroke site. Stroke causes a sudden loss of inputs and hence function in these remote connected areas, an effect known as diaschisis[17,18]. While it is recognized that stroke affects a distributed motor network, past studies have focused mainly on cortical areas[8,19,20] or structural connectivity between cortical and brain stem areas[21,22]. The role of subcortical motor areas after cortical strokes have been especially overlooked. One subcortical area of interest is the dorsolateral striatum (DLS), which is one synapse downstream of the motor cortex and is involved in the learning and execution of motor actions[23–25]. DLS loses input projections after a motor cortical stroke and is reinnervated during recovery[26]. Whether and how DLS neural activity reorganize during motor recovery post-stroke have not been explored. Additionally, increased coordination and connectivity strength among brain areas in the motor network, particularly the cortex and striatum[27], is a hallmark of motor learning in intact subjects but has not been studied in context of rehabilitation post-stroke.

In this thesis, I aimed to fill the gaps in previous literature by (1) linking neural activity post-stroke to motor behavior during recovery by measuring neural changes with high temporal and spatial resolution during movement throughout rehabilitation, (2) developing and testing the effectiveness of electrical stimulation to modulate ongoing neural dynamics during movement and to improve motor function and (3) investigating the role of a remote area previously connected to the stroke site, specifically the DLS, and its interactions with the PLC during motor recovery. We used rodent models of stroke and chronic in vivo electrophysiology to characterize the neurophysiological changes in PLC and DLS at the level of spiking and local field potentials (LFP) during rehabilitation post-stroke. Rodent models have been well-characterized and validated for the study of upper limb motor control and stroke[28–32]. Specifically, we used

photothrombotic stroke and middle cerebral artery occlusion to create strokes in the forelimb motor cortex of rats. To assess upper limb motor function, we used a reach-to-grasp task that requires coordination of gross proximal and dexterous distal movements and which performance depends on the motor cortex[28,33–35]. Chronic in vivo electrophysiology is a promising method of tracking neural activity during behavior, with both high temporal and spatial resolution. It has been performed extensively in studies of motor control and learning in intact subjects but not yet widely applied to studies of motor recovery post-stroke. In intact animals, motor learning is associated with increased movement-related neuronal spiking modulation, LFP power and coherence across the motor network [27,36–40]. Whether similar changes occur during motor rehabilitation is unknown.

Chapter 2 examined the neural dynamics in PLC after stroke and during rehabilitation training. By tracking spiking and LFP activity with high temporal resolution throughout rehabilitation, we identified low frequency oscillations as a stable biomarker of motor function post-stroke. Movement-related low frequency oscillations were diminished after stroke and increased with improvements in the reach-to-grasp task. Furthermore, we found that epidural direct current stimulation, when applied during movement, increased the amplitude of ongoing low frequency oscillations and improved motor function.

Using the same experimental approach as in Chapter 2, Chapter 3 examined the role of DLS and interactions between PLC and DLS in stroke recovery. We found that DLS was also disrupted after stroke and was reorganized simultaneously with PLC. Reorganization in both areas was closely linked to motor improvements post-stroke. Furthermore, spiking activity between DLS and PLC was more coordinated after rehabilitation. These results highlight the importance of considering remote motor areas and multi-area interactions in stroke recovery.

Finally, Chapter 4 summarizes key ideas, discusses limitations and makes recommendations for future studies.

References

1. Feigin, V. L. *et al.* Global and regional burden of stroke during 1990-2010: Findings from the Global Burden of Disease Study 2010. *Lancet* **383**, 245–255 (2014).

2. Lawrence, E. S. *et al.* Estimates of the prevalence of acute stroke impairments and disability in a multiethnic population. *Stroke.* **32**, 1279–1284 (2001).

3. Jones, T. A. & Adkins, D. L. Motor System Reorganization After Stroke: Stimulating and Training Toward Perfection. *Physiology (Bethesda).* **30**, 358–70 (2015).

4. Houwink, A., Nijland, R. H., Geurts, A. C. & Kwakkel, G. Functional Recovery of the Paretic Upper Limb After Stroke: Who Regains Hand Capacity? *Arch. Phys. Med. Rehabil.* **94**, 839–844 (2013).

5. Nudo, R. J. Recovery after brain injury: mechanisms and principles. *Front. Hum. Neurosci.* **7**, 887 (2013).

6. Nudo, R. J. Neural bases of recovery after brain injury. *J. Commun. Disord.* **44**, 515–520 (2011).

7. Carmichael, S. T. Cellular and molecular mechanisms of neural repair after stroke: Making waves. *Ann. Neurol.* **59**, 735–742 (2006).

8. Corbetta, M. Functional connectivity and neurological recovery. *Dev. Psychobiol.* **54**, 239–253 (2012).

9. Carmichael, S. T. Plasticity of cortical projections after stroke. *Neurosci.* **9**, 64–75 (2003).

10. Carmichael, S. T., Wei, L., Rovainen, C. M. & Woolsey, T. A. New Patterns of Intracortical

Projections after Focal Cortical Stroke. *Neurobiol. Dis.* **8**, 910–922 (2001).

11. Ramanathan, D., Conner, J. M. & Tuszynski, M. H. A form of motor cortical plasticity that correlates with recovery of function after brain injury. *Proc. Natl. Acad. Sci. U. S. A.* **103**, 11370–5 (2006).

12. Castro-Alamancos, M. A. & Borrell, J. Functional recovery of forelimb response capacity after forelimb primary motor cortex damage in the rat is due to the reorganization of adjacent areas of cortex. *Neuroscience* **68**, 793–805 (1995).

13. Nudo, R. J., Wise, B. M., SiFuentes, F. & Milliken, G. W. Neural Substrates for the Effects of Rehabilitative Training on Motor Recovery After Ischemic Infarct. *Science (80-.).* **272**, 1791–1794 (1996).

14. Whishaw, I. Q. Loss of the innate cortical engram for action patterns used in skilled reaching and the development of behavioral compensation following motor cortex lesions in the rat. *Neuropharmacology* **39**, 788–805 (2000).

15. Gharbawie, O. A., Karl, J. M. & Whishaw, I. Q. Recovery of skilled reaching following motor cortex stroke: Do residual corticofugal fibers mediate compensatory recovery? *Eur. J. Neurosci.* **26**, 3309–3327 (2007).

16. Perlmutter, J. S. & Mink, J. W. Deep Brain Stimulation. *Annu. Rev. Neurosci.* **29**, 229–257 (2006).

17. Carrera, E. & Tononi, G. Diaschisis: past, present, future. *Brain* **137**, 2408–2422 (2014).

18. von Monakow, C. *Lokalisation im Gehirn und Funktionelle Sta'rungen Induziert Durch Kortikale Läsionen.* (Bergmann JF, 1914).

19. Grefkes, C. & Fink, G. R. Recovery from stroke: current concepts and future perspectives. *Neurol. Res. Pract.* **2**, 17 (2020).

20. Rehme, A. K., Eickhoff, S. B., Wang, L. E., Fink, G. R. & Grefkes, C. Dynamic causal modeling of cortical activity from the acute to the chronic stage after stroke. *Neuroimage* **55**, 1147–1158 (2011).

21. Ishida, A. *et al.* Causal Link between the Cortico-Rubral Pathway and Functional Recovery through Forced Impaired Limb Use in Rats with Stroke. *J. Neurosci.* **36**, 455–467 (2016).

22. Ishida, A. *et al.* Dynamic Interaction between Cortico-Brainstem Pathways during Training-Induced Recovery in Stroke Model Rats. *J. Neurosci.* **39**, 7306–7320 (2019).

23. Yin, H. H. The sensorimotor striatum is necessary for serial order learning. *J Neurosci* **30**, 14719–14723 (2010).

24. Jin, X., Tecuapetla, F. & Costa, R. M. Basal ganglia subcircuits distinctively encode the parsing and concatenation of action sequences. *Nat. Neurosci.* **17**, 423–430 (2014).

25. Markowitz, J. E. *et al.* The Striatum Organizes 3D Behavior via Moment-to-Moment Action Selection. *Cell* **174**, 44-49.e17 (2018).

26. Napieralski, J. A., Butler, A. K. & Chesselet, M.-F. Anatomical and functional evidence for lesion-specific sprouting of corticostriatal input in the adult rat. *J. Comp. Neurol.* **373**, 484–497 (1996).

27. Lemke, S. M., Ramanathan, D. S., Guo, L., Won, S. J. & Ganguly, K. Emergent modular neural control drives coordinated motor actions. *Nat. Neurosci.* **22**, 1122–1131 (2019).

28. Alaverdashvili, M. & Whishaw, I. Q. Motor cortex stroke impairs individual digit movement in

skilled reaching by the rat. *Eur. J. Neurosci.* **28**, 311–322 (2008).

29. Gharbawie, O. A., Williams, P. T. J. A., Kolb, B. & Whishaw, I. Q. Transient middle cerebral artery occlusion disrupts the forelimb movement representations of rat motor cortex. *Eur. J. Neurosci.* **28**, 951–963 (2008).

30. Gharbawie, O. A., Gonzalez, C. L. R., Williams, P. T., Kleim, J. A. & Whishaw, I. Q. Middle cerebral artery (MCA) stroke produces dysfunction in adjacent motor cortex as detected by intracortical microstimulation in rats. *Neuroscience* **130**, 601–610 (2005).

31. Carmichael, S. T. Rodent models of focal stroke: size, mechanism, and purpose. *NeuroRx* **2**, 396–409 (2005).

32. Balbinot, G. *et al.* Post-stroke kinematic analysis in rats reveals similar reaching abnormalities as humans. *Nat. Sci. Reports* **8**, 1–13 (2018).

33. Wong, C. C., Ramanathan, D. S., Gulati, T., Won, S. J. & Ganguly, K. An automated behavioral box to assess forelimb function in rats. *J. Neurosci. Methods* **246**, 30–7 (2015).

34. Gulati, T. *et al.* Robust Neuroprosthetic Control from the Stroke Perilesional Cortex. *J. Neurosci.* **35**, 8653–8661 (2015).

35. Guo, J. Z. *et al.* Cortex commands the performance of skilled movement. *Elife* **4**, 1–18 (2015).

36. Karni, A. *et al.* The acquisition of skilled motor performance: fast and slow experience-driven changes in primary motor cortex. *Proc. Natl. Acad. Sci. U. S. A.* **95**, 861–868 (1998).

37. Hyland, B. Neural activity related to reaching and grasping in rostral and caudal regions of rat motor cortex. *Behav. Brain Res.* **94**, 255–269 (1998).

38. Peters, A. J., Chen, S. X. & Komiyama, T. Emergence of reproducible spatiotemporal activity during motor learning. *Nature* **510**, 263–7 (2014).

39. Sauerbrei, B. A. *et al.* Cortical pattern generation during dexterous movement is input-driven. *Nature* **577**, 386–391 (2020).

40. Laubach, M., Wessberg, J. & Nicolelis, M. A. Cortical ensemble activity increasingly predicts behaviour outcomes during learning of a motor task. *Nature* **405**, 567–571 (2000).

CHAPTER 2 : LOW FREQUENCY CORTICAL ACTIVITY IS A NEUROMODULATORY TARGET THAT TRACKS RECOVERY AFTER STROKE

Abstract

Recent work has highlighted the importance of transient low-frequency oscillatory (LFO, < 4 Hz) activity in the healthy motor cortex (M1) during skilled upper-limb tasks. These brief bouts of oscillatory activity may establish the timing or sequencing of motor actions. Here we show that LFOs track motor recovery post-stroke and can be a physiological target for neuromodulation. In rodents, we found that reach-related LFOs, as measured in both the LFP and related spiking activity, were diminished after stroke and that spontaneous recovery was closely correlated with their restoration in perilesional cortex. Sensorimotor LFOs were also diminished in a human subject with chronic disability after stroke in contrast to two non-stroke subjects who demonstrated robust LFOs. Therapeutic delivery of electrical stimulation time-locked to the expected onset of LFOs was found to significantly improve skilled reaching in stroke animals. Together, our results suggest that restoration or modulation of cortical oscillatory dynamics is important for recovery of upper-limb function and that they may serve as a novel target for clinical neuromodulation.

Introduction

An emerging view of primary motor cortex (M1) sees it as an engine for movement governed by transient oscillatory dynamics present during both preparation and generation of movement [1–7]. Movement-related, low-frequency quasi-oscillatory activity (LFO), at the level of both spiking and local field potentials (LFP), has also been observed in the intact non-human primate M1 and human motor regions during reaching tasks [2–5,8–13]. Such quasi-oscillatory activity can be as brief as 1-2 cycles for rapid movements or longer during sustained movements, and appears to be closely correlated with sub-movement timing [4,5,14]. They may also be related to the multiphasic muscle activations required for precise kinetics during actions[15,16]. Thus, LFOs appear to represent an intrinsic property of motor circuits involved in the production of fast and accurate movements.

Here we hypothesized that monitoring and manipulating movement-related LFOs after stroke may offer new avenues to understand motor recovery. Prior research using invasive electrophysiological approaches has largely focused on measurements of nervous system function that occur at rest and/or away from motor tasks 17–20. For this reason, surprisingly little is known about how stroke and recovery affects task-related neural dynamics at the level of single neurons and mesoscopic circuit function. Non-invasive studies in human subjects have found that EEG movement-related potentials (e.g. slow-cortical potentials or SCPs[21–23]) are affected by stroke[24–27]. Furthermore, changes in SCP are correlated with motor impairments post-stroke[26]. One limitation of EEG, however, is the uncertainty regarding specific anatomical generators and neural processes that contribute to the recorded potentials; moreover, SCPs include a variety of pre-movement and movement related phemonenon[22,23], further limiting their interpretation.

A generative model of cortical dynamics in both the healthy and recovering nervous system may guide the development of novel, closed-loop neuromodulatory approaches that dynamically target transient

task-related processes. Despite our knowledge that neural networks are highly non-stationary, the vast majority of prior studies applying electrical or magnetic stimulation to the brain post-injury have applied it continuously, without explicitly targeting intrinsic neural dynamics[28–30] and with a primary goal of generally increasing excitability and/or plasticity[31–33]. However, recent work has suggested that therapeutic electrical stimulation can be used to target phasic oscillatory dynamics[34,35], an idea has been successfully implemented in Parkinson's disease [36] and epilepsy [37]. Implementing such an approach post-stroke requires detailed knowledge of normal and abnormal neural dynamics, and a better understanding of how to modulate them. Here we aimed to identify neurophysiological dynamics associated with skilled execution; assess whether these same dynamics are related to recovery; and finally, to evaluate whether temporally precise electrical neuromodulation of these dynamics can improve motor function post-stroke.

Results

Long Evans male rats (n = 4) were implanted with microwire arrays in M1 after learning a skilled forelimb reach task[38] (**Fig 2.1a-b**). Animals were trained over multiple days using an automated reach-box[39]. In addition to movement-related spiking activity in M1 in well-trained rats[40,41] (**Fig 2.1c**), we also observed quasi-oscillatory low-frequency activity at the level of both LFP and spiking activity (**Fig 1d**, example trial; **Fig 2.S1** for description of quasi-oscillatory population dynamics; **Fig 2.S2a** additional trial examples). We found strong movement-related power predominately in lower LFP frequencies that began prior to reach onset; neurons showed coherent spiking with the LFP at these frequencies (**Fig 2.1e-f**). We quantified these effects by calculating the mean 1.5-4 Hz LFP power and spike-field coherence or SFC (-0.25 to +0.75 s around reach onset) across channels/units from all animals. There was a significant increase in both power (mixed-effects model with 118 channels and 4 rats as random effect, $t(117) = 6.77$, $p = 5.37e\text{-}10$) and SFC (mixed-effects model with 170 units and 4 rats as random effect, $t(170) = 8.07$, $p = 1.24e\text{-}13$) during the reach as compared to the pre-reach "baseline". Because power and SFC were computed for each trial and then averaged, these values are not related to the mean evoked "event related potential" or ERP, but rather to single-trial dynamics. Together, these findings indicate that rodent M1 also demonstrates similar task-related low-frequency quasi-oscillatory activity described in non-human-primates[2–4,14]. A dynamic increase in SFC associated with movement suggests one of two possibilities: single units and LFP could both be phase-locked to the motor action and thus simply appear phase-locked to each other; or, by contrast, there may be independent phase-locking between units and LFP. One approach of teasing this apart is to subtract out the average ERP, which represents the dominant "phase-locked" LFP activity across trials, and then recalculate power/SFC. By subtracting the ERP, we were left with "induced" oscillations (the non-phase-locked changes in power associated with movement); thus, the subsequent SFC measure indicates a more direct relationship between LFP phase and spiking that is less contaminated by phase-

locked LFP activity to the reach. Using this approach, we again found a strong increase in task-evoked low-frequency SFC (**Fig 2.S2b**) and power (**Fig 2.S2c**) evoked by reaching.

One advantage of LFP recordings over spiking is stability over long-time periods[14,42,43]. In contrast, spike recordings are easily affected by micro-motion, making it difficult to follow the same ensemble across days. Notably, we found remarkable stability in the measured task-related low frequency LFP power across trials and days (**Fig 2.S2d-f**). Finally, LFP measurements provide information about mesoscale organization of neural activity (**Fig 2.1g**)[8,44]. Interestingly, we found that only a subset of channels demonstrated an increase in task-related low frequency power; there appeared to be spatial clustering of channels, suggesting that M1 activation is not uniform at the mesoscale level.

After collecting electrophysiological data in the healthy state (**Fig 2.1**), we performed a distal MCA-occlusion stroke on these same animals (**Fig 2.2a**). Induction of this type of stroke could be performed without perturbing implanted electrodes, thus allowing for a direct comparison of neural activity pre/post stroke in the same animals and cortical region. The distal-MCA model stroke resulted in a large area of damage within sensorimotor cortex (**Fig 2.2b, Fig 2.S3a**). Animals were tested again after at least a 5-day rest post-stroke; neural activity was measured again once animals could attempt reaches and at least occasionally retrieve the pellet (**Fig 2.S3b** shows example hand trajectories). The stroke resulted in impaired skilled motor function (**Fig 2.2c**). Importantly, neural probes were positioned such that at least some electrodes remained in viable tissue (**Fig 2.2b, Fig 2.S3a**); even post-stroke, single units remained on a subset of electrodes (**Fig 2.2d**). There were fewer units post-stroke (average of 1.45 vs. 0.453 units/channel pre vs. post-stroke), but those that remained continued to demonstrate task-related increases in activity, though demonstrating significantly less modulation on average (**Fig 2.2d, Fig 2.S3c-d**). Reach-related LFOs were perturbed (**Fig 2.2e-i**). Low-frequency SFC was reduced after stroke (**Fig 2.2g,** mixed effects model $t(221) = 7.45$, $p = 2.07e\text{-}12$; **Fig 2.S3e-f**); changes in firing rate could not explain the observed changes in SFC (**Fig 2.S3g-h**). To further probe the relationship between spiking activity and LFP using a

method that is not confounded by potential changes in firing rate, we calculated the preferred phase of spiking. We found strong phase-locking to the trough of the low frequency LFP pre-stroke, and no preferred phase of spiking post-stroke (**Fig 2.S3i-j**). LFP power also reduced after stroke (**Fig 2.2h-i,** mixed-effects model t(100) = 6.01, p = 3.06e-8; **Fig 2.S3k-l**). As task-related units were present, the loss of the reach-related LFP power was not simply a product of probes being in infarcted tissue (**Fig 2.2i**). The decrease in LFP power was also not due to changes in movement speed; power was not correlated with movement duration (**Fig 2.S3m**). As before, subtracting the mean ERP to isolate "induced" activity did not significantly change results (**Fig 2.S3n-q**). Together, these analyses clearly demonstrated that stroke resulted in a striking loss of LFOs and phase-locked quasi-oscillatory spiking activity.

Having observed a clear decrease in LFOs in M1 after stroke, we next wondered if recovery of function might be associated with its restoration in peri-lesional cortex. Because of variability in the location of damage after distal MCA occlusion [45], we performed this next set of experiments using a focal photothrombotic stroke model [46] to generate a relatively reproducible area of damage (**Fig 2.S4a**); hence allowing us to know *a priori* the location of the perilesional cortex and to target neural probes to the appropriate rostral location where rehabilitation-induced plasticity has been shown to occur[17,47] . Immediately after stroke induction, a 16 or 32-channel microelectrode array was implanted anterior to the site of the injury [48] (**Fig 2.3a-b**). Animals were given 5 days to recover from the stroke and electrode implantation; they then underwent motor training on the same task to assess the relationship between recovery and task-related LFOs in perilesional cortex. Injury resulted in impaired motor performance (73.6% ± 12.21% vs. 35.1% ± 11.9%, 2-tailed paired t-test, t(5) = 3.35, p = 0.0204) which improved over the course of subsequent training (69.1% ± 9.01% last session; 2-tailed paired t-test comparing first vs last session, t(5) = 3.03, p = 0.0290; **Fig 2.3c**, see **Fig 2.S4b** for example paw trajectories).

With recovery of function, spiking activity in perilesional cortex became sharper, more task-related and more similar to that observed in the healthy M1 (**Fig 2.3d, Fig 2.S4c-d**). There was a clear emergence

of low-frequency task-related activity in both spiking and LFP in perilesional cortex (**Fig 2.3e-k**). This increase in LFO can be observed in single trial examples (**Fig 2.3e**) and across trials/sessions within the same animals (**Fig 2.3f**). Statistically, there was a strong increase in 1.5-4Hz SFC (**Fig 2.3g-h,** mixed effects model $t(387) = 8.94$, $p = 1.59e\text{-}17$; **Fig 2.S4e**). Changes in SFC could not be explained by changes in firing rate (**Fig 2.S4f-i**). 1.5-4 Hz power also increased significantly (**Fig 2.3i-j**, mixed effects model $t(175) = 3.11$, $p = 0.00217$; **Fig 2.S4j-k**). Moreover, subtracting the ERP did not change the results (**Fig 2.S4l-o**).

There was a significant positive relationship between the restoration of low-frequency power and improvements in accuracy on the task (**Fig 2.3f**, example animal; **Fig 2.3l**, all animals, Pearson's correlation $r = 0.576$, $p = 1.18e\text{-}7$). There was also a significant correlation between the restoration of SFC and recovery of function ($r = 0.554$, $p = 4.60e\text{-}7$) and between single unit modulation change and recovery ($r = 0.561$, $p = 3.01e\text{-}7$). A multi-variate linear regression model with all three variables significantly predicted motor improvements ($r = 0.737$, $p = 1.28e\text{-}11$). Each variable had significant partial correlation ($r = 0.428$, $p = 2.21e\text{-}4$ for power; $r = 0.339$, $p = 0.00410$ for SFC; $r = 0.398$, $p = 6.29e\text{-}4$ for unit modulation), suggesting that all variables could independently account for variance in recovery of function.

We next assessed whether our observed phenomena in rodent models were relevant in human stroke[46] by reanalyzing invasive human ECoG (ElectroCortiocoGraphy) data collected from three human subjects undergoing invasive epilepsy monitoring to identify seizure foci[8,44]. Physiological data were recorded during a center-out reach task in which subjects were instructed to wait for a start cue and then reach as fast as possible to a target (**Fig 2.4a**). Two of these patients had intact sensorimotor cortices (hereafter Non-Stroke or NS1/NS2); the third patient, however, had experienced an ischemic cortical stroke four years prior to the monitoring (hereafter Stroke Subject or SS) (**Fig 2.4b**). The stroke subject had persistent motor deficits involving arm and hand movements (Fugl-Meyer upper-limb score of 35). He also showed impairments in speed of execution. Reaction time from "Go" to movement onset (i.e. rise in mean EMG) was slower for the affected versus unaffected arm (reaction time of 635 ± 40 and 423 ± 72 ms,

respectively, t(56) = -2.7, p = 0.009, two-tailed two-sample t-test). Similarly, the reach time from movement onset to target acquisition was longer for the affected arm (reach time of 1266 ± 58 ms vs. 914 ± 51 ms, t(56) = -4.42, p = 4.65e-5, two-tailed two-sample t-test).

For ECoG recordings from NS1/NS2, we found evidence for robust task-related LFOs centered around sensorimotor cortex (**Fig 2.4c**). The time course and pattern of this activity (**Fig 2.4d**) appeared to closely resemble that observed in rodents (**Fig 2.1f**). In the SS, however, there was a striking loss of this sensorimotor reach-related low-frequency activity (**Fig 2.4c-e**). The mean normalized 1.5-4Hz LFP power for sensorimotor electrodes (from -300ms to + 300ms) was significantly positive for the two non-stroke subjects: NS1, normalized mean activity 0.55 ± 0.2 (n = 18 SM electrodes, two-tailed one-sample t-test, t(17) = 7.16, p = 2e-6) and 0.93 ± .25 in NS2, (n = 16 SM electrodes, two-tailed one-sample t-test, t(15)=5.47, p = 6.5e-5), while the stroke subject showed no significant increase in power (-0.12 ± 0.12, n = 91 SM electrodes, two-tailed one-sample t-test, t(90) = -1.03, p = 0.304). There was a highly significant difference in task-related low frequency power between SS and NS1/NS2. We analyzed all channels from all subjects comparing healthy vs. stroke, including subject as a factor in the model to account for differences between the two healthy subjects. Using this approach, we found a highly significant overall effect (F(2,122) = 9.80, p = 1.13e-4, and more importantly, a highly significant effect of stroke (F(1,122) = 18.76, p = 3.1e-5). It is possible these results were observed because, while in healthy subjects, the LFO was dominant near the central sulcus, in stroke, due to cortical reorganization, the LFO could be observed in other regions of the brain. Indeed, prior analyses of the data from SS demonstrated intact high-gamma activity away from the central sulcus, that were correlated with muscle synergies, suggesting functional reorganization[44]. To account for functional reorganization, we thus selected channels that showed increased activity in the high-gamma band between -300 to 300 ms prior to reach. This was performed blind to location, in an un-biased manner for all three subjects. Using this method of functional[49] rather than anatomic selection, we found overall similar results (**Fig 2.S5**). These results suggest that low-frequency

quasi-oscillatory activity is a common electrophysiological signature of healthy motor circuit function across both rats and humans.

A key goal of this project was to assess whether we could modulate task-related oscillations and thereby develop a targeted neuromodulation approach post-stroke. Prior research has demonstrated that direct current stimulation (DCS) can modulate spiking activity [50] and on-going, carbachol-induced gamma-oscillatory dynamics[34]. It has also been recently reported that low-frequency oscillatory activity observed during ketamine anesthesia is similar to the brief, low-frequency spiking/LFP dynamics during natural reaching[3]. To study the effects of DCS *in vivo*, we analyzed the effects of DCS on M1 low-frequency oscillatory activity during ketamine anesthesia (10 rats, 11 sessions). Neural recordings during anesthesia are of substantially greater quality; we can move electrodes to optimize location near neurons and greatly increase signal to noise, a requirement for monitoring spiking during stimulation. After anesthesia induction, we implanted epidural electrodes for stimulation and M1 microwire electrodes to measure neural activity (**Fig 2.5a**). Baseline spiking/LFP activity was recorded for 15 minutes, followed by recordings during the application of a 1–5 minute long DCS (mean duration 2.909 ± 0.607 mins, mean amplitude: 106.364 ± 44.526 μA) via the epidural electrodes adjacent to the implanted recording electrodes**.** We found that DCS could effectively modulate ongoing LFO dynamics during ketamine anesthesia (**Fig 2.5b-d**). Specifically, DCS significantly increased LFP power in the lower frequencies (**Fig 2.5b** 1.5-4Hz LFP power, baseline 0.266 ± 0.047 and with DCS 0.314 ± 0.062; two-tailed paired t-test $t(10) = -2.49$, $p = 0.032$). DCS also generally increased phasic spiking (**Fig 2.5c**) and significantly increased 1.5-4Hz SFC (**Fig 2.5d,** SFC without DCS: 0.278 ± 0.016 and during DCS 0.316 ± 0.022; one-tailed paired t-test $t(49) = -1.73$, $p = 0.0452$). Moreover, 40% of neurons changed their firing rate significantly. More specifically, 30% increased and 10% decreased their firing rates over the baseline period. SFC analyses were performed after controlling for any firing rate changes[51]. This was important as firing rate changed significantly for these neurons at a population level (n= 50, two-tailed paired t-test, $t(49) = -2.65$, $p = 0.0109$).

We next performed experiments to assess whether shorter pulses of DCS (<5 seconds in duration), applied directly during reaching behaviors could improve motor function after stroke. Importantly, we avoided the significantly longer duration stimulation (e.g. continuous stimulation for 5 minutes) that are known to induce long-lasting changes in excitability[31,32], as we wanted to specifically assess whether transient "on-demand" stimulation could induce behavioral improvements. For these experiments, animals underwent either a photothrombotic (n = 4) or distal-MCA (n = 3) stroke induction and were implanted with cranial screws for stimulation both anterior and posterior to the injury site (**Fig 2.6a**). Animals then underwent motor training until their level of performance plateaued (see methods); DCS was then performed. Stimulation experiments occurred between 20-150 days after the stroke, with no clear relationship between time after stroke and efficacy of stimulation. We compared the effects of stimulation with a "no-stimulation" and a "sham-stimulation" condition (**Fig 2.6b**). Using this paradigm, we found that stimulation effects were "on-demand" and did not persist across blocks, allowing us to test, daily, all three conditions (blocks of trials of no stimulation, sham-stimulation or stimulation). The order of these blocks was pseudo-randomized across days in every animal, and across sessions. We calculated the percentage improvement in accuracy for each daily stimulation and sham condition relative to the no-stimulation condition for that day, and then calculated the mean improvement across days for each animal to perform statistics. Animals showed an improvement of 73 ± 12% in accuracy following stimulation compared with no stimulation (one-sample, two-tailed t-test, $t(6) = 6$, $p = 9.6e\text{-}4$) and a non-significant change of -4 ± 5% in the sham stimulation group (one-sample, two-sided t-test, $t(6) = -0.77$, $p = 0.47$, **Fig 2.6c**). There was also a significant difference in the observed behavioral effects between the stim and sham conditions (two-tailed paired-t test, $t(6) = 4.91$, $p = 0.003$). Further analyses describing stroke-type and variation in effects across days as well as additional experiments using cathodal stimulation, are described in online methods.

We next assessed whether DCS could enhance task-related LFOs. We recorded neural signals from four post-stroke rats with persistent deficits, while they attempted the reach-to-grasp task over a total of 24

sessions (total of 1031 trials, 532 reach trials with 'Stim On' and 499 trials without DCS). Simultaneous recording of neural signals during brief epochs of stimulation is particularly challenging as the stimulation onset/offset triggers large distortions in both LFP and spiking. We thus had to substantially alter the stimulation parameters. We used significantly lower current amplitudes (81.654 ± 12.414 μA vs 321.4 ± 12.2 μA in behavioral experiments above), longer duration pulses (DCS pulses were typically 15 seconds long) and more distant stimulation sites to accommodate recording probe (see methods). The average z-scored 1.5-4Hz LFP power was higher during DCS trials (0.201 ± 0.076) compared to no stimulation trials (0.059 ± 0.038, t(1029) = 7.425, p = 2.361e-13, mixed effects model, **Fig 2.6d-f**). We observed a trend towards increased accuracy with DCS in this set of animals 21.069 ± 14.963% increase (one-tailed paired t-test, t(3) = –1.830, p = 0.082). The reduced efficacy was likely the result of the lower current amplitude used. Consistent with this notion is the data from our early pilot experiments (see Methods) and in the behavior-only animals (**Fig 2.6c**) where stimulation currents of >150 μA per screw were required to observe consistent behavioral improvements.

Lastly, we designed a separate set of stimulation experiments using one second long pulses in a new group of animals to replicate the prior effect and more precisely determine the temporal relationship between electrical stimulation and the neural processes underlying reach control after stroke. More specifically, we pseudo-randomly varied the timing of stimulation onset (in blocks of 25 trials) relative to the trial onset (i.e., door opened to allow reach) (**Fig 2.6g**). Importantly, the only parameter varied was the timing of the stimulation onset relative to this cue; stimulation was delivered on all trials**.** Next, we calculated the ΔT between stimulation onset and the actual reach onset for each trial, thereby allowing us to precisely assess the relationship between the timing of stimulation and change in motor function. We then calculated the % accuracy for all trials at a particular ΔT by binning all trials in a window of ± 50 ms around that time-point (100 ms bins). We observed a significant improvement in accuracy only when ΔT occurred between 500 - 400ms from the reach (**Fig 2.6h,** two-tailed, one-sample t-test, t(3) = 9.035, p =

0.0458, Bonferroni-Holm correction for 16 time points, also see **Fig 2.S6** for individual animal traces). It is important to note that, with 1 second pulses, stimulation around this time point is likely to maximally overlap with the expected LFO (visualized on the plot, though the mean LFP trace was taken from different animals). Given the brief duration of stimulation pulses, 1 second long stimulation pulses at other times were likely to begin or end during the LFO; and, interestingly, did not appear to be beneficial. Together, our data demonstrates that DCS improved motor function in a temporally restricted manner and could enhance the LFO after stroke, suggesting a novel mechanism by which neuromodulation can work to improve motor function post-stroke.

Discussion

Our results identified low-frequency quasi-oscillatory activity as an important neurophysiological marker of skilled motor control. We found evidence of such activity at the level of neural spiking and LFP during the performance of a dexterous task in rats, and in ECoG signals in human subjects without stroke. In both rodents and humans, cortical stroke appeared to significantly disrupt low-frequency activity and its reemergence strongly tracked recovery of motor performance in rats. We also found that pulses of electrical stimulation enhanced entrainment of spiking, increased LFOs, and also improved motor performance in animals with persistent deficits. Consistent with this model, electrical stimulation was primarily effective when it started prior to and lasted through the reach, suggesting that applied electrical fields directly modulated neural dynamics linked to task execution.

There is growing literature demonstrating that quasi-oscillatory low-frequency activity can capture reach dynamics [21,22,26]; our results provide evidence that this activity is relevant during recovery as well. Are these events truly "oscillatory", given their relatively brief nature? In this study, we used an established analytic framework [52,53] for time-frequency decomposition of motor evoked activity to assess the spectral content of evoked activity. Using these methods, we were able to: 1) quantify the relationship between spiking and LFP (i.e. SFC), (2) develop a model for how DC stimulation effects neural circuits, and (3) link our findings with human ECoG recordings. All of this suggests that LFOs provide a useful framework for characterizing important cortical dynamics during recovery. A final point in favor of this framework is that we found significant partial correlations between behavioral improvements separately for both SFC and low frequency LFP power; this suggests that specific aspects of the oscillatory dynamics (spiking and LFP) provide independent explanatory power about motor recovery. This does raise a concern regarding the correct interpretation of the SFC. Specifically, task-evoked SFC could arise simply because both LFP and spiking are phase-locked to behavior, even if they are not directly related to each other. To address this, we subtracted the average ERP, which represents the phase-locked component of the LFP[53]; we still observed

task-related increase in power and SFC, suggesting the two signals are related to each other, and not simply similarly phase-locked to behavior. Together, our results indicate that restoration of oscillatory dynamics observed both in spiking and LFP data, is important for motor recovery.

What is the possible relationship between LFOs, skilled behaviors, and motor recovery? Low-frequency oscillations can be used to decode reach-related activity[7,14] and predict spiking phase across multiple behavioral states[7,14]. Such activity is also correlated with multiphasic muscle activations and movement timing [2,4,5,14,15]. Recent work also suggests that oscillatory dynamics reflect an underlying dynamical system[2]. This prior work argues that LFOs represent an intrinsic property of motor circuits associated with precise temporal control of movements. Our findings extend this body of work by linking restoration of LFO dynamics in perilesional cortex to motor recovery. Our results directly implicate LFOs in the re-instantiation of cortical control of complex limb dynamics during reaching[17]. In our human stroke subject, persistent loss of cortical LFOs may suggest a mechanism for why reaching behaviors continued to be impaired. Of course, as we were only able to get data from one stroke patient, the generalizability of these findings remains unknown. The results need confirmation in a larger cohort. Nonetheless, given the concordance with our extensive rodent-based investigations, it is reasonable to propose that recovery of LFOs may represent a marker of restored circuit dynamics after stroke important for skilled reaching.

The exact origin of LFOs and underlying generators remains unknown. While our finding that a focal cortical stroke can perturb LFOs might indicate a local source, it is also increasingly clear that local perturbations can affect large-scale networks [19,54]. Indeed, reach-related LFOs may involve striatal [55] or thalamocortical activity [56]; with impairments and recovery after stroke a function of network plasticity rather than local effects restricted to M1. It is possible that these LFOs are related to slow-cortical potentials associated with actions measured using EEG[22]. However, because those potentials may involve multiple cortical/subcortical networks, it is difficult to directly compare to our observed phenomenon. Further work

specifically probing interactions between perilesional cortex and the broader motor network can clarify what drives our observed electrophysiological changes during recovery.

We found that pulses of DC stimulation (i.e. **Fig 2.6**) could improve motor function when timed to start prior to and last through the reach period. How might electrical stimulation improve motor function after stroke; and how does this differ from prior neuromodulation methods in stroke [29,30,33,57]? In many prior animal and human studies (best exemplified in the EVEREST trial[30]), sub-threshold high-frequency epidural stimulation over perilesional cortex was used to generally enhance cortical plasticity. Stimulation was delivered for an extended period of time in an 'open-loop' manner, i.e. not-timed with behavior, and the primary outcome measures were long-term changes in map plasticity (in animals[57]) and long-lasting changes in motor function (in both animals/humans)[30,57]. Such stimulation protocols are thought to induce lasting changes in excitability[31] that likely requires BDNF[32]. A more novel form of stimulation used a closed-loop paradigm in which stimulation in one region was linked with firing activity in different region[33], but again the primary goal was to induce long-term changes in network-plasticity. In contrast to these prior efforts, our study was designed to test whether electrical stimulation could specifically modulate the brief, movement-locked neural activity identified here and thereby improve motor function, i.e. apart from any long-term changes in cortical excitability or plasticity. Indeed, we show that brief, DC pulses can modulate movement-locked low-frequency activity and can improve motor function post-stroke. Our study, therefore, provides a theoretical basis for designing a rationale, on-demand and neurally-targeted stimulation paradigm for improving motor function. Moreover, our method of delivering stimulation (i.e. via cranial-screws) is potentially translatable as a novel class of invasive medical device. Such a device could address growing concerns that non-invasive stimulation may not reliably modulate cortex[58].

Stroke is one of the primary causes of long-term motor disability. Most current therapies, including task-specific rehabilitation training, are designed to enhance endogenous neural plasticity[59]. Here we have identified a novel neurophysiological target and tested a dynamic neuromodulation approach for improving

motor function post-stroke. Moreover, because LFOs can be recorded in human subjects both non-invasively (i.e. task-evoked delta/theta power using EEG) [5] and invasively (i.e. using ECoG)[8] there is a potential path to translate our results to stroke patients. These results may provide the basis for a new generation of "smart" stimulation devices that can precisely target neuromodulation to improve motor function after stroke.

Materials and Methods

Animal Care and Surgery

All procedures were in accordance with protocols approved by the Institutional Animal Care and Use Committee at the San Francisco Veterans Affairs Medical Center. Adult male Long Evans rats (n = 34, 250-400g, Charles River Laboratories) were housed in a 12h:12h light: dark cycle. All surgical procedures were performed using sterile technique under 2-4% isoflurane or a ketamine/xylazine cocktail. Surgery involved cleaning and exposure of the skull, preparation of the skull surface (using cyanoacrylate), and then implantation of skull screws for referencing, stimulation and overall head-stage stability. Reference screws were implanted posterior to lambda, ipsilateral to the neural recordings. The ground screw was placed in the skull contralateral to the neural recordings and either placed posterior to lambda or over the nasal bone. For experiments involved physiological recordings, craniotomy and durectomy were performed, followed by implantation of neural probes. The postoperative recovery regimen included administration of buprenorphine at 0.02 mg/kg b.w for 2 days, and meloxicam at 0.2 mg/kg b.w. dexamethasone at 0.5 mg/kg b.w and trimethoprim sulfadiazine at 15 mg/kg b.w for 5 days. All animals were allowed to recover for one week prior to further behavioral training.

Behavior

Animals were acclimated and then trained to plateau level of performance in a reach to grasp single pellet task before neural probe implantation. Probe implantation was performed contralateral to the preferred hand. Animals were allowed to rest for 5 days before the start of experimental/recording sessions. During behavioral assessments, we monitored the animals and ensured that body weights did not drop below 90% of the initial weight.

We used an automated reach-box, controlled by custom MATLAB scripts and an Arduino micro-controller. This setup required minimal user intervention, as described previously[39]. Each trial consisted of a pellet dispensed on the pellet tray; followed by an alerting beep indicating that the trial was beginning and then the door opening. Animals then had to reach their arm out, grasp and retrieve the pellet. A real-time "pellet-detector" using an IR detector centered over the pellet was used to determine when the pellet was moved, indicating the trial was over, and the door was closed. All trials were captured by video, which was synced with electrophysiology data using Arduino digital output. The video frame rate was 30Hz for the animals in the photothrombotic stroke electrophysiology experiments (n=6), and 75Hz for those in the MCA stroke electrophysiology experiments (n=4) and stimulation experiments (n=14). Physiological data presented in this paper were generally time-locked to the onset of the reach movement. Onset of reach was determined manually from recorded video, and defined as the start of paw advancement towards the slot.

In Vivo Electrophysiology

We recorded extracellular neural activity using tungsten microwire electrode arrays (Tucker-Davis Technologies). We used either 16- or 32-channel arrays (33 μm polyamide-coated tungsten microwire arrays). Arrays were lowered down to a depth of ~ 1200 - 1500μm. In healthy animals, neural probes were centered over the forelimb area of M1[17], at 3 mm lateral and 0.5 mm anterior from bregma. In photothrombotic stroke animals, the neural probe was placed immediately anterior to the stroke site, typically centered around 3-4 mm anterior and 2.5-3 mm lateral to bregma.

Units and LFP activity were recorded using a 128-channel TDT-RZ2 system (Tucker-Davies Technologies). Spike data were sampled at 24414 Hz and LFP data at 1017.3 Hz. ZIF-clip-based analog headstages with a unity gain and high impedance (~1 GΩ) were used. Threshold for spiking activity was set on-line using a standard deviation of 4.5 (calculated over a 1 minute period using the TDT-RZ2 system), and waveforms and timestamps were stored for any event that crossed that threshold. Sorting was performed

using Plexon OfflineSorter v4.3.0, using a PCA-based method followed by manual inspection and sorting. We included both clearly identified single-units and multi-unit activity for this analysis (results were pooled as there were not clear differences in single and multi-unit responses). A total of 171 single and multi-units were recorded from healthy animals, 53 from those same animals post MCA stroke, 170-219 from animals after photothrombotic stroke, and 50 units in the ketamine experiment (only single units with SNR > 5.5 were used in this DC stimulation experiment in order to minimize stimulated-related contamination of neural signals). Behavior-related timestamps (i.e., trial onset, trial completion) were sent to the RZ2 analog input channel using an Arduino digital board and synchronized to neural data.

MCA Stroke

For this procedure[60], adult rats were placed in the supine position, and a ventral cervical midline skin incision was made under the surgical microscope. Both the common carotid arteries (CCAs) were carefully isolated from the adjacent vagus nerve. The animal was then placed in the lateral position, and an incision was made over the temporalis muscle, which was then retracted. The main trunk of the left middle cerebral artery (MCA) was exposed and occluded with an AVM micro clip (Codman & Shurtleff, Inc., MA) and the CCAs was occluded using micro clamps, both for 60 minutes. After ischemia, micro clip and micro clamps were removed to restore blood flow after which the wound was sutured. This procedure has been previously shown to result in long-term loss of cortical tissue, and long-term impairments in motor cortical function [61].

Photothrombotic Stroke and Electrophysiology

After craniotomy, rose-bengal dye was injected into the femoral vein using an intravenous catheter. Next, the surface of the brain was illuminated with white light (KL-1500 LCD, Schott) using a fiber optic cable for 20 minutes. We used a 4 mm aperture for stroke induction (centered in the M1 area based on stereotactic coordinates) and covered the remaining cortical area with a custom aluminum foil mask to

prevent light penetration. After induction, a probe was implanted in the perilesional cortex (PLC) immediately anterior to the stroke site[48]. The craniotomy/implanted electrodes were covered with a layer of silicone (Quiksil), followed by dental cement.

Direct Current Stimulation (DCS)

Anesthesia (Ketamine) Experiment

Animals (n = 10) were initially anesthetized using a ketamine/xylazine cocktail (85 mg/kg ketamine, and 10 mg/kg xylazine), with supplemental ketamine given ~ every 40-60 minutes as needed to maintain a stable anesthetic level, and also to maintain anesthesia at stage III characterized by predominantly slow oscillations[62]; 0.05 mg/ kg atropine was also given separately to help decrease secretions and counteract cardiac and respiratory depression. After anesthesia and craniotomy was performed, epidural stimulation electrodes were implanted (using skull-screws embedded in the skull), in the configuration noted in Fig 2.5. The ground screw for this and all other stimulation experiments was implanted over the contralateral nasal bone, suggesting current flow would likely go through cortex and associated pathways in an anterior-medial direction from the site of stimulation. These screws were connected to a Multi-Channel Systems Stimulus Generator (MCS STG4000 series) to deliver direct-current stimulation. In 3 animals, ~2mm tungsten wire was placed on epidural surface in the craniotomy well instead of using skull screws to deliver the electrical stimulation. 32-ch multi-electrode arrays were implanted into Layer 5 of motor cortex (1200 – 1500 μm deep). Single-unit and LFP activity was recorded for 1 hour to ensure stability of recordings and minimize drift during stimulation experiment. Then, we recorded a base-line period of neural activity (~ 15 minutes), followed by neural activity during direct-current stimulation (typically using 10 – 100 μA currents, applied for 1 - 5 minutes).

In vivo DCS Experiments

Fixed Stimulation-Behavioral experiments

After a stroke was induced (photothrombotic n = 4 and distal-MCA n = 3), two stainless steel skull-screws were implanted 1mm anterior and posterior to the stroke site; we ensured that the electrodes were as close as possible to the stroke site and that they were located near the midline of the stroke area. Ground screw was implanted over contra-lesional nasal bone. Following a one-week recovery period animals were tested several times each week and those showing no persistent motor deficit (n = 3) were excluded from further testing. Animals were tested until their behavior was at a plateau, with reach accuracies at least > 15%. Direct-current stimulation, applied using an IZ2 stimulus isolator (TDT), was administered on both variable and fixed schedules. Stimulation was delivered on 2 screws in each animal, with a maximum stimulation amplitude of 200 μA/screw. Pilot studies in the first two animals suggested that accuracy on the skilled forelimb reach task was improved with > 150μA of current/screw; based on this pilot data, we provided at least 150μA of current/screw in all animals undergoing behavioral testing. Stimulation current was increased up to the point of tolerability by the subject; with a max amplitude of 200 μA /screw. Tolerability was defined as animals not making any observable behavioral response to the onset/offset of stimulation pulse. We tested both cathodal and anodal polarities of stimulation, as described in results and below.

The current densities used in our study appear to be less that what has been used in previous studies. For example, a 2016 study used epidural electrodes for language mapping[63]. The authors report using 5-15 mA of current delivered through 2.3 mm electrodes (area of 4.15 mm^2); this results in a current density of 2.4 mA/mm^2. Similarly, the current densities used for epidural stimulation in the Everest Trial were also comparable[30]. The study reported using currents up to 13 mA using four electrodes with 3 mm diameter. Thus, each electrode could have a density of 0.46 mA/mm^2. There are also multiple non-human primate

studies using epidural stimulation. We estimate the following densities for the two example studies: 0.92 mA/mm^2 [64] & 1.41 mA/mm^2 [65]. In comparison, we used 1 mm diameters screws. We typically used between 150 - 200 μA /skull screw when delivering stimulation. Our estimated current density was 0.25 mA/mm^2. Thus, to the best of our knowledge, our current densities are comparable to those used in invasive human and non-human primate studies. Fixed stimulation (n = 7, i.e. Fig 2.6a-c data) began 500 ms prior to the door opening (i.e. signal of trial starting), and lasted up to 5s total (encompassing the entire reach period, with stimulation turned off after the trial ended). 30-trial blocks of stimulation "on," "off" and "sham," (a 200 ms pulse that ended prior to the door opening, to mimic the sensory or possible alerting effects of the stimulation onset) were counterbalanced and interleaved across days. Effects of stimulation and sham were made based on percent improvements compared to temporally adjacent no-stimulation blocks. We made a decision to randomize at the level of blocks (i.e., blocks of 30 trials; 25 trials in DC Stim with physiology experiments) rather than at the level of trials because of pilot data (in 2 animals) that there were more robust behavioral effects when randomized in this manner.

Because we performed stim/sham stim sessions across days, we also calculated the standard deviation in the percentage improvement for each animal across days to see if this differed between conditions. We did not find a significant difference between the two conditions ($t(6) = 1.37$, $p = 0.21$). We did observe improvements in performance in both stroke models with no significant differences by stroke model type ($t(5) = 1.24$, $p = 0.271$). While the above experiments were all conducted using cathodal stimulation, we found similar effects using anodal stimulation condition (anodal-stimulation showed an improvement of 60 ± 12% (one-sample t-test, $t(4) = 4.95$, $p = 0.008$, n = 5 animals, which included experiments performed in two of the animals used above for cathodal stimulation and 3 additional animals, all in a photothrombotic stroke model). There was no difference between anodal and cathodal stimulation on motor improvement (ANOVA, $t(10) = 0.736$, $p = 0.479$).

Joint Stimulation-Physiology Experiments

In studies combining electrophysiology and DC stimulation (Fig 2.6d-e, n = 4), we found that high stimulation currents resulted in artifacts that were difficult to remove. For this reason, we utilized smaller currents (81.654 ± 12.414 μA mean current amplitudes in these experiments vs 321.4 ± 12.2 μA in behavioral experiments above), with the primary goal of understanding whether DC stim could affect the LFO in any way. DC stimulation started 9 seconds before the door opened for the reach to start, and lasted 7 seconds after the door opened in these experiments, to minimize stim-related artifact in LFP recordings of interest (n = 4 rats, i.e. Fig 2.6d-e data). Photothrombotic stroke was used in the joint stimulation and physiological recording experiments (n = 4). Furthermore, since the aim was to see if LFO was boosted with DCS, in these experiments, we started these experiments immediately after stroke (after a 14 day recovery period). For all fixed stimulation DCS experiments, the stimulation screws were placed anterior/posterior to the lesion/electrodes, and the "ground screw" was placed on the contra-lateral hemisphere on the nasal bone. For the joint stimulation and physiology experiments, the stimulation screws were placed somewhat diagonally and at further distance from stroke to accommodate recording array. Thus, the fixed stimulation versus joint stimulation and recording were optimized for behavioral effects versus physiologic recordings/ effects respectively.

Variable Stimulation Experiment

Variable timing stimulation (Fig 2.6 f-g, n = 4) began at six time-points with respect to door-open (-1s, -.5s, 0s, .5s, 1s, 1.5s) and lasted 1 second to ensure a spread of temporal relationships between stimulation start and reach onset (ΔT). Stimulation was delivered in blocks of 25 trials with stimulation start time consistent within-block. Animals underwent 12 random-ordered blocks each day with each time-point tested in a total of 50 trials in two non-consecutive blocks. For each trial in each animal we calculated the exact time between stimulation and reach onset (ΔT) for analysis. Data was pooled in each animal from

both anodal and cathodal stimulation experiments; there was no evidence that one form of stimulation worked consistently or significantly more than the other, consistent with data from the longer-duration stimulation experiments described above. Because there is some variability between the trial start (i.e. door opening), and the actual reach onset, the exact ΔT varied quite a bit from trial to trial even in the same stim block, thus helping to increase the randomization of this experiment.

Immunohistochemistry

Rats were anesthetized and transcardially perfused with 0.9% sodium chloride, followed by 4% formaldehyde. The harvested brains were post-fixed for 24 hours and immersed in 20% sucrose for 2 days. Coronal cryostat sections (40 □m thickness) were incubated with blocking buffer (10% Donkey serum and 0.1% Triton X-100 in 0.1 M PB) for 1 hr, and then incubated with mouse anti-NeuN (1:1000; Millipore, Billerica, MA) for overnight. After washing, the sections were incubated with biotinylated anti-mouse IgG secondary antibody (1:300; Vector Lab, Burlingame, CA) for 2 hrs. Sections were incubated with avidin-biotin peroxidase complex reagents using a Vector ABC kit (Vector Labs). The horseradish peroxidase reaction was detected with diaminobenzidine and H2O2. The sections were washed in PB, and then mounted with permount solution (Fisher scientific) on superfrosted coated slides (Fisher Scientific, Pittsburgh, PA). The images of whole section were taken by HP scanner, and the microscope image was taken by Zeiss microscope (Zeiss, Thornwood, NY).

Human ECoG Experiments

We utilized data that had been collected and described in two previous manuscripts[8,44]. As previously described, these studies were conducted using a protocol approved by the UCSF CHR; all studies were conducted after obtaining informed consent from subjects. Data were collected from two subjects without stroke and one subject with documented cortical stroke. All subjects had epilepsy, and had chronic ECoG grids implanted for pre-surgical monitoring/localization of seizure. Consent and details of recordings

and of the specific aspects of the behavioral paradigm in healthy subjects were previously reported here[8]; and for the stroke subject here[44]. In brief, all subjects performed a center-out reaching task, in which trials began with the appearance of a target at the center of the reach field, followed, after a variable delay, with a cue indicating subjects should perform a reach to one of 4 targets.

Data analysis

LFP/ECOG and Single-Unit Analyses

Analyses were conducted using a combination of custom-written routines in MATLAB 2015a/2017a (Math Works), along with functions/routines from the EEGLAB toolbox (http://sccn.ucsd.edu/eeglab/) and the Chronux toolbox (http://chronux.org/). Pre-processing steps for LFP/ECOG analysis included: artifact rejection (removing broken channels and noisy trials); z-scoring; and common-mode referencing using the median signal (at every time-point, the median signal across the remaining electrodes, was calculated; and this median signal was subtracted from every channel to decrease common noise and minimize volume conduction). We used median referencing rather than mean referencing to minimize the effect of channels with high noise/impedance that were not discsarded). For the joint stimulation and physiology experiments, we witnessed crosstalk between channels in two animals, and thus non-median subtracted LFP was analyzed. Filtering of data at specified frequency bands was performed using the EEGLAB function eegfilt(). Calculation of power was performed with wavelets using the EEGLAB function newtimef(). All time-frequency decompositions were performed on data on a trial by trial basis to capture the "total power" (that is, both the phase-locked, i.e., "evoked" and non-phase-locked, or "induced") power. To isolate and also study only the "induced" oscillatory activity, we performed a similar analysis after subtracting the mean evoked potential from the single trial data. By subtracting this out, we removed on each trial the predominant phase-locked activity in the LFP, and what remained was the "induced" activity in which power is increased in a non-phase-locked way. Channels used for ECoG

analysis were chosen by locating, for each subject, the central sulcus and selecting anatomically adjacent electrodes both anterior and posterior to the central sulcus. We performed the analysis using electrodes as far ventral as the Sylvian fissure for this paper; however, we also performed an analysis in which we subsampled only the dorsal half of these electrodes from each subject presumably closer to the hand knob, and found similar results.

Statistical quantification of how stroke/recovery affected power and spike-field-coherence in rodents was calculated by taking the mean power/SFC from -0.25s to 0.75s around reach onset. Only trials where the rat managed to at least touched and knocked off the pellet were included in the analysis. In Fig 2.1, the baseline period is -3 to -2s relative to reach onset. In Fig 2.2, quantifications were made between all valid trials (at least 50) in the recording block before and after stroke. In Fig 2.3, comparisons were made across the first 50 and last 50 trials or the first and last recording block, for power and SFC respectively, for each animal. In humans, we used data from -0.3s to + 0.3s from reach onset across all trials performed in each subject. Calculation of spike-field coherence values was performed using the Chronux function cohgramcpt. For awake task-related experiments, SFC calculations were performed using 1s windows moving by 0.025s. For the anesthetized DCS experiments, multitaper and window parameters used for sleep-epoch analyses were utilized[51,66].

Sorted spikes were binned at 20 ms unless otherwise stated. After spikes were time-locked to behavioral markers, the peri-event time histogram (PETH) was estimated by Bayesian Adaptive Regression Splines (BARS)[67]. Unit modulation was calculated as (max-min)/(max+min) firing rate from -4 to 2.5s around reach, after spline-fitting. Gaussian process factor analysis (GPFA)[68], in Fig 2.S1, was done using DataHigh[69], with spikes from -1s to +1.5s around grasp onset.

Spike-phase histograms in Fig 2.S3 and 4 were calculated by first taking the Hilbert transform of the LFP filtered from 1.5-4 Hz, and then finding the phases of the LFP at which spikes (between -0.25 and +0.75 seconds from reach onset) occurred. For every spike-LFP pair (all spikes and LFP channels from each animal, across all 4 animals), we calculated the Rayleigh's z-statistic for circular non-uniformity, and then obtained the percentage of significant pairs ($p<0.05$).

Statistical Analysis

Parametric statistics were generally used in this study (ANOVA, t-tests, Pearson's correlation and linear regression, unless otherwise stated), implemented within either MATLAB or SPSS. Linear mixed effects model (implemented using MATLAB fitlme) was used to compare the differences in unit modulation, SFC and LFP power in Fig 2.1-3 and the LFP power for stimulation on and off trials in Fig 2.6. This model accounts for the fact that units, channels or trials from the same animal are more correlated than those from different animals, and is more stringent than computing statistical significance over all units/channels/trials[70]. We fitted random intercepts for each rat, and reported the p-values for the regression coefficients associated with pre/post stroke, early/late recovery or stimulation on/off.

In Fig 2.4, we used anatomically defined sensorimotor electrodes (electrodes that laid on either side of the central sulcus), and performed an ANOVA between conditions (stroke vs. non-stroke), with subject included as an additional factor. In Figure 5, we analyzed data from only one channel in each animal (non-referenced), and calculated parametric statistics across animals (5b) or units (5d). In Figure 6, we performed parametric statistics across animals. In figure 6f-g, to calculate significance, we performed two-tailed, one-sample t-tests at each time point displayed followed by Bonferroni-Holm correction for family-wise error. To confirm the effect, using a permutation test, we performed the following analysis. For each trial in each animal we calculated the time between stimulation and reach onset (ΔT) and the accuracy (success/fail) of that trial. We then randomized the accuracies relative to the (ΔT) 1000 times for each animal, maintaining

in each animal the overall distribution of times (i.e. ΔT and accuracy. Then we computed for each animal the percentage accuracy at any particular ΔT (around a window of $\pm$ 50 ms); and also the 1000 surrogate (i.e., randomized) accuracy at these time points. Across animals, we then calculated the mean accuracy, and compared this to the distribution of mean accuracies across the 4 animals generated from the randomized surrogates. Significance was assigned according to 2-tailed probabilities, such that at any point in time, accuracy > or < the 97.5^{th} percentile in either direction at that particular ΔT was assigned a significance of <0.05. The significance values derived from this approach are more conservative than p-values derived from a more standard one-sample t-test at each time point, and likewise confirmed significance of the time-point in question (-450 ms prior to reach onset).

Figures

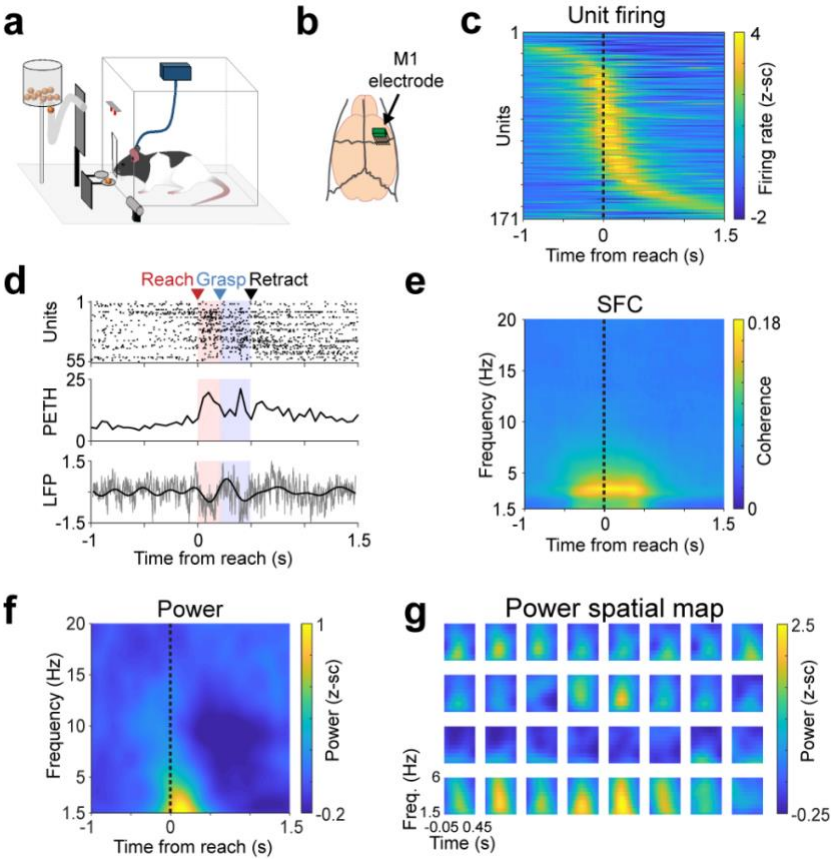

Figure 2.1: Low-frequency quasi-oscillatory (LFO) activity during a skilled forelimb reach task in healthy rats

a. Behavioral setup for skilled forelimb reach task with simultaneous neurophysiological recording. b. Fixed 32-channel micro-wire arrays were implanted in motor cortex. c. Z-scored firing rate changes (171 units from 4 rats) aligned to reach onset. d. Single trial example of brief low-frequency oscillatory activity during reaching (top: spike raster of all units in this example trial, middle: population peri-event time histogram for all spikes shown on top, bottom: z-scored raw LFP in gray and LFP filtered from 1.5 – 4 Hz in black from an example channel). This trial is representative example of trials that show high SFC and high power, as quantified subsequently. e. Mean spike-field coherence (SFC) across 171 units from 4 rats. f. Mean LFP power across 118 channels from 4 rats. g. 4 x 8 grid of electrodes from one animal, in actual spatial configuration, with 375 □m spacing in the y-direction and 250 □m spacing in the x-direction, plotting only power from 1.5 – 6 Hz, and from - .05 to 0.45 seconds from reach onset.

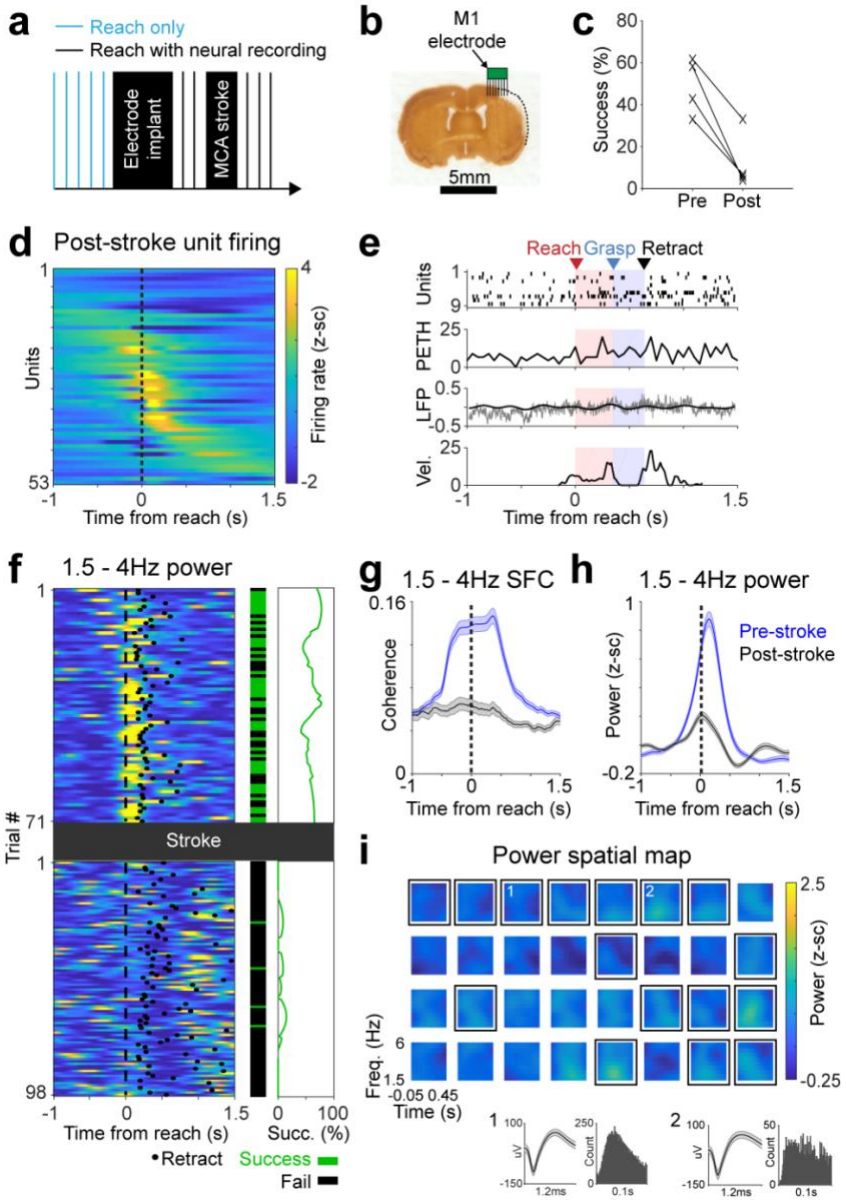

Figure 2.2: Stroke diminished LFO activity in M1

a. Experimental paradigm. After the MCA stroke, we continued recording neural activity from M1 during the reach task in same animals as Fig 3.1. b. Histological section showing stroke and approximate location of electrodes from one animal. We performed a similar histological analysis in 4 animals to verify that there was some observable lesion resulting from the stroke. c. Pellet retrieval success rate before (mean 48.9%, SD 13.4%) and after (mean 12.4%, SD 13.8%) distal MCA stroke in 4 rats (2-sided paired t-test, $t(3)= 5.77$, $*p = 0.010$). d. Z-scored unit firing rate changes relative to reach onset (53 units from 4 rats). e. Single trial example of diminished LFO activity. Labeling convention is the same as Fig 2.1d. Bottom panel shows paw velocity in arbitrary units. This is representative of trials that show low SFC and LFP power, quantified in subsequent panels (g/h) f. Trial-by-trial low frequency LFP power decrease after stroke shown in an example channel, paralleled by decrease in success rate. Left: 1.5-4 Hz LFP power, middle: trial by trial

success rate, right: success rate smoothed over 25 trials. Only trials in which rat reached and touched the pellet were included. This is representative of a channel that shows high power prior to stroke and low power after, as quantified in subsequent panels (g/h) g. Quantification of 1.5-4 Hz SFC before (n = 171 units) and after (n = 53 units) stroke in 4 rats. Thick lines show mean and shaded area is SEM. h. Quantification of changes in low frequency LFP power after stroke, comparing all paired channels (n = 101) from all 4 animals. Shaded area is SEM. i. Example grid of channels from the same rat as in Fig 2.1 and in the same scale. Channels with spiking activity are enclosed by black squares. Insets 1 and 2 show mean unit waveforms (shaded area is SEM) and inter-spike interval histograms from 2 selected channels. All 4 animals demonstrated a similar loss of low frequency power across channels after the stroke.

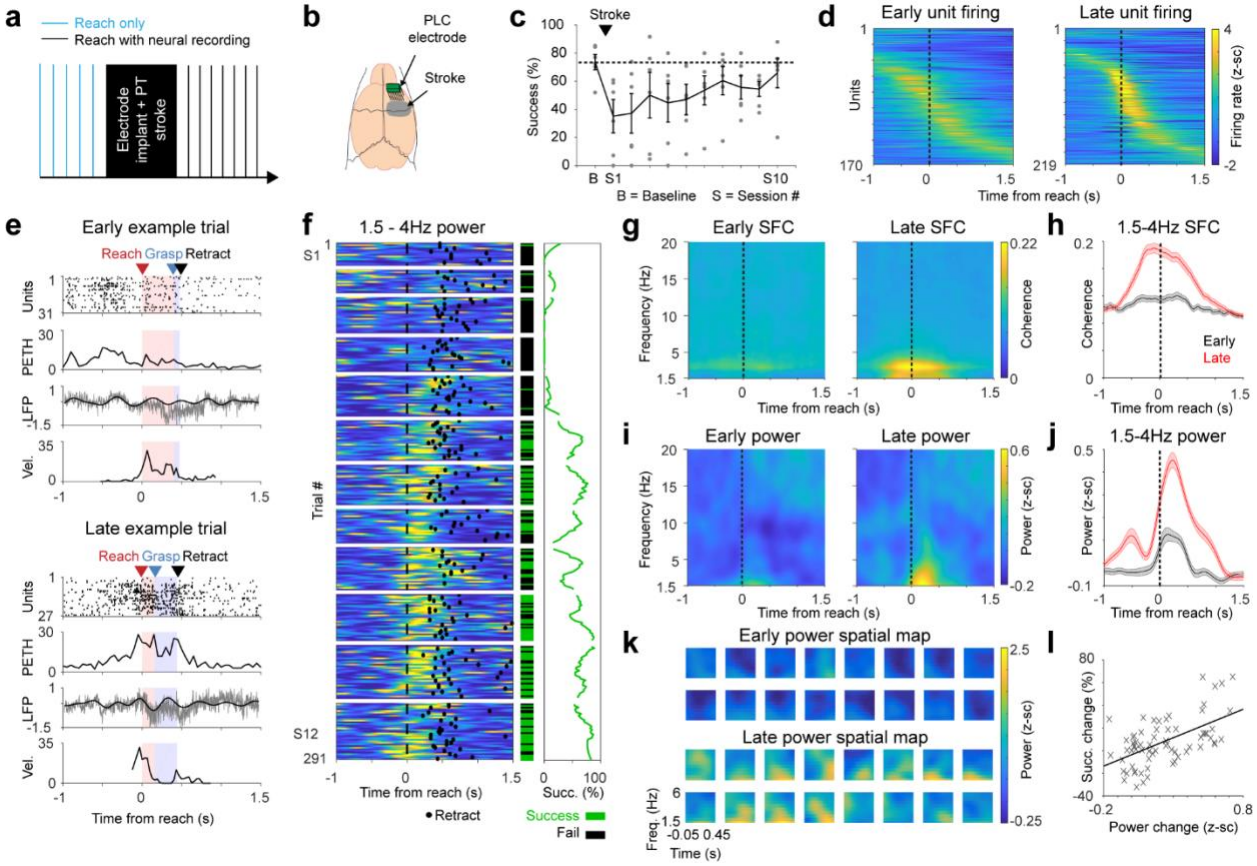

Figure 2.3: Restoration of LFOs in perilesional motor cortex tracked motor recovery

a. Experimental paradigm. b. Schematic showing location of stroke and electrode. c. Mean pellet retrieval success rate before stroke and during rehabilitation training sessions (n = 6, error bars show SEM, grey dots show mean of individual rats). Session 1 or S1 was 1 week post stroke for all. Each animal typically attempted 2 sessions of 25-35 trials each per day. d. Firing rate changes relative to reach onset in early (the first) and late (the last) sessions (for all units from all 6 rats). e. Example of increased LFO activity with rehabilitation, both at the level of spiking and LFP, in two trials with similar paw velocity. Labeling convention are the same as Fig 2.2e. f. Example channel from one animal showing trial by trial 1.5-4 Hz LFP power increase, along with success rate increase, over the course of rehabilitation training. Quantification of this effect across channels is in panels i/j. Labeling convention is the same as Fig 2.2f. Horizontal white lines separate training sessions. g-h. Mean SFC, calculated from units (n = 170 early, n = 219 late) in all 6 animals. Shaded area in h is SEM. i-j. Mean LFP power across channels (n = 176) from all 6 animals in early and late trials. Shaded area in j is SEM. k. Spatial topography of the low-frequency LFP power increase. Plot shows example channels from one animal. All 6 animals showed similar patterns of recovery, as quantified in panels i/j. l. Scatter showing significant correlation between restoration of low frequency power (mean 1.5-4Hz power from –0.25 to 0.75s around reach onset) and improvements on the motor task (r = 0.576, two-tailed Pearson's correlation, *p = 1.18e-7). Each x represents one session from one rat (n = 72 sessions), with values normalized for each animal to first session post-stroke.

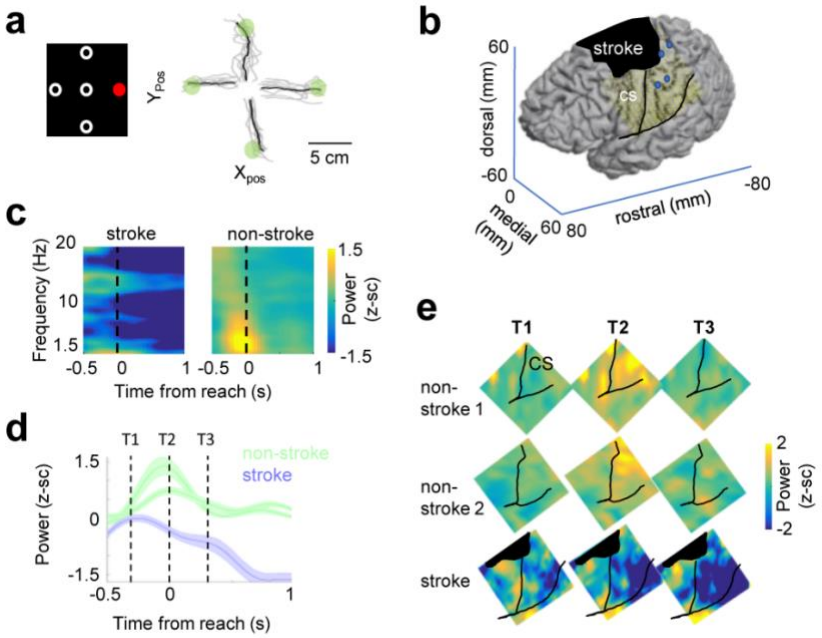

Figure 2.4: Movement-related LFOs in sensorimotor cortex of a human stroke patient relative to non-stroke subjects

a. Left: center-out paradigm used in patients with ElectroCorticoGraphy (ECoG) recordings. In each trial, subjects were given a hold cue, followed by a "reach" cue (red) that indicated which target to move to. Right: example of trajectories in the stroke patient. Movement-related data was recorded from 2 subjects with no stroke (NS) and 1 stroke subject (SS). Analyses were collapsed across all movement directions in each subject. b. Placement of ECoG grid in the stroke subject, and location of stroke. Blue dots on image indicate where intracortical stimulation evoked hand movements. c. Event-related spectral power across sensorimotor electrodes from one intact subject, and the stroke subject. Power normalized to a baseline time period for each channel (activity prior to the hold-cue). This experiment was not repeated on a subsequent day. d. Temporal plot of mean low-frequency power (1.5-4 Hz) from sensorimotor electrodes in each of the 2 intact subjects (NS1, n = 18 electrodes, NS2, n = 16 electrodes and the stroke subject (n = 91 electrodes). Shaded error bars display SEM for each subject across electrodes. e. Spatiotemporal plot at the 3 time-points indicated in panel (d), demonstrating increase in low frequency power along the CS (sensorimotor strip) in the two healthy subjects, and absence of this power in the stroke subject. Z-score scale displayed to the right of the image is identical for all subjects and time points. Experiments were not repeated in these subjects.

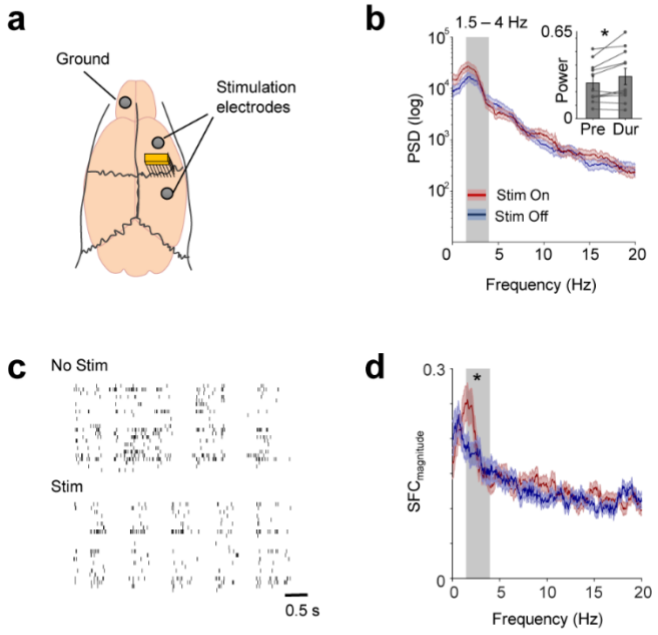

Figure 2.5: LFO activity increased with Direct Current Stimulation (DCS) in acute (anesthetized) recording sessions

a. Recording and stimulation arrangement in acute experiments. b. LFP power before and during DCS shown in one session. Grey shaded area shows 1.5-4Hz frequency range. Thick lines in blue and red show mean and shaded areas show SEM. Inset shows 1.5-4Hz power in pre-DCS and during-DCS in all 11 sessions from 10 rats (mean and SEM shown in bar plots with individual values, two-tailed paired t-test, $t(10)= -2.493$, $*p = 0.032$). c. Spiking activity of the same neurons from a session before and during stimulation, showing increased coherent spiking during DCS. d. Mean SFC (dark red/blue line - conventions as previous) of 50 neurons from 10 rats. Shaded area represents SEM. 1.5-4Hz SFC (grey shaded area) increased with DCS (one-tailed paired t-test, $t(49) = -1.727$, $*p = 0.045$).

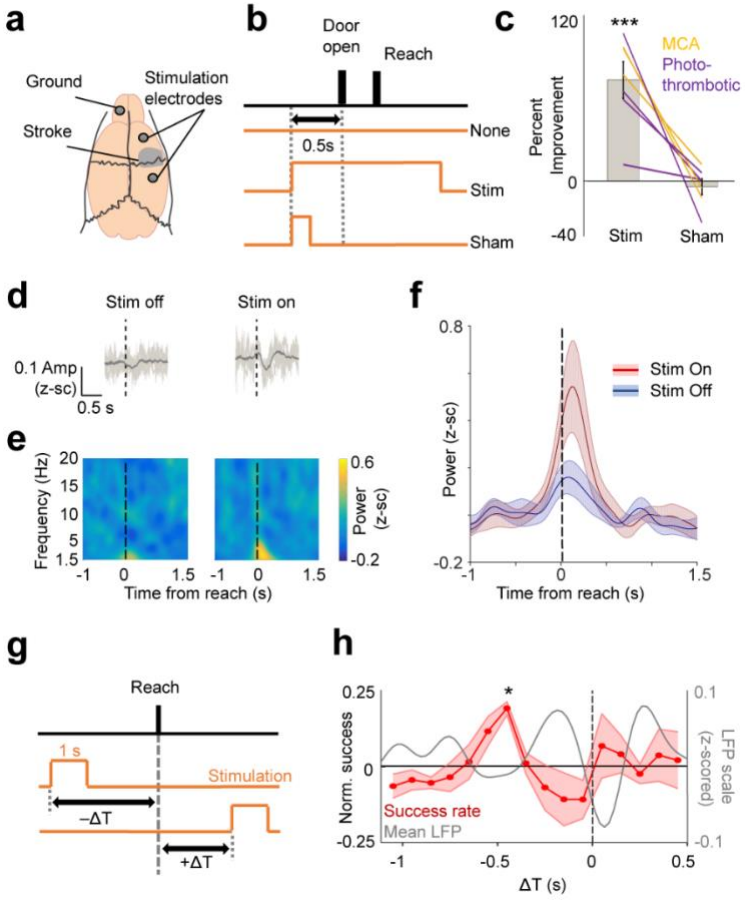

Figure 2.6: Task-dependent DCS improved motor function post-stroke

a. Cranial-screws placement for stimulation in relation to stroke lesion along with the ground screw. b. Pseudo-randomized stimulation design indicating the trial with either DC stimulation, a "sham-stim" control (stimulation turned on for only 200 ms), or no stimulation. c. Effects of DC vs. sham-stim on motor accuracy on the skilled forelimb reach task post-stroke. Bar plots demonstrate mean/SEM % improvement in accuracy, and lines show the effects in each animal (n = 7). We performed one-sample, two-sided t-test performed separately for the Stim ($t(6) = 6.004$, ***p = 9.6e-4) and Sham ($t(6) = -0.77$, p = 0.47) group, followed by a paired two-sample two-sided t-test to compare the effects between groups ($t(6) = 4.91$, p = 0.003)). d. Mean raw LFP trace (bold line, n = 70 trials stim off, n = 66 trials stim on) from one animal comparing DCS on vs. off; light grey lines show 6 example single trial traces. Dotted line indicates reach onset time. Quantification performed in next panel. e-f. Mean LFP power for all sessions (n = 13 stim on, n = 11 stim off sessions) across 4 animals. Bold line in f is the mean and the shaded area is SEM. g. Pseudo-randomized stimulation onset design depicting how a 1s stimulation was triggered in relation to reach onset. □T was negative if the stimulation occurred prior to reach onset, and it was positive if stimulation onset occurred after reach onset. h. Percentage accuracy as a function of □T (n = 4 animals). Shaded area displays SEM. (* indicates significant improvement in accuracy at □T between 500 - 400ms from the reach onset, $t(3) = 9.035$, *p = 0.046, after Bonferroni-Holm correction for 16 different time points). Grey line shows the mean 1.5-4Hz LFP from healthy animals, taken from Fig 2.1.

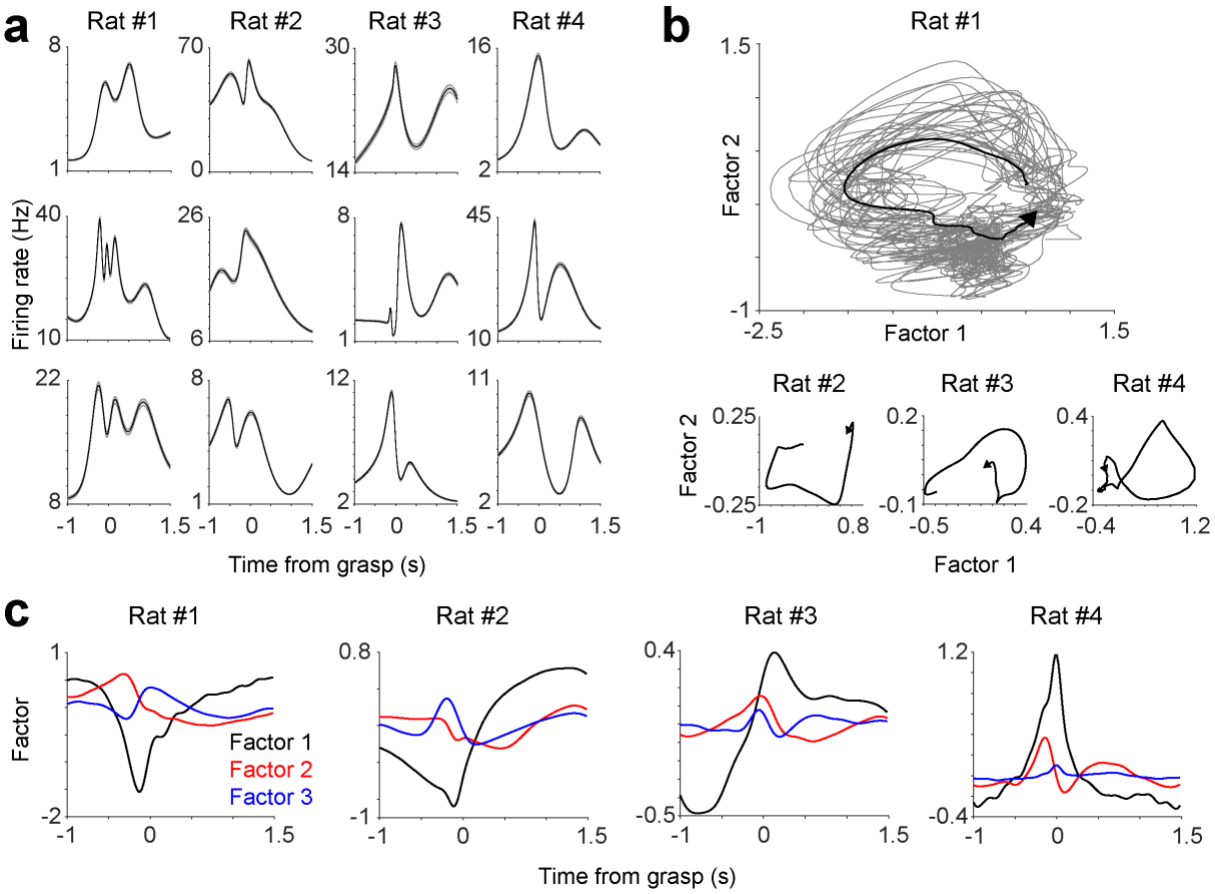

Figure 2.S1: Low frequency quasi-oscillatory dynamics in unit spiking during reaching in healthy rats

a. Examples of smoothed peri-event time histograms of single unit spiking from all 4 rats, showing multiphasic changes in firing rate relative to grasp onset. These are representative examples of unit firing and population dynamics were examined in subsequent panels. **b.** Neural population trajectory during reach, from -1s to +1.5 around grasp, calculated using gaussian process factor analysis[68,69]. Thick black line shows mean across all trials (n = 91, 145, 100 and 73 trials for rats 1-4 respectively), and grey lines in top plot represent 30 example trials. **c.** Top 3 factors from GPFA, in terms of variance accounted for, from all 4 rats showing multi-phasic changes in population neural activity during reaching.

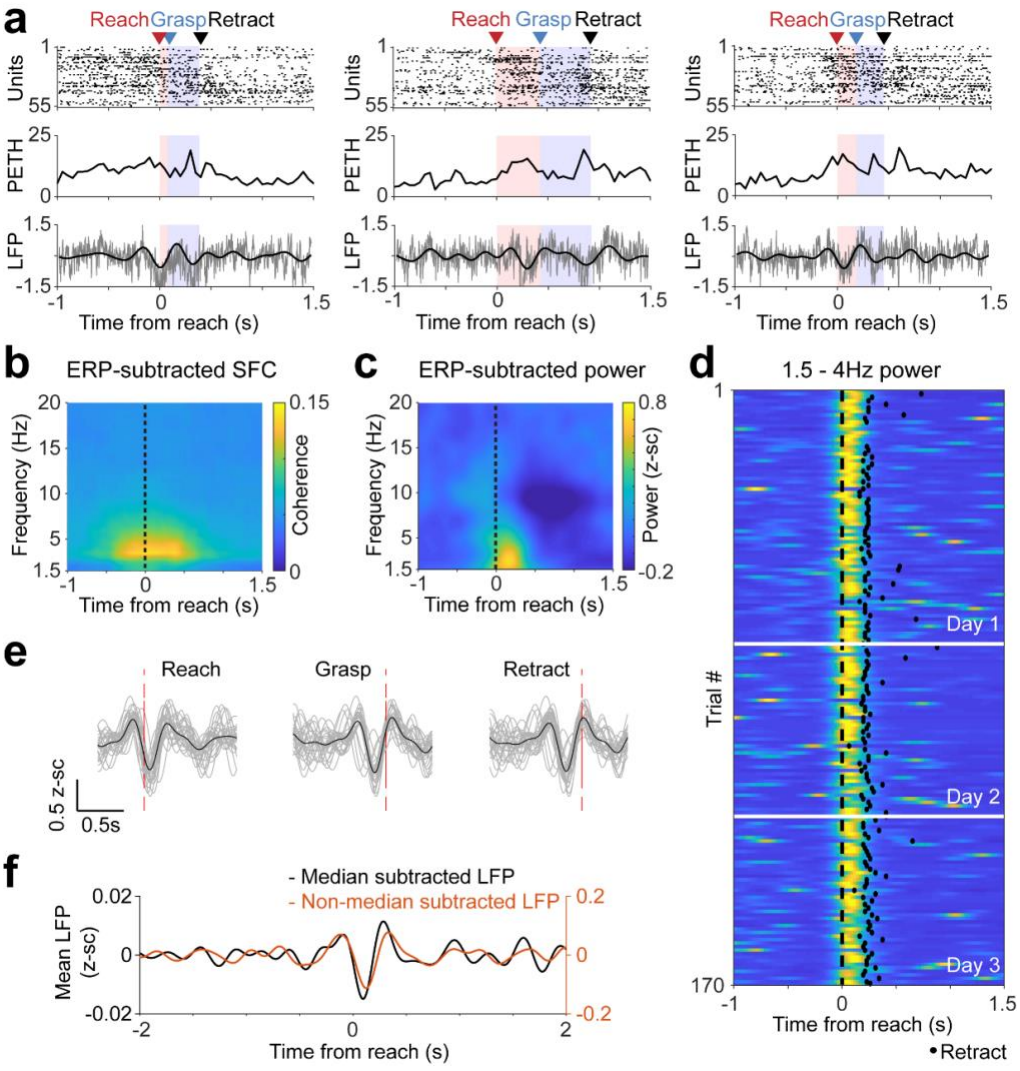

Figure 2.S2: Task-related LFO in healthy rats

a. Example single trials from healthy rodents during reaching, showing quasi-oscillatory activity in both unit spiking and LFP. Top: spike raster of all units in example trial, middle: population peri-event time histogram for all spikes shown on top, bottom: raw LFP in gray and LFP filtered from 1.5 – 4 Hz in black from an example channel. These trials are representative examples of trials that show high SFC and power, as quantified in Fig 2.1. **b-c.** Mean spike-field coherence (n = 171 units) and LFP (n = 118 channels) spectrograms from all 4 animals after the mean evoked potential (ERP) was subtracted. **d.** 1.5-4Hz LFP power of single trials over 3 recording sessions (1 session per day) from an example channel. Similar patterns of power increases can be observed across trials/days. **e.** Example data from one animal demonstrating single-trial LFP signals from 20 trials, filtered from 1.5-4Hz. There was striking phase-locking to behavioral markers. **f.** Comparison of the median-referenced and unreferenced LFP signal (mean activity across all 118 channels from 4 healthy animals). Other than the exact amplitude of the signal, there was no observed difference in the temporal features. Data presented in this paper primarily used from median referenced data.

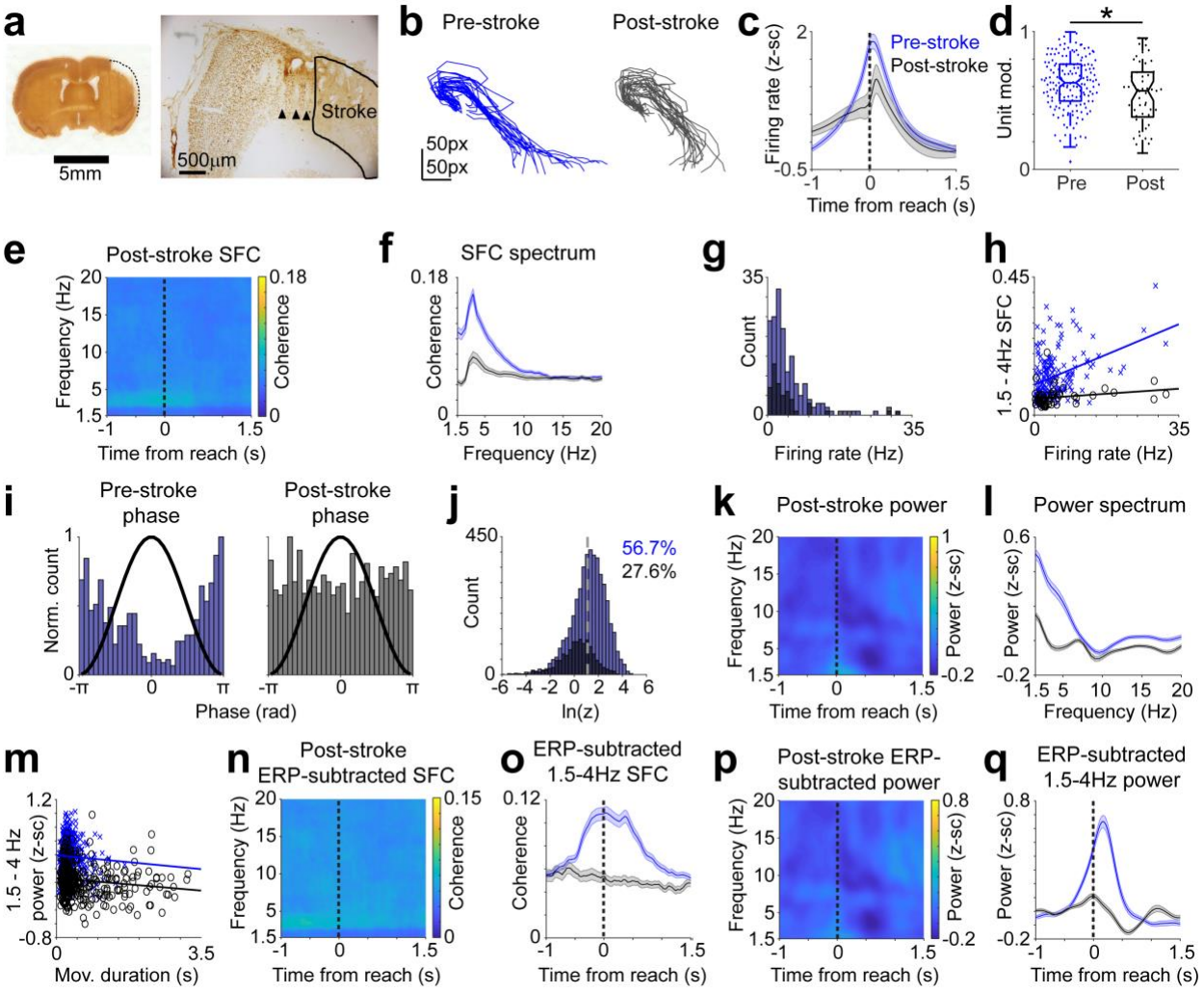

Figure 2.S3: Reduction in LFO after stroke

a. Left: coronal histology section showing lesion caused by MCA stroke. Right: Magnified coronal section showing electrode tracks (black arrows) next to stroke lesion. We performed a similar histological analysis in 4 animals to verify that there was a lesion from stroke. **b.** Example paw trajectories during reach in the same animal before and after MCA stroke (25 trials each). Color code is maintained for the rest of the figure. Axis refers to both plots. px=pixel. **c.** Mean z-scored firing rate of all units pre- (n = 171) and post- (n = 53) stroke from 4 rats. Shaded area represents SEM. **d.** Unit modulation decreased after stroke (mixed-effects model $t(221) = 2.51$, $*p = 0.0128$). Each dot represents modulation of one unit. Center line in boxplot is median and the tops and bottoms are the 25th and 75th percentiles. Whiskers indicate range excluding outliers (>1.5 times interquartile range). **e.** Mean SFC spectrogram after stroke (n = 53 units from 4 rats). **f.** Mean SFC spectrum –0.25 to 0.75s around reach (n = 171 pre and 53 post stroke, from 4 rats). Shaded area shows SEM. **g.** Firing rate histograms of units before (n = 171) and after (n = 53) stroke. There was no significant difference in mean firing rate (across both baseline and task periods) of units pre- and post-stroke (2-sided rank-sum test, $z = 0.48$, $p = 0.63$). **h.** Scatter of 1.5-4Hz task-related SFC (-0.25 to 0.75s around reach) versus mean firing rate of each unit. Least squares lines were fitted for units pre- (n = 171) and post- (n = 53) stroke. There is a reduction in low frequency SFC even when comparing units with

similar firing rates before and after stroke. **i.** Histograms of spike phases (-0.25 to 0.75 around reach) relative to 1.5-4Hz LFP for example units pre- and post-stroke. **j.** Histogram of natural log of Rayleigh's z (from Rayleigh's test of circular uniformity) in all spike-LFP pairs pre (n = 4700) and post stroke (n = 1263). Values greater than grey dotted line (ln(z)>1.09) have p-values <0.05. Numbers indicate the percentage of spike-LFP pairs with significantly non-uniform phase histograms. **k.** Mean post-stroke power spectrogram (n = 117 channels from 4 rats). **l.** Mean power spectrum –0.25 to 0.75s around reach (n = 117 channels from 4 rats). Shaded area is SEM. **m.** Scatter of 1.5-4Hz task-related power versus movement duration (from reach onset to retract) for each trial from all 4 animals before (n = 389 trials) and after (n = 355) stroke, fitted with least squares lines. Power and duration were not correlated (Pearson's correlation r = -0.0765, p = 0.132 pre-stroke and r = -0.0888, p = 0.0947 post-stroke) and there was a reduction in low frequency power post-stroke regardless of movement duration. **n-o.** Mean SFC after mean evoked potential (ERP) was subtracted (53 units from 4 rats). **o.** Mean 1.5-4Hz SFC before (n = 171) and after (n = 53) ERP was subtracted. Shaded area is SEM. **p.** Mean LFP power spectrogram after ERP subtraction (n = 117 channels). **q.** Mean 1.5-4Hz LFP power before and after stroke (n = 101 paired channels from 4 rats). Shaded area is SEM.

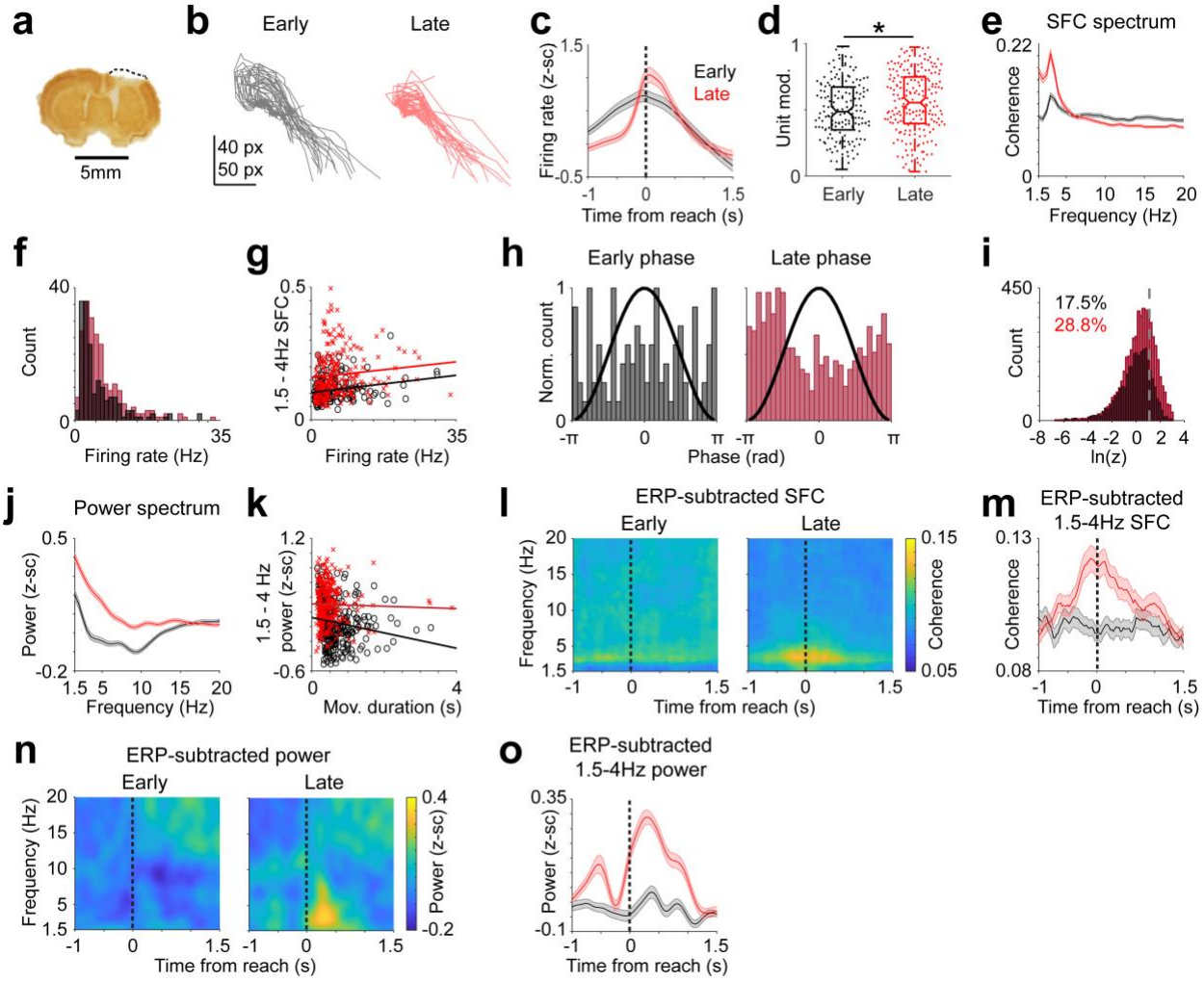

Figure 2.S4: Restoration of LFO in perilesional cortex with rehabilitation

a. Coronal histology section showing lesion caused by photothrombotic stroke. We performed a similar histological analysis in 6 animals to verify that there was a lesion from stroke. **b.** Example early (first 25 trials in first session) and late (last 25 in last session) paw trajectories in the same animal. px=pixel. Color code is maintained for the rest of the figure **c.** Mean z-scored firing of all units in all 6 animals in early (first, n = 170) and late (last, n = 219) sessions. Shaded area is SEM. **d.** Units became more task-modulated from early (n = 170) to late (n = 219) rehabilitation sessions (mixed-effects model t(387) = 3.30, *p = 0.00104). Each dot represents one unit. Center line in boxplot is median and the tops and bottoms are the 25th and 75th percentiles. Whiskers indicate range excluding outliers (>1.5 times interquartile range). **e.** Mean SFC spectrum across all units in early (n = 170) and late (n = 219) sessions from –0.25 to 0.75 around reach. **f.** Histogram of mean firing rate (across both baseline and task periods) of all units in early (n = 170) and late (n = 219) sessions. There was a significant increase in firing rate of units from early to late (2-sided rank-sum test, z=3.96, p=7.61e-5). **g.** Scatter of 1.5-4Hz SFC versus firing rate for each unit (n = 170 early and n = 219 late), with fitted least squares lines. Units show higher low-frequency SFC in late compared to early sessions, even when comparing units with similar firing rates. **h.** Histograms of spike phases (-0.25 to 0.75 around reach) relative to 1.5-4Hz LFP for 2 example units in early and late rehabilitation sessions.

i. Histogram of natural log of Rayleigh's z (from Rayleigh's test of circular uniformity) in all spike-LFP pairs in early (n = 3649 pairs) and late sessions (n = 5675). Values greater than grey dotted line (ln(z)>1.09) have p-values <0.05. Numbers indicate the percentage of spike-LFP pairs with significantly non-uniform phase histograms. **j.** Mean power spectrum across all channels (n = 176 channels from 6 rats) in early (first 50) and late (last 50) trials, from –0.25 to 0.75s around reach. Shaded area is SEM **k.** Scatter of 1.5-4Hz task-related power versus movement duration for each trial (n = 300 trials for both early and late, from 6 rats), with fitted least squares lines. Low frequency power increased from early to late trials, even when comparing trials with similar movement duration. **l-m.** Mean ERP-subtracted SFC spectrograms early (n = 170) and late (n = 219). Shaded area is in m SEM. **n-o.** Mean ERP-subtracted LFP power spectrograms (n = 176 channels from 6 rats). Shaded area is in o SEM.

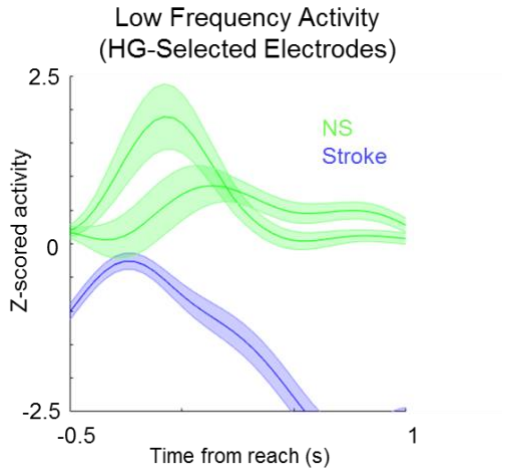

Figure 2.S5: Functional selection of electrodes

We used a blind/automated approach of selecting electrodes based on significant increases in high-gamma (70 – 150 Hz) activity. For each channel, we quantified the 95% CI in the high-gamma band (70 – 150 Hz). If the mean activity between -300 ms before and 100 ms after reach was greater than the 95% CI, we included that channel in our analysis. Using this method, the low-frequency activity in the stroke subject was significant lower than the healthy subjects activity during the time-points of interest (-300 to + 300 msec after reach). NS1 (n = 8 electrodes), NS2 (n = 7 electrodes), SS1 (n = 103 electrodes). Using this approach, we still found a significant increase in LFO in NS1/NS2($t(7) = 4.57$, $p = 0.003$ for NS1; $t(6) = 2.46$, $p = 0.049$ for NS2) and significant a reduction in LFO in SS ($t(102) = -4.18$, $p = 6.1e\text{-}5$). As before, we assessed the overall effect of stroke by performing an ANOVA across all channels from stroke vs. healthy subjects, with subject included as a fixed effect in the model; the overall model was significant ($F(2,115) = 8.08$, $p = 0.001$; with a highly significant effect of stroke ($F(1,115) = 15$, $p = 1.82e\text{-}4$). All subjects showed the expected significant increase in high-gamma activity ($t(7) = 4.21$, $p = 0.004$ for NS1; $t(6) = 5.82$, $p = 0.001$ for NS2; and $t(102) = 21.3$, $p = 2.14e\text{-}39$) for the stroke subject, demonstrating our technique for electrode selection was effective at selecting channels with high-gamma activity, which is widely thought to reflect local spiking activity.

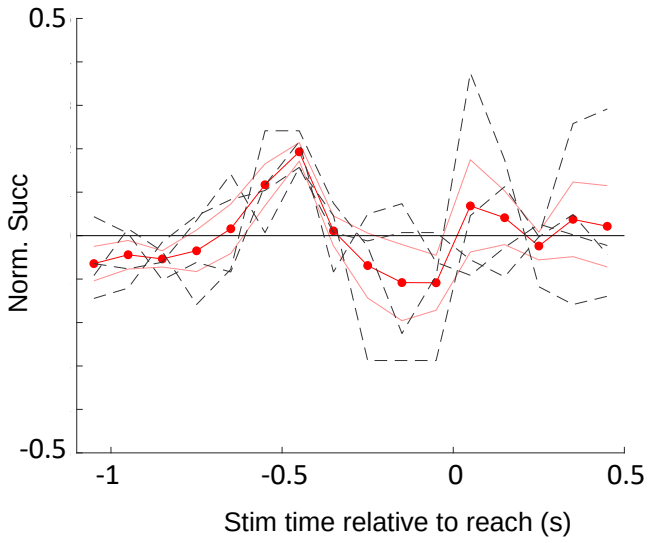

Figure 2.S6: Single animal data of brief-stimulation paradigm

Dark red line represents mean, variance shown with red shading, each of the gray dotted lines are the individual 4 animal traces. Across animals, there was a consistent increase in performance when stimulation occurs between -0.5 and -0.4s relative to reach onset.

References

1. Churchland, M. M., Cunningham, J. P., Kaufman, M. T., Ryu, S. I. & Shenoy, K. V. Cortical Preparatory Activity: Representation of Movement or First Cog in a Dynamical Machine? *Neuron* **68,** 387–400 (2010).

2. Churchland, M. M. *et al.* Neural population dynamics during reaching. *Nature* **487,** 51–56 (2012).

3. Hall, T. M., de Carvalho, F. & Jackson, A. A Common Structure Underlies Low-Frequency Cortical Dynamics in Movement, Sleep, and Sedation. *Neuron* **83,** 1185–1199 (2014).

4. Bansal, A. K., Vargas-Irwin, C. E., Truccolo, W. & Donoghue, J. P. Relationships among low-frequency local field potentials, spiking activity, and three-dimensional reach and grasp kinematics in primary motor and ventral premotor cortices. *J. Neurophysiol.* **105,** 1603–1619 (2011).

5. Stefanics, G. *et al.* Phase Entrainment of Human Delta Oscillations Can Mediate the Effects of Expectation on Reaction Speed. *J. Neurosci.* **30,** 13578–13585 (2010).

6. Mollazadeh, M. *et al.* Spatiotemporal Variation of Multiple Neurophysiological Signals in the Primary Motor Cortex during Dexterous Reach-to-Grasp Movements. *J. Neurosci.* **31,** 15531–15543 (2011).

7. Mollazadeh, M. *et al.* Coherency between spike and LFP activity in M1 during hand movements. in *2009 4th International IEEE/EMBS Conference on Neural Engineering* 506–509 (2009). doi:10.1109/NER.2009.5109344

8. Ganguly, K. *et al.* Cortical Representation of Ipsilateral Arm Movements in Monkey and Man. *J. Neurosci.* **29,** 12948–12956 (2009).

9. Rickert, J. *et al.* Encoding of Movement Direction in Different Frequency Ranges of Motor Cortical Local Field Potentials. *J. Neurosci.* **25,** 8815–8824 (2005).

10. Donoghue, J. P., Sanes, J. N., Hatsopoulos, N. G. & Gaál, G. Neural Discharge and Local Field Potential Oscillations in Primate Motor Cortex During Voluntary Movements. *J. Neurophysiol.* **79,** 159–173 (1998).

11. O'Leary, J. G. & Hatsopoulos, N. G. Early Visuomotor Representations Revealed From Evoked Local Field Potentials in Motor and Premotor Cortical Areas. *J. Neurophysiol.* **96,** 1492–1506 (2006).

12. Sasaki, K., Gemba, H. & Hashimoto, S. Premovement slow cortical potentials on self-paced hand movements and thalamocortical and corticocortical responses in the monkey. *Exp. Neurol.* **72,** 41–50 (1981).

13. Hashimoto, S., Gemba, H. & Sasaki, K. Analysis of slow cortical potentials preceding self-paced hand movements in the monkey. *Exp. Neurol.* **65,** 218–229 (1979).

14. Hall, T. M., Nazarpour, K. & Jackson, A. Real-time estimation and biofeedback of single-neuron firing rates using local field potentials. *Nat. Commun.* **5,** 5462 (2014).

15. Flint, R. D., Ethier, C., Oby, E. R., Miller, L. E. & Slutzky, M. W. Local field potentials allow accurate decoding of muscle activity. *J. Neurophysiol.* **108,** 18–24 (2012).

16. Krasoulis, A., Hall, T. M., Vijayakumar, S., Jackson, A. & Nazarpour, K. Generalizability of EMG decoding using local field potentials. in *2014 36th Annual International Conference of the IEEE Engineering in Medicine and Biology Society* 1630–1633 (2014). doi:10.1109/EMBC.2014.6943917

17. Ramanathan, D., Conner, J. M. & Tuszynski, M. H. A form of motor cortical plasticity that correlates with recovery of function after brain injury. *Proc. Natl. Acad. Sci.* **103,** 11370–11375 (2006).

18. Nudo, R. J., Wise, B. M., SiFuentes, F. & Milliken, G. W. Neural Substrates for the Effects of Rehabilitative Training on Motor Recovery After Ischemic Infarct. *Science* **272,** 1791–1794 (1996).

19. Lim, D. H., LeDue, J. M., Mohajerani, M. H. & Murphy, T. H. Optogenetic Mapping after Stroke Reveals Network-Wide Scaling of Functional Connections and Heterogeneous Recovery of the Peri-Infarct. *J. Neurosci.* **34,** 16455–16466 (2014).

20. Brown, C. E., Wong, C. & Murphy, T. H. Rapid Morphologic Plasticity of Peri-Infarct Dendritic Spines After Focal Ischemic. *Stroke* **39,** 1286–1291 (2008).

21. Rockstroh, B. *Slow Cortical Potentials and Behaviour*. (Urban & Schwarzenberg, 1989).

22. Birbaumer, N., Elbert, T., Canavan, A. G. & Rockstroh, B. Slow potentials of the cerebral cortex and behavior. *Physiol. Rev.* **70,** 1–41 (1990).

23. *Preparatory States and Processes*. (Psychology Press, 1984).

24. Honda, M. *et al.* Movement-related cortical potentials and regional cerebral blood flow change in patients with stroke after motor recovery. *J. Neurol. Sci.* **146,** 117–126 (1997).

25. Kitamura, J., Shibasaki, H. & Takeuchi, T. Cortical potentials preceding voluntary elbow movement in recovered hemiparesis. *Electroencephalogr. Clin. Neurophysiol.* **98,** 149–156 (1996).

26. Yilmaz, O., Birbaumer, N. & Ramos-Murguialday, A. Movement related slow cortical potentials in severely paralyzed chronic stroke patients. *Front. Hum. Neurosci.* **8,** (2015).

27. Yilmaz, O., Cho, W., Braun, C., Birbaumer, N. & Ramos-Murguialday, A. Movement related cortical potentials in severe chronic stroke. in *2013 35th Annual International Conference of the IEEE Engineering in Medicine and Biology Society (EMBC)* 2216–2219 (2013). doi:10.1109/EMBC.2013.6609976

28. Allman, C. *et al.* Ipsilesional anodal tDCS enhances the functional benefits of rehabilitation in patients after stroke. *Sci. Transl. Med.* **8,** 330re1-330re1 (2016).

29. Elsner, B., Kugler, J., Pohl, M. & Mehrholz, J. Transcranial direct current stimulation (tDCS) for improving activities of daily living, and physical and cognitive functioning, in people after stroke. in *Cochrane Database of Systematic Reviews* (John Wiley & Sons, Ltd, 2016).

30. Levy, R. M. *et al.* Epidural Electrical Stimulation for Stroke Rehabilitation Results of the Prospective, Multicenter, Randomized, Single-Blinded Everest Trial. *Neurorehabil. Neural Repair* **30,** 107–119 (2016).

31. Nitsche, M. A. & Paulus, W. Sustained excitability elevations induced by transcranial DC motor cortex stimulation in humans. *Neurology* **57,** 1899–1901 (2001).

32. Fritsch, B. *et al.* Direct Current Stimulation Promotes BDNF-Dependent Synaptic Plasticity: Potential Implications for Motor Learning. *Neuron* **66,** 198–204 (2010).

33. Guggenmos, D. J. *et al.* Restoration of function after brain damage using a neural prosthesis. *Proc. Natl. Acad. Sci.* **110,** 21177–21182 (2013).

34. Reato, D., Rahman, A., Bikson, M. & Parra, L. C. Low-Intensity Electrical Stimulation Affects Network Dynamics by Modulating Population Rate and Spike Timing. *J. Neurosci.* **30,** 15067–15079 (2010).

35. Ali, M. M., Sellers, K. K. & Fröhlich, F. Transcranial Alternating Current Stimulation Modulates Large-Scale Cortical Network Activity by Network Resonance. *J. Neurosci.* **33,** 11262–11275 (2013).

36. Rosin, B. *et al.* Closed-Loop Deep Brain Stimulation Is Superior in Ameliorating Parkinsonism. *Neuron* **72,** 370–384 (2011).

37. Berényi, A., Belluscio, M., Mao, D. & Buzsáki, G. Closed-Loop Control of Epilepsy by Transcranial Electrical Stimulation. *Science* **337,** 735–737 (2012).

38. Whishaw, I. Q. & Pellis, S. M. The structure of skilled forelimb reaching in the rat: A proximally driven movement with a single distal rotatory component. *Behav. Brain Res.* **41,** 49–59 (1990).

39. Wong, C. C., Ramanathan, D. S., Gulati, T., Won, S. J. & Ganguly, K. An automated behavioral box to assess forelimb function in rats. *J. Neurosci. Methods* **246,** 30–37 (2015).

40. Kargo, W. J. & Nitz, D. A. Improvements in the Signal-to-Noise Ratio of Motor Cortex Cells Distinguish Early versus Late Phases of Motor Skill Learning. *J. Neurosci.* **24,** 5560–5569 (2004).

41. Ramanathan, D. S., Gulati, T. & Ganguly, K. Sleep-Dependent Reactivation of Ensembles in Motor Cortex Promotes Skill Consolidation. *PLOS Biol* **13,** e1002263 (2015).

42. Flint, R. D., Wright, Z. A., Scheid, M. R. & Slutzky, M. W. Long term, stable brain machine interface performance using local field potentials and multiunit spikes. *J. Neural Eng.* **10,** 056005 (2013).

43. Flint, R. D., Scheid, M. R., Wright, Z. A., Solla, S. A. & Slutzky, M. W. Long-Term Stability of Motor Cortical Activity: Implications for Brain Machine Interfaces and Optimal Feedback Control. *J. Neurosci.* **36,** 3623–3632 (2016).

44. Godlove, J., Gulati, T., Dichter, B., Chang, E. & Ganguly, K. Muscle synergies after stroke are correlated with perilesional high gamma. *Ann. Clin. Transl. Neurol.* **3,** 956–961 (2016).

45. Gharbawie, O. A., Gonzalez, C. L. R., Williams, P. T., Kleim, J. A. & Whishaw, I. Q. Middle cerebral artery (MCA) stroke produces dysfunction in adjacent motor cortex as detected by intracortical microstimulation in rats. *Neuroscience* **130,** 601–610 (2005).

46. Carmichael, S. T. Rodent Models of Focal Stroke: Size, Mechanism, and Purpose. *NeuroRX* **2,** 396–409 (2005).

47. Nishibe, M., Edward T. R. Urban, I., Barbay, S. & Nudo, R. J. Rehabilitative Training Promotes Rapid Motor Recovery but Delayed Motor Map Reorganization in a Rat Cortical Ischemic Infarct Model. *Neurorehabil. Neural Repair* **29,** 472–482 (2015).

48. Gulati, T. *et al.* Robust Neuroprosthetic Control from the Stroke Perilesional Cortex. *J. Neurosci.* **35,** 8653–8661 (2015).

49. Chang, E. F. Towards Large-Scale, Human-Based, Mesoscopic Neurotechnologies. *Neuron* **86,** 68–78 (2015).

50. Bikson, M. *et al.* Effects of uniform extracellular DC electric fields on excitability in rat hippocampal slices in vitro. *J. Physiol.* **557,** 175–190 (2004).

51. Gulati, T., Ramanathan, D. S., Wong, C. C. & Ganguly, K. Reactivation of emergent task-related ensembles during slow-wave sleep after neuroprosthetic learning. *Nat. Neurosci.* **17,** 1107–1113 (2014).

52. Delorme, A. & Makeig, S. EEGLAB: an open source toolbox for analysis of single-trial EEG dynamics including independent component analysis. *J. Neurosci. Methods* **134,** 9–21 (2004).

53. Makeig, S. *et al.* Dynamic Brain Sources of Visual Evoked Responses. *Science* **295,** 690–694 (2002).

54. Corbetta, M. *et al.* Common Behavioral Clusters and Subcortical Anatomy in Stroke. *Neuron* **85,** 927–941 (2015).

55. DeCoteau, W. E. *et al.* Oscillations of Local Field Potentials in the Rat Dorsal Striatum During Spontaneous and Instructed Behaviors. *J. Neurophysiol.* **97,** 3800–3805 (2007).

56. Dossi, R. C., Nuñez, A. & Steriade, M. Electrophysiology of a slow (0.5-4 Hz) intrinsic oscillation of cat thalamocortical neurones in vivo. *J. Physiol.* **447,** 215–234 (1992).

57. Plautz, E. J. *et al.* Effects of Subdural Monopolar Cortical Stimulation Paired With Rehabilitative Training on Behavioral and Neurophysiological Recovery After Cortical Ischemic Stroke in Adult Squirrel Monkeys. *Neurorehabil. Neural Repair* **30,** 159–172 (2016).

58. Lafon, B. *et al.* Low frequency transcranial electrical stimulation does not entrain sleep rhythms measured by human intracranial recordings. *Nat. Commun.* **8,** 1199 (2017).

59. Dimyan, M. A. & Cohen, L. G. Neuroplasticity in the context of motor rehabilitation after stroke. *Nat. Rev. Neurol.* **7,** 76–85 (2011).

60. Longa, E. Z., Weinstein, P. R., Carlson, S. & Cummins, R. Reversible middle cerebral artery occlusion without craniectomy in rats. *Stroke* **20,** 84–91 (1989).

61. Rogers, D. C., Campbell, C. A., Stretton, J. L. & Mackay, K. B. Correlation Between Motor Impairment and Infarct Volume After Permanent and Transient Middle Cerebral Artery Occlusion in the Rat. *Stroke* **28,** 2060–2066 (1997).

62. Friedberg, M. H., Lee, S. M. & Ebner, F. F. Modulation of Receptive Field Properties of Thalamic Somatosensory Neurons by the Depth of Anesthesia. *J. Neurophysiol.* **81,** 2243–2252 (1999).

63. Taplin, A. M. *et al.* Intraoperative mapping of expressive language cortex using passive real-time electrocorticography. *Epilepsy Behav. Case Rep.* **5,** 46–51 (2016).

64. Plautz, E. J. *et al.* Post-infarct cortical plasticity and behavioral recovery using concurrent cortical stimulation and rehabilitative training: A feasibility study in primates. *Neurol. Res.* **25,** 801–810 (2003).

65. Levy, R. *et al.* Cortical stimulation for the rehabilitation of patients with hemiparetic stroke: a multicenter feasibility study of safety and efficacy. *J. Neurosurg.* **108,** 707–714 (2008).

66. Gulati, T., Guo, L., Ramanathan, D. S., Bodepudi, A. & Ganguly, K. Neural reactivations during sleep determine network credit assignment. *Nat. Neurosci.* **20, 3-5** (2017).

67. Wallstrom, G., Liebner, J. & Kass, R. E. An Implementation of Bayesian Adaptive Regression Splines (BARS) in C with S and R Wrappers. *J. Stat. Softw.* **26,** 1–21 (2008).

68. Yu, B. M. *et al.* Gaussian-process factor analysis for low-dimensional single-trial analysis of neural population activity. in *Advances in Neural Information Processing Systems 21* (eds. Koller, D., Schuurmans, D., Bengio, Y. & Bottou, L.) 1881–1888 (Curran Associates, Inc., 2009).

69. Cowley, B. R. *et al.* DataHigh: graphical user interface for visualizing and interacting with high-dimensional neural activity. *J. Neural Eng.* **10,** 066012 (2013).

70. Aarts, E., Verhage, M., Veenvliet, J. V., Dolan, C. V. & Sluis, S. van der. A solution to dependency: using multilevel analysis to accommodate nested data. *Nat. Neurosci.* **17,** 491 (2014).

CHAPTER 3 : COORDINATED INCREASE OF RELIABLE CORTICAL AND STRIATAL ENSEMBLE ACTIVATIONS DURING RECOVERY AFTER STROKE

Abstract

Skilled movements rely on a distributed cortical and subcortical network, but how this network supports motor recovery after stroke is unknown. Previous studies focused on the perilesional cortex (PLC); how and if connected subcortical areas reorganize and coordinate with PLC is unclear. Of particular interest is the dorsolateral striatum (DLS), which is one synapse downstream of PLC and is important for learning and generation of fast reliable actions. Using a rat stroke model, we performed chronic electrophysiological recordings in motor PLC and DLS during long-term recovery of a dexterous skill. Remarkably, we found that recovery was associated with the simultaneous emergence of reliable movement-related single-trial ensemble spiking in both structures along with fine timescale cross-area alignment of spiking. Our study highlights the importance of consistent neural activity patterns across brain structures during recovery and suggests that modulation of cross-area coordination could be a therapeutic target for enhancing motor function post-stroke.

Introduction

Both the learning and execution of new motor skills are increasingly recognized to require contributions from a distributed motor network[1–8]. How movement-related activity in this network is altered by brain injuries such as stroke and how it changes with recovery remain unclear. The overwhelming majority of studies investigating stroke have focused solely on the role of cortical structures, particularly the perilesional cortex (PLC), as primary substrates for recovery of dexterous function[9–13]. This suggests that restoration of cortical activity patterns is sufficient to account for motor recovery. However, subcortical motor areas which receive inputs from the stroke site can experience acute changes in activity, known as diaschisis[14,15], following stroke. It remains unknown if a previously connected area that experiences diaschisis participates, over longer time periods, in the process of recovery.

We specifically monitored neural activity patterns in a connected area, the dorsolateral striatum (DLS), that is a single synapse downstream from the stroke site, i.e. the primary motor cortex (M1), and the motor PLC. Given that stroke survivors are known to demonstrate reduced movement vigor as well as movement fragmentation[16,17] and that the basal ganglia is implicated in regulating both[6,18,19], examining how the DLS contributes to recovery might be particularly revealing. Changes in DLS neural activity during recovery may also better account for the impaired "speed and accuracy" tradeoff frequently seen after stroke[20–22]. Importantly, both DLS and coordinated cortico-striatal interactions are known to be important for the learning and control of skilled (fast, accurate and consistent) movements in intact individuals[3,6,23–25]. Precisely how DLS activations and interactions between DLS and PLC contribute to the recovery of coordinated reaching and grasping function after stroke, if at all, has not been explored.

We thus performed chronic dual site multielectrode electrophysiological recordings in PLC, i.e., premotor cortex (M2) and areas anterior to M1 that are adjacent to the stroke site, and DLS during motor rehabilitation after a primary motor cortex (M1) stroke in rats. Recordings were conducted with high

temporal resolution during movement and throughout recovery. Importantly, given the growing understanding that neural ensemble dynamics at the level of single trials – i.e., not averaged across multiple trials – can better explain complex behaviors[26], we analyzed the local and cross-area ensemble dynamics at both the single trial and trial averaged levels. We found that task-related activity in both PLC and DLS were disrupted after stroke and reorganized together during rehabilitation. Specifically, we observed simultaneous increases in movement modulation of neurons, trial to trial reliability of neural patterns and the ability to decode instantaneous movement speed from PLC and DLS. These increases were significantly correlated with the animals' abilities to perform coordinated reaching and grasping actions during rehabilitation. Strikingly, fine timescale coordination of spiking activity between PLC and DLS was also evident with recovery. Our results thus highlight the importance of reliable cross-area activations during motor recovery after stroke.

Results

Corticostriatal neural activity was monitored during motor recovery after stroke

We trained Long Evans rats (see Table 3.S1 for total numbers of subjects per group) on a reach-to-grasp task that requires coordination of gross proximal movements and fine distal movements (Fig 3.1A) using an automated behavior box[27]. When rats reached plateau performance levels, we induced a photothrombotic stroke over the primary motor cortex forelimb area (Fig 3.1B). After at least 1 week of recovery from surgery, rats were retrained on the same task as part of physical rehabilitation. In a subset of animals with neural implants, simultaneous *in vivo* electrophysiology recording of neural activity from both anterior PLC and DLS was conducted over this period (n=8 animals, *see* Methods, Fig 3.1B-C, Fig 3.S1A-B).

We first assessed whether our anterior PLC recording site (which is a combination of premotor forelimb areas and surrounding areas anterior to M1, Fig 3.S1C) was indeed connected to the DLS recording site (which is strongly coupled to the intact M1, i.e. the stroke site in these animals). We found that the PLC and DLS sites remained physically (Fig 3.1D shows retrograde labelling at the PLC site when a viral vector was injected in the DLS recording site) and functionally connected after stroke (Fig 3.S1D shows short-latency evoked potentials recorded at the DLS site during PLC stimulation). This indicated that there was a physical substrate for connectivity that can support possible changes in coupling between PLC and DLS with recovery.

To monitor recovery, we used three behavioral metrics to characterize motor deficits and improvements over time (Fig 3.1E-F): pellet retrieval success rate, paw average speed and speed consistency (correlation of the instantaneous speed change of individual trials with the pre-stroke median template). All measures decreased significantly after stroke (2-tail paired t-test, $t(6) = 8.0947$, $p = 1.9059e-$

4, $t(6) = 5.6853$, $p = 0.0013$, and $t(6) = 13.8028$, $p = 1.4954e\text{-}4$ respectively). Moreover, all three measures also increased significantly with rehabilitation (linear mixed effects model, $b = 2.3256$, $t(77) = 6.189$, $p = 2.7235e\text{-}8$, $b = 0.17815$, $t(77) = 7.7367$, $p = 3.2635e\text{-}11$, and $b = 0.01751$, $t(77) = 4.1574$, $p = 8.2784e\text{-}5$ respectively). These results show that overall movement, including gross movement components as measured by paw speed and consistency, were impaired after a M1 stroke and improved with rehabilitation. This is consistent with previous studies that showed similar deficits with motor cortex inactivation/lesion[3,12,28,29].

DLS was partially disrupted but still involved in reaching early after stroke

First, we assessed if DLS activity patterns were altered in the early period after stroke. Even though motor behavior was disrupted in this period, it is possible that DLS activity remained unchanged after stroke and continued to support gross movements (animals were still able to make reaching movement and knock off the pellet). We compared DLS neural activity in rats during the first rehabilitation session post-stroke and in a separate group of sham/control animals (n=7), i.e. intact animals implanted with electrodes (Fig 3.2A, Table S1). At the trial average level, we found that the proportion of movement modulated DLS units in the stroke rats was lower than that in the intact rats (Fig 3.2A-C). Fig 3.2A-B show all neurons and their trial-averaged time course of activity, and Fig 3.2C shows the proportion of modulated units per animal (2-tailed 2 sample t-test, $t(11) = 3.2894$, $p = 0.0072$). The distribution of baseline firing rates of units during spontaneous periods (-6 to -3s relative to trial start) were unchanged (2-sample Kolmogorov-Smirnov test, $D = 0.1906$, $p = 0.0671$). Importantly, only trials in which rats managed to touch the pellet were included in analysis. Further, only trials with durations of less than 0.5s and with one reach attempt were included (see Methods) to control for intact and stroke animals exhibiting different behaviors. Hence, the decreased proportion of modulated units was not merely due to differences in reaching behaviors between the two groups.

Since DLS neural activity was affected post-stroke, we next asked if DLS was still required for the observed movements post-stroke. These movements primarily consisted of reaching attempts that could touch the pellet but did not end with a functional grasp. We implanted infusion cannulas in a separate cohort of stroke rats (n=4) and inactivated DLS using the GABA agonist muscimol (Fig 3.S2A-B) during rehabilitation once rats were able to reach independently. Compared to saline infusions, we found that muscimol inactivation of DLS post-stroke resulted in more variable paw trajectories (Fig 3.S2C, D, linear mixed effects model, b = 0.5113, $t(11)$ = 3.3011, p = 0.0071) and shorter reaches (Fig 3.S2C, E, linear mixed effects model, b = -0.2047, $t(11)$ = -2.7764, p = 0.0180), consistent with previous experiments in healthy animals[3].

In the intact brain, DLS is thought to modulate movement vigor and/or speed[20,30,31]. Given that DLS was still necessary for some aspects of movement in stroke animals, we wondered if the remaining DLS neural activity still represented hand speed. We used regularized multiple linear regression to predict instantaneous arm endpoint speed from DLS neural activity or shuffled activity (Fig 3.2D, see Methods). Binned spiking activity at 10 different time lags relative to paw speed were used as inputs in the decoder. In the fitted regression, different DLS units tended to have high weights at different time lags (Fig 3.2E), likely related to the general sequential activation of neurons. Interestingly, across animals, DLS neural activity even in the first rehabilitation session post-stroke predicted arm speed significantly better than chance (Fig 3.2F, 2-tailed paired t-test, $t(6)$ = 3.1229, p = 0.0205).

Overall, we showed that DLS was partially disrupted after a M1 stroke. Despite this, ensemble activity in the DLS still represented movement speed during reaching and was necessary for consistent and high amplitude movements.

DLS neural dynamics reorganized during rehabilitation

Next, we examined how DLS neural activity patterns changed and whether they tracked improvements in motor function over the course of rehabilitation. We computed the peri-event time histogram (PETH) for all units to examine changes at the trial average level and observed an increase in the proportion of movement modulated units (Fig 3.3A). We also investigated the consistency of single trial population activity. In early rehabilitation sessions, trial to trial neural firing was inconsistent among kinematically matched trials (Fig 3.3B). However, in later rehabilitation sessions, trials with similar kinematics were consistently associated with a stereotyped sequence of unit activations that also matched the trial averaged PETH. To quantify this, we computed the correlations between single trial neural activity and the trial averaged template across all units in a rehabilitation session. Across the sessions from all rats, we observed a significant increase in the single trial to template correlation (Fig 3.3C, linear mixed effects model, b = 0.0117, $t(72)$ = 5.0044, p = 3.8323e-6), indicating that trial to trial variability in DLS neural activity reduced with recovery. Additionally, template correlation was a significant predictor of task success rate (Fig 3.3D, linear mixed effects model, b = 72.074, $t(72)$ = 4.0165, p = 0.00014). As our past work in the PLC[12] suggested a link between single-trial neural firing and low frequency (1.5-4Hz) local field potential (LFP) power during movement, we performed the same quantification in DLS. We found that 1.5-4Hz DLS LFP power, -0.75s to 0.25s around pellet touch, increased over rehabilitation (linear mixed effects model, b = 0.0141, $t(75)$ = 5.6624, p = 2.605e-7), similar to what we observed previously in PLC during stroke rehabilitation[12] and in DLS during motor learning in intact animals[3].

To directly link the neural changes to behavior, we calculated the arm endpoint speed decoding ability of DLS neural activity throughout rehabilitation, using the same method as in Fig 3.2. As the DLS firing patterns were more consistent for kinematically similar trials after rehabilitation (Fig 3.3C), we expected that decoding accuracy would increase as well. This was indeed the case (Fig 3.3E-F, linear mixed effects mode, b = 0.008491, $t(72)$ = 2.8222, p = 6.1615e-3). Although DLS neural activity already

represented speed better than chance from the first rehabilitation session (Fig 3.2F), the relationship between DLS neural activity and endpoint speed strengthened even more with rehabilitation and motor recovery. The improved decoding ability also supports the notion that the neural changes in DLS were not just due to behavioral differences across rehabilitation. Specifically, decoding was done on a moment by moment basis for concatenated single trials and hence not influenced by average behavioral differences across sessions. Together, this indicated that DLS activity became more closely tied to arm kinematics during the recovery process.

Changes in PLC activity paralleled changes in DLS

Given the importance of PLC in motor recovery[9,32] and our results demonstrating that DLS reorganized with changes in motor behavior, we wondered about the comparative change in PLC. We recorded neural activity from the "future PLC" (i.e. premotor and surround regions anterior of M1) and the PLC in the same two groups of animals as in Fig 3.2 (Fig 3.4A). Similar to our observations in the DLS, the proportion of movement modulated units in the PLC was lower in stroke compared to intact animals and increased over rehabilitation (Fig 3.4B). The single trial to template correlation in PLC also increased (Fig 3.4C-D, linear mixed effects model, b = 0.0143, $t(47)$ = 6.0579, p = 2.1999e-7), and was positively correlated with success rate (Fig 3.4E, linear mixed effects model, b = 113.25, $t(47)$ = 4.9776, p = 9.0736e-6). PLC neural activity predicted paw speed better over rehabilitation as well (Fig 3.4F-G, linear mixed effects model, b = 0.007355, $t(47)$ = 2.6117, p = 0.0121). Hence, neural activity in both PLC and DLS were affected early after stroke and reorganized post-stroke, becoming more movement modulated and less variable.

Neural changes in PLC and DLS occurred simultaneously across rehabilitation sessions

Although we observed similar patterns of reorganization in PLC and DLS, they may or may not occur simultaneously. For example, as PLC is thought to be the primary site of plasticity for stroke recovery,

it is possible that reorganization in PLC recruits and drives subsequent changes in downstream areas such as the DLS. If so, we would expect to see reorganization in PLC earlier than that in DLS. We thus directly compared the timescale of neural changes in PLC and DLS by correlating the neural measures (proportion of modulated units, template correlation and speed decoding ability) on a session by session basis at different session lags. Interestingly, we found that the correlation for all neural measures were the highest at zero-session lag (Fig 3.5A-C), indicating that PLC and DLS were changing simultaneously instead of one leading or lagging the other. Fig 3.5D shows the significant positive correlation for template correlation at zero session lag. Altogether, the results support the idea that PLC and DLS are interdependent throughout rehabilitation and affecting each other's activity through the cortico-basal ganglia loop.

Fine-timescale coordination between PLC and DLS increased after rehabilitation

In the previous sections, our evidence for the close relationship between PLC and DLS was based on session by session changes in neural measures local to each area. This does not necessarily indicate that the neural activity patterns in the two structures are coordinated across single trials. Past studies in intact brains have shown that single trial coordination across cortex and striatum increases during motor learning[3], but it is unknown if this fine-timescale coordination also increases during rehabilitation post-stroke. We first tested LFP coherence between PLC and DLS, as previous studies in intact animals have found increases in M1-DLS theta coherence with learning[3,33]. Interestingly, we found that there were instead significant decreases in broadband low frequency PLC-DLS LFP coherence over time and with recovery (Fig 3.S3). This might mean that the two structures are less rhythmically coupled, i.e. because coherence relies on spectral analysis. However, recent studies have indicated that fine-time scale coordination may be evident at the level of spiking[34,35]. Importantly, such methods used statistical methods to measure "communication subspaces" based on ensemble patterns and do not rely on aggregate measures such as the LFP.

Here we used canonical correlation analysis (CCA) to assess fine-timescale coordination between PLC and DLS during movement (Fig 3.6A). CCA has been used in various neuroscience studies to extract correlated population activity between two areas[34–37]. Specifically, CCA finds a linear combination of units in PLC and DLS that project to PLC and DLS subspaces respectively, and where activity in these subspaces is maximally correlated (Fig 3.6B). We used CCA because it allowed us to extract a time series of correlated population activity across two structures, used to analyze coordination at a fine timescale (we used concatenated single trial spiking activity binned at 100ms). The top component produced by CCA is the axis of the PLC and DLS subspaces that has the maximum correlation between the two areas. We found that this maximum correlation increased with rehabilitation (Fig 3.6C shows example sessions from a single animal, 6D shows all sessions from all animal across rehabilitation, linear mixed effects model, $b = 0.01363$, $t(44) = 4.1562$, $p = 1.4694e\text{-}4$), showing that activity in the two structures became more precisely temporally correlated with recovery. Interestingly, top component activity increased during movement (Fig 3.6E) and became more movement-specific on a trial by trial basis after rehabilitation (Fig 3.6F). This indicated that correlated activity across PLC and DLS was increasingly movement related. The maximum canonical correlation was also a significant predictor of success rate across sessions (linear mixed effects model, $b = 89.977$, $t(44) = 4.1712$, $p = 1.4017e\text{-}4$). Together, these results highlighted the emergence of fine timescale coordinated activity between PLC and DLS with rehabilitation of reaching and grasping actions during stroke recovery, in addition to simultaneous changes in neural measures that were local to each area.

Discussion

Our main goal was to determine how a subcortical motor site, the DLS, was affected by a M1 stroke and how potential changes in DLS related to known reorganization of neural activity patterns in the PLC. We found that DLS was partially disrupted by the stroke in the early recovery period, but it still played a role in the smoothness and amplitude of reaching movements and its activity contained information that could be decoded to predict movement speed trajectories. With rehabilitation, DLS neural activity became more movement modulated, demonstrated greater trial to trial consistency and better represented single trial movement speed. Similar changes were evident in the PLC. Our analysis also revealed that these changes in both structures took place simultaneously. Notably, we also found that precise temporal coordination of neural activity patterns between PLC and DLS increased over rehabilitation and could account for recovery. Together, these results demonstrate that recovery of fast, accurate and consistent dexterous actions was closely tied to the emergence of reliable (from trial to trial and with respect to behavior) and precisely aligned neural activity patterns across PLC and DLS.

Effect of cortical stroke on downstream subcortical areas

The general concept of a connected downstream region being disrupted by stroke was described over a century ago and termed diaschisis. While other studies have found, mostly through anatomical tracing, evidence for disruption of connected areas after a focal stroke[38–41], it remained unclear how such a disrupted site experiencing diaschisis changed with and contributed to recovery. We specifically monitored a site in the DLS that was a single synapse downstream of M1 and PLC. We found that DLS task related activity patterns were altered early after stroke. Specifically, the proportion of movement modulated units was reduced. As DLS receives most of its inputs from the cortex, this could be due to the loss of motor cortical inputs and hence insufficient input strength to drive neuronal firing during movement. The finding that cortical stroke affected DLS activity suggests that the behavioral deficits observed could be attributed

partially to the indirect effects of stroke on DLS and highlights the importance of studying other connected areas[4,41].

Although DLS activity was affected by stroke, it still represented movement speed better than chance. This remaining movement related activity in DLS was likely driven by persisting cortical and thalamic inputs or internal dynamics within DLS[24,42]. Temporary DLS inactivation further disrupted movements, supporting a causal role in movement control post-stroke. With rehabilitation and recovery, DLS activity became more consistent from trial to trial and better predicted movement kinematics. This could be due to a strengthening of connections between the PLC, other connected motor areas and the DLS, or modification within DLS itself, leading to more reliable firing of DLS neurons. These findings, together with the observation that activity in both DLS and PLC reorganized in a near synchronous manner, suggest that understanding how PLC recruits previously connected areas is important to gain a complete view of the recovery process.

Coordination between PLC and DLS

Our results revealed that behavioral recovery was associated with more consistent sequential activation of neurons in both structures. Furthermore, our CCA analysis, designed to define axes of maximal correlation between cortical and striatal ensembles, revealed increased fine timescale alignment of activity between PLC and DLS. What mechanisms might drive the observed changes in cross area coordination? One possibility is that there are changes in cortico-striatal synaptic strength over the recovery process[6]. There is a large body of literature using largely *in vitro* preparations that indicate that long-term potentiation (LTP) can be induced at this connection in an activity dependent manner[43]. Alternatively, structural changes (e.g. axon sprouting) could change the strength of corticostriatal connections[38,39]. Future studies could use a combination of viral tracing and imaging techniques to directly monitor structural or synaptic changes in corticostriatal inputs. Moreover, it is also possible that a third area is driving changes in both structures or

that rehabilitation training modifies the entire motor network simultaneously. To distinguish between these possibilities, future studies could record from more sites in the brain, such as the contralateral motor cortex, motor thalamus, and cerebellum.

Role of DLS in dexterous motor control post-stroke

A wealth of studies has implicated M1 in the control of gross and fine motor control[44–46]. Especially for fine motor control, descending cortical inputs to brainstem and spinal regions appear to be important both for learning and skilled execution[47,48]. In contrast, for isolated gross movements, previous work has indicated that while motor cortical areas are required for learning, well-trained gross movements can rapidly recover after M1 injury (and without further training) and is dependent on DLS [24,25,49]. In our case, consistent with past literature[3,12], coordinated gross and fine control was impaired after cortical stroke and slowly recovered with rehabilitation training. The main uncertainty was whether recovery was exclusively a cortical phenomenon or recruited the distributed motor network. As outlined above, our results clearly demonstrate the involvement of DLS in the recovery process.

Notably, past studies have shown that coordination between M1 and DLS is important for learning and skilled execution. Specifically, our previous study in intact animals learning a reach-to-grasp task showed that M1 and DLS became increasingly coordinated with the achievement of skilled motor control[3]. We also found that gross and fine movement control was linked to different M1 and DLS activity patterns. While gross movements were linked to coordinated "quasi-oscillatory" activity between areas, grasping was shown to be more cortically dependent. Consistent with this, DLS activity was also closely linked to more reliable timing between reaching and grasping. With DLS inactivation or lesion, proximal movements were altered but the grasping action was not, i.e. animals were able retrieve the pellet when the task was made easier by reducing the transport distance. Together, this suggests that DLS has a role in regulating the timing and the reliability of an action that is composed of multiple sub-movements[3,6,18,19]. In this study,

animals slowly improved both gross and fine control, as shown by increases in accuracy, speed and consistency during rehabilitation. Throughout this process, we observed that PLC and DLS reorganized in a temporally coordinated manner. Moreover, activity in each area was linked to instantaneous reaching speed as well as task accuracy. This suggests that recovery of skilled movements that are fast and accurate may rely on reestablishment of PLC-DLS coordination. Interestingly, this might also suggest that the known deficits in stroke survivors of reduced movement speed and inconsistent transitions between movements, often referred to as fragmentation[16], may be attributable to incomplete recruitment of the striatum after stroke.

Implications for stroke rehabilitation and therapies

Overall, our results suggest that the processes driving coordination of PLC and DLS can be a novel target for therapies to improve recovery. Consistent with stroke studies in human subjects as well as in animals, our animals displayed variable degrees of recovery and this could be accounted for by the extent of coordinated activity between cortex and striatum. Poor recovery in some animals may be related to weaker neurophysiological coupling between PLC and DLS after stroke, in comparison to the intact M1 and striatum. Thus, increasing coupling between PLC and DLS, with novel therapies to either improve structural or functional connectivity, might further improve speed, consistency and accuracy. A particularly promising option is electrical stimulation[12] to increase the synchrony between PLC and DLS. Subcortical areas like DLS are also attractive targets for neuromodulation as they are more compact, hence easier to target compared to the cortex, and have widespread connections throughout the brain[50]. Our work provides the starting point for future studies to further delineate the role of DLS and other connected subcortical structures in motor function after cortical stroke, and for the development of therapies targeting subcortical areas.

Interestingly, there is also a long history of testing dopamine agonists in clinical stroke populations; both preclinical and clinical studies have shown promising results[51]. However, the precise mechanism remains unclear. Our results suggest possible mechanisms for this treatment approach. For example, it is known that dopamine activation during training can aid action selection and ultimately result in consolidated skilled actions[19,43]. Our finding showing that cortico-striatal interactions are important for recovery suggest a more direct link. Future studies can determine how dopamine dynamics directly interact with recovery; they can also suggest approaches to optimize dopamine agonist treatment. For example, such studies can reveal whether treatments should be given only during rehabilitation training or in a continuous manner such that it also interacts with offline processing.

Summary

We found that recovery of fast and accurate movement control was associated with reliable neural activation in both PLC and DLS and increased fine timescale alignment of activity between PLC and DLS. Together, our results highlight the importance of examining distributed network changes after stroke and suggests that modulation of coordination can be a novel therapeutic target.

Materials and Methods

Animal care and surgery

All procedures were in accordance with protocols approved by the Institutional Animal Care and Use Committee at the San Francisco Veterans Affairs Medical Center. Adult male Long Evans rats (n = 23, 250–400 g; Charles River Laboratories; see Table S1 for the number of rats used in each experiment) were housed in a 12-h/12-h light–dark cycle. All experiments were done during the light cycle. All surgical procedures were performed using sterile techniques under 2–4% isoflurane. Surgery involved cleaning and exposure of the skull and preparation of the skull surface using cyanoacrylate and then implantation of the skull screws for referencing and overall head-stage stability. The postoperative recovery regimen included the administration of 0.02 mg per kg body weight buprenorphine for 2 days, and 0.2 mg per kg body weight meloxicam, 0.5 mg per kg body weight dexamethasone and 15 mg per kg body weight trimethoprim sulfadiazine for 5 days. All animals were allowed to recover for 1 week prior to further behavioral training.

Surgery for electrophysiology recordings

Reference and ground screws were implanted posterior to lambda, ipsilateral and contralateral, respectively, to the neural recordings. Craniotomy and durectomy were performed, followed by stroke induction (if any) and then implantation of the neural probes. We used either 32- or 64-channel arrays (33/35-μm polyamide-coated tungsten microwire arrays, Tucker-Davis Technologies and Innovative Neurophysiology). Arrays targeting the perilesional cortex were centered at 4mm anterior and 2 mm lateral to the bregma and lowered to a depth of 1.5mm from the brain surface, and arrays targeting the dorsolateral striatum were centered at 0.5mm anterior and 4mm lateral to bregma and lowered to a depth of 4mm from the brain surface. The final locations of electrodes were confirmed by electrolytic lesions.

Photothrombotic stroke

After craniotomy, rose bengal dye was injected into the femoral vein using an intravenous catheter. Next, the surface of the brain was illuminated with white light (KL-1500 LCD, Schott) using a fiber optic cable for 20 min. We used a 4-mm aperture for stroke induction, centered at 3mm lateral and 0.5mm anterior to bregma, and covered the remaining cortical area with a custom aluminum foil mask to prevent light penetration. If no neural probes were needed, the craniotomy was covered with a layer of silicone (Kwik-Sil) and the incision was closed with sutures.

Surgery for infusions

After craniotomy and stroke induction, cannulas (PlasticsOne) were implanted to target the DLS (same coordinates as electrode arrays). The location and spread of muscimol was determined by infusing a fluorescent muscimol (Invitrogen BODIPY TMR-X Conjugate) right before perfusion and histology.

Viral injection

750-1500nl of retrogradeAAV-hSyn-JAWs-KGC-GFP-ER2 (Addgene) was injected in the DLS (same coordinates as before) of 3 stroke rats, using a Hamilton syringe and needle. Injection was performed one week after stroke induction. Rats used for viral injection were not trained on the reach-to-grasp task. 4 weeks after viral injection, rats were anesthetized and perfused as described in the immunohistochemistry section.

Electrolytic lesion

Rats were anesthetized with 2% isoflurane and electrical current (-300μA for 10s) was passed through every channel, 2 at a time, of the implanted electrode arrays using the TDT IZ2 system. Rats were perfused right after the electrolytic lesions were completed.

Immunohistochemistry

After all experiments, rats were anesthetized and transcardially perfused with 0.9% sodium chloride, followed by 4% formaldehyde. The harvested brains were post-fixed for 24 h and immersed in 20% sucrose for 2 days. NeuN staining was used for stroke and electrode localization. Coronal cryostat sections (40-μ m thickness) were incubated with blocking buffer (10% Donkey serum and 0.1% Triton X-100 in 0.1 M phosphate buffer) for 1 hour and then incubated overnight with mouse anti-NeuN (1:1,000; Millipore). After washing, the sections were incubated with biotinylated anti-mouse IgG secondary antibody (1:300; Vector Lab) for 2 hours. Sections were incubated with avidin–biotin peroxidase complex reagents using a Vector ABC kit (Vector Labs). The horseradish peroxidase reaction was detected with diaminobenzidine and H_2O_2. The sections were washed in phosphate buffer and then mounted with permount solution (Fisher Scientific) on superfrosted coated slides (Fisher Scientific). For fluorescent imaging (viral tracing and muscimol localization), 40um sections were mounted directly with mounting media containing DAPI (VectorShield). Images of whole sections with NeuN staining were taken by a HP scanner, and fluorescent images were taken by a Zeiss microscope.

In vivo electrophysiology

Units and LFP activity were recorded using a 128-channel TDT-RZ2 system (Tucker-Davis Technologies). Spike data were sampled at 24,414 Hz and LFP data at 1,017.3 Hz. ZIF clip-based analog head stages with a unity gain and high impedance (~ 1 GΩ) were used. The threshold for spiking activity was set online using a standard deviation of 4.5 (calculated over a 1-min period using the TDT-RZ2 system), and waveforms and timestamps were stored for any event that crossed that threshold. Sorting was performed using Plexon OfflineSorter v4.3.0, using a principal component analysis (PCA)-based method followed by manual inspection and sorting. We included both clearly identified single-units and multi-unit activity for this analysis (results were pooled as there were not clear differences in single-unit and multi-unit responses).

Behavior-related timestamps (trial onset and trial completion) were sent to the RZ2 analog input channel using an Arduino digital board and synchronized to neural data.

Evoked potentials

To probe the functional connectivity between PLC and DLS, we measured short latency evoked potentials in DLS from PLC stimulation in 3 of the 8 chronically implanted stroke animals. This was done after all rehabilitation and electrophysiology recordings were completed. While animals were awake and resting, biphasic pulses (20-100μA, 200μs per phase with 100μs inter-phase interval, 5 pulses per current condition, Tucker Davis Technologies (TDT), IZ2) were applied in PLC at four tungsten microwire array electrodes (TDT, ~50 kOhm input impedance at 1000 Hz) with recording of DLS LFP short-latency evoked potentials (5-10ms after stimulation offset) in all striatal array channels (TDT, PZ2). DLS LFP was median-referenced, without z-scoring, and trials with motion artifact were excluded. Evoked response was averaged for each current amplitude condition and tested again two weeks later to confirm mapping stability. Channel pairs that demonstrated increased short-latency EP amplitude with increased current injection were deemed to reflect monosynaptic connections.

Intra-cortical microstimulation (ICMS) mapping

We conducted ICMS motor mapping in an intact animal not used for other experiments to confirm placement location of the PLC/M2 array and that movements can be evoked from the PLC/M2 area. This animal was anesthetized with a mixture of ketamine (100 mg/kg) and xylazine (16.67 mg/kg) delivered intraperitoneally. Supplementary 0.5-1ml doses of the mixture were provided as needed, based on toe pinch response. 32-channel multi-electrode arrays (TDT), the same type of electrodes we used for chronic *in vivo* electrophysiology were implanted in the PLC/M2 area (+4mm anterior and +2mm lateral from bregma) at a depth of 1.5mm from the brain surface. Triplet biphasic trains of 200μs per phase (100μs interphase interval, 333Hz triplet) were delivered at each electrode using a constant current stimulator (IZ2, TDT).

The trains were delivered with 50-150μA amplitude. Stimulation was delivered to each electrode in the array with video recording of forelimb at 20Hz.

Behavior

Training

Rats were acclimated to the behavioral box for at least 2 days and then trained to a plateau level of performance (>50% success rate for 4 consecutive days, Fig 3.1F shows pre-stroke baseline values) in a reach-to-grasp task before neural probe implantation. Rats typically took 1 to 2 weeks of daily training (~100 trials per day) to reach plateau performance. Probe implantation was performed contralateral to the preferred hand. Rats were allowed to recover for at least 5 days before the start of experimental sessions. During behavioral assessments, we monitored the animals and ensured that their body weights did not drop below 90% of their initial weight. We used an automated reach-box, controlled by custom MATLAB scripts and an Arduino microcontroller. This setup requires minimal user intervention, as described previously[27]. Each trial consisted of a pellet dispensed on the pellet tray, followed by an alerting beep indicating that the trial was beginning. Rats had to first move to the back of the box, breaking an infrared sensor which opens the door to the pellet. They then had 20s to reach their arms through the slot, grasp and retrieve the pellet. A real-time 'pellet detector' using an infrared detector centered over the pellet was used to determine when the pellet was moved, which indicated that the trial was over and the door was closed. All trials were captured by video through a camera placed on the side of the behavioral box. The camera was synced with the electrophysiology data either using Arduino digital output or directly through TTL pulses to the TDT RZ2 system. The video frame rate was 65-75 Hz.

Stroke rehabilitation

Rats began rehabilitation training 5-7 days after surgery by performing the same reach-to-grasp task. Electrophysiology recordings began after rats were able to reach independently without experimenter prompting. Rehabilitation training consisted of one to two sessions of 100-150 trials per day for 7-12 days. Sessions within a day were spaced by at least 2 hours. Rehabilitation training was stopped when single units could no longer be reliably recorded.

Muscimol experiments

After stroke induction and recovery from surgery, rats (n=4) were trained in the same reach-to-grasp task (2 sessions of 100 trials per day, spaced by 3 hours) until they can reach independently (perform task without prompting from experimenter) and achieved a success rate of at least 20%. Infusions began after these criteria were met. On each infusion day, rats first performed a baseline session of 100 trials. They were then anesthetized with 2% isoflurane and injected with 100-400nl (1μg/μl) of the GABA receptor agonist muscimol (Tocris Bioscience) or equal volume of saline (0.9% sodium chloride) into the dorsolateral striatum. Injection was done at a rate of 100nl/min through a chronically implanted cannula (PlasticsOne) using a Hamilton infusion syringe. The infusion syringe was left in place for 10 minutes post-infusion. Rats were allowed to recover for 2 hours in their home cage before starting the next session of 100 trials. Muscimol and saline infusion days were alternated for each animal and randomized across animals.

Behavioral analysis

Behavioral analysis was done based on video recorded during experimental sessions. The rats' dominant paws were painted with an orange marker at the beginning of each session to facilitate tracking of their paw positions. Reach videos were viewed and semi-automatically scored to obtain trial success,

hand position and time points for reach onset, pellet touch and retract onset. To characterize motor performance, we quantified pellet retrieval success rate (percentage of pellets successfully retrieved into the box), average paw speed (average speed from reach onset, the start of the last paw advancement towards the pellet, to time of pellet touch) and speed consistency (median correlation between single trial instantaneous paw speed from 0.4s to 0.05s around pellet touch and the median paw instantaneous speed before stroke/ infusion). Only trials in which the rat touched or knocked off the pellet were included in analysis. In muscimol experiments, we also quantified paw position variability (the closest euclidean distance between paw position in each frame and the mean paw trajectory) and reach amplitude (the farthest distance the paw travelled beyond the slot).

Neural data analysis

Analyses were conducted using custom-written scripts and functions in MATLAB 2018b (MathWorks).

Trial matching

For unit modulation and trial to template neural correlation analyses, only trials with one reach attempt and a reach to pellet touch duration of <0.5s were included. This was to account for the differences in behavioral variability across sessions.

Unit modulation

Spikes were binned at 50ms and time locked to behavioral markers. For visualization purposes, the peri-event time histogram (PETH) was estimated by Bayesian adaptive regression splines[52]. To determine if a unit was significantly modulated during movement, circular shuffling was performed on the binned firing rate data (without spline fitting). The firing rate from -2 to 2s around pellet touch for each trial of a unit was shifted circularly by a random time. The PETH was then recomputed from the shuffled data and

the mean squared error (the difference between the firing rate in each bin and the mean across all bins from -2 to 2s around pellet touch) of the PETH was calculated. This was repeated 5000 times to obtain a distribution of mean squared error values. The actual mean squared error of the real PETH was compared to this distribution to obtain a p-value. A p-value of <0.05, after bonferroni correction for multiple comparisons, was considered significant.

Single trial to template correlation

Spikes from -2s to 2s around pellet touch were binned at 20ms, smoothed with a gaussian kernel with a standard deviation of 60ms and then z-scored. Binned, smoothed and standardized spike counts for all units of a single trial were then concatenated into one long vector. The correlation between each concatenated single trial neural activity and the mean template (mean of all trials excluding current trial) was computed and the median correlation for each session was reported. To account for different numbers of units across rehabilitation sessions, units were subsampled to the lowest number across sessions for each animal (units were randomly sub-selected with replacement 1000 times). Only sessions with more than 5 units were included.

Speed decoding

A multiple linear regression with LASSO (Least Absolute Shrinkage and Selection Operator) regularization was used to predict paw speed, using PLC or DLS spiking activity. The regression was implemented using the MATLAB function *fitrlinear*. Spikes were binned at 20ms and instantaneous paw speed from the first reach to the last retract of each trial was interpolated to match the neural time bin. Predictors were binned spike counts of units at 10 time lags, spaced equally from 0 to -180ms relative to paw speed. The regularization parameter lambda was determined separately for each run of the regression using 5-fold cross validation. The lambda value that gave the lowest mean squared error was chosen. The final model was fitted using the best lambda value and the r^2 value was computed on 5-fold cross-validated

data. For a fairer comparison of r^2 values across different rehabilitation sessions with different numbers of units, units were subsampled to the lowest number of units across sessions (units were randomly sub-selected with replacement 500 times). Only sessions with more than 5 units were included. To obtain a chance level of decoding ability, neural activity was shuffled relative to paw speed (e.g. trial 1's speed is matched with trial 5's neural activity) and r^2 was recomputed.

Session by session cross-correlation between PLC and DLS

The correlation between PLC and DLS neural measures (proportion of modulated units, trial to mean neural correlation and speed decoding) were calculated at different time lags, by shifting the DLS measure by -2, -1, 0, +1 and +2 rehabilitation sessions relative to the PLC measures. If the lagged DLS/PLC session did not have a matching PLC/DLS session, the session was removed from analysis, instead of padding the other session. To obtain the shuffled null distribution, we randomly permuted the sequence of the sessions within each animal and recalculated the cross-correlation across all sessions from all animals 1000 times.

Canonical correlation analysis (CCA)

CCA identifies maximally correlated linear combinations between two groups of variables. Unit spiking data in PLC and DLS from -1.5s to 1.5s around pellet touch for each trial were binned at 100ms and concatenated. CCA models were then fit using the MATLAB function *canoncorr*. Only the top canonical component was used in this paper. Only sessions with more than 5 units in both PLC and DLS were included. To account for different numbers of units across rehabilitation sessions, PLC and DLS units were subsampled to the lowest number across sessions for each animal.

Local field potential (LFP) analyses

Artifact reject was first performed on LFP signals to remove broken channels and noisy trials. LFPs were then z-scored and median referenced separately for PLC and DLS. There were no detected PLC units in 2 of the 8 animals with simultaneous PLC and DLS recordings post-stroke. Hence, the PLC LFP activity from those two animals were excluded from analysis. LFP power was calculated on a trial-by-trial basis and then averaged across channels and animals, with wavelet decomposition using the EEGLAB function *newtimef*. PLC-DLS LFP coherence was calculated for each pair of channels using the Chronux function *cohgramc* with 0.75s windows moving by 0.01s.

Statistical analysis

Parametric statistics were generally used in this study (t-tests, Pearson's correlation and linear regression, unless otherwise stated), implemented within MATLAB. The linear mixed-effects model (implemented using MATLAB *fitlme*) was used to compare the differences in behavior, trial to mean correlation, speed decoding and canonical correlation. This model accounts for the fact that units or sessions from the same animal are more correlated than those from different animals and is more stringent than computing statistical significance over all units and sessions. We fitted random intercepts for each rat and reported the p-values for the regression coefficients associated with muscimol or saline, pre-stroke or post-stroke, or rehabilitation session.

Figures

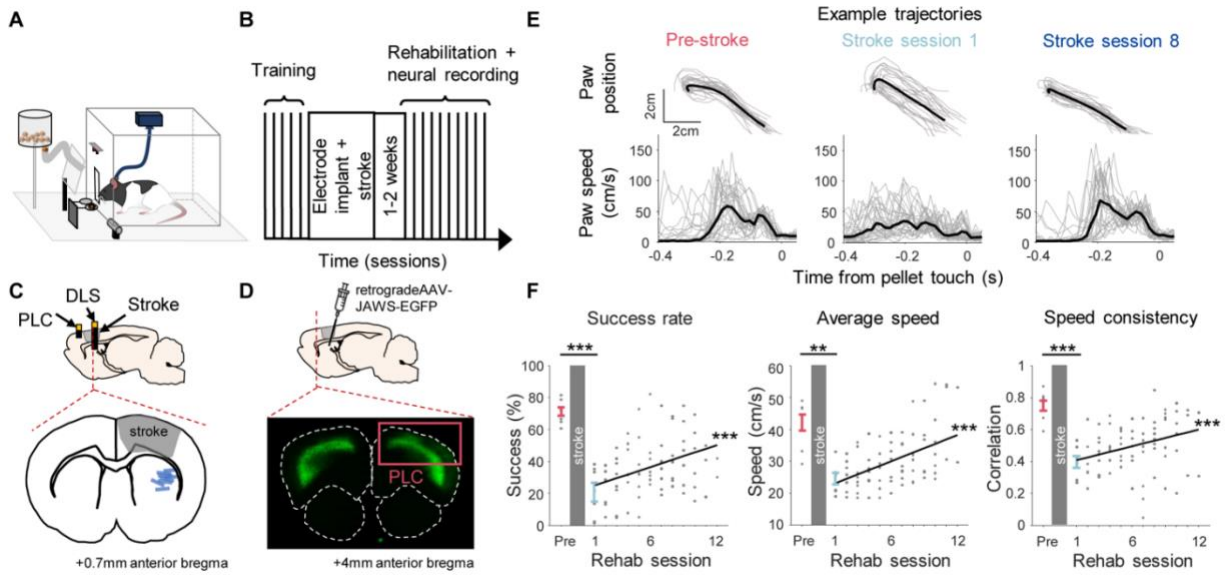

Figure 3.1: Corticostriatal neural activity was monitored during motor recovery after stroke

(**A**) Set up for reach to grasp task. (**B**) Behavioral paradigm. (**C**) Top: diagram of sagittal section, showing stroke and electrode locations. Bottom: diagram of coronal section, showing stroke and DLS electrode locations for the 8 stroke rats used for electrophysiology recordings. PLC = perilesional cortex, DLS = dorsolateral striatum. (**D**) Top: diagram of retrograde tracing from DLS to PLC in stroke rat. Bottom: fluorescent imaging of coronal section showing projections from PLC to DLS. (**E**) Paw position (top) and speed (bottom) trajectories for an example rat. (**F**) From left to right: pellet retrieval success rate, average speed from reach to pellet touch and single trial speed trajectory correlation with pre-stroke mean trajectory over rehabilitation sessions. Each point represents one session from one rat. Error bars represent SEM. Black line is best fit line over rehabilitation using linear mixed effects model with session as fixed effect and rat identity as random effect. Asterisks indicate significant difference between pre-stroke and post-stroke session one using paired t-test, and significant improvement over rehabilitation sessions using linear mixed effects model. **p<0.01, ***p<0.001.

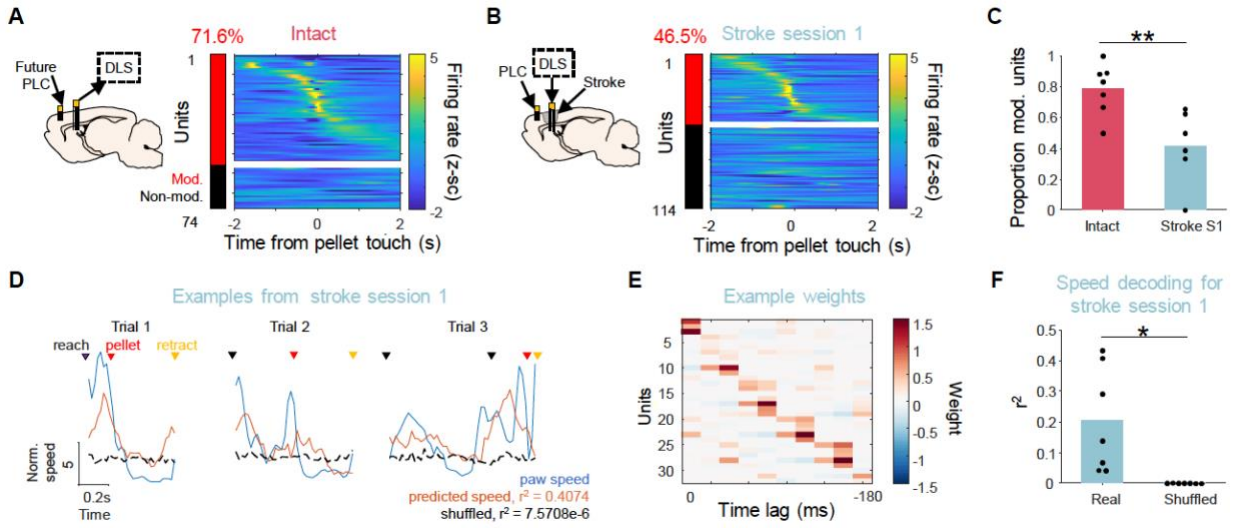

Figure 3.2: DLS was partially disrupted but still involved in reaching early after stroke

(**A**, **B**) Electrode locations (left) and peri-event time histograms (PETH, right) for all DLS units from 7 intact rats and 8 stroke rats, respectively, during the first rehabilitation session. (**C**) Proportion of significantly modulated DLS units in intact rats vs. in stroke rats during session 1. Each dot represents one rat and bar indicates mean across rats. *p<0.05, **p<0.01 from paired t-test. (**D**) Example trials from the first rehabilitation session of a stroke rat, showing the actual paw speed, predicted paw speed from DLS unit activity, and predicted speed from shuffled activity. (**E**) Weights of the multiple linear regression for one example stroke rat. (**F**) R^2 values of speed prediction using DLS unit activity vs. shuffled activity for the first rehabilitation session post-stroke. Labeling conventions are the same as (C).

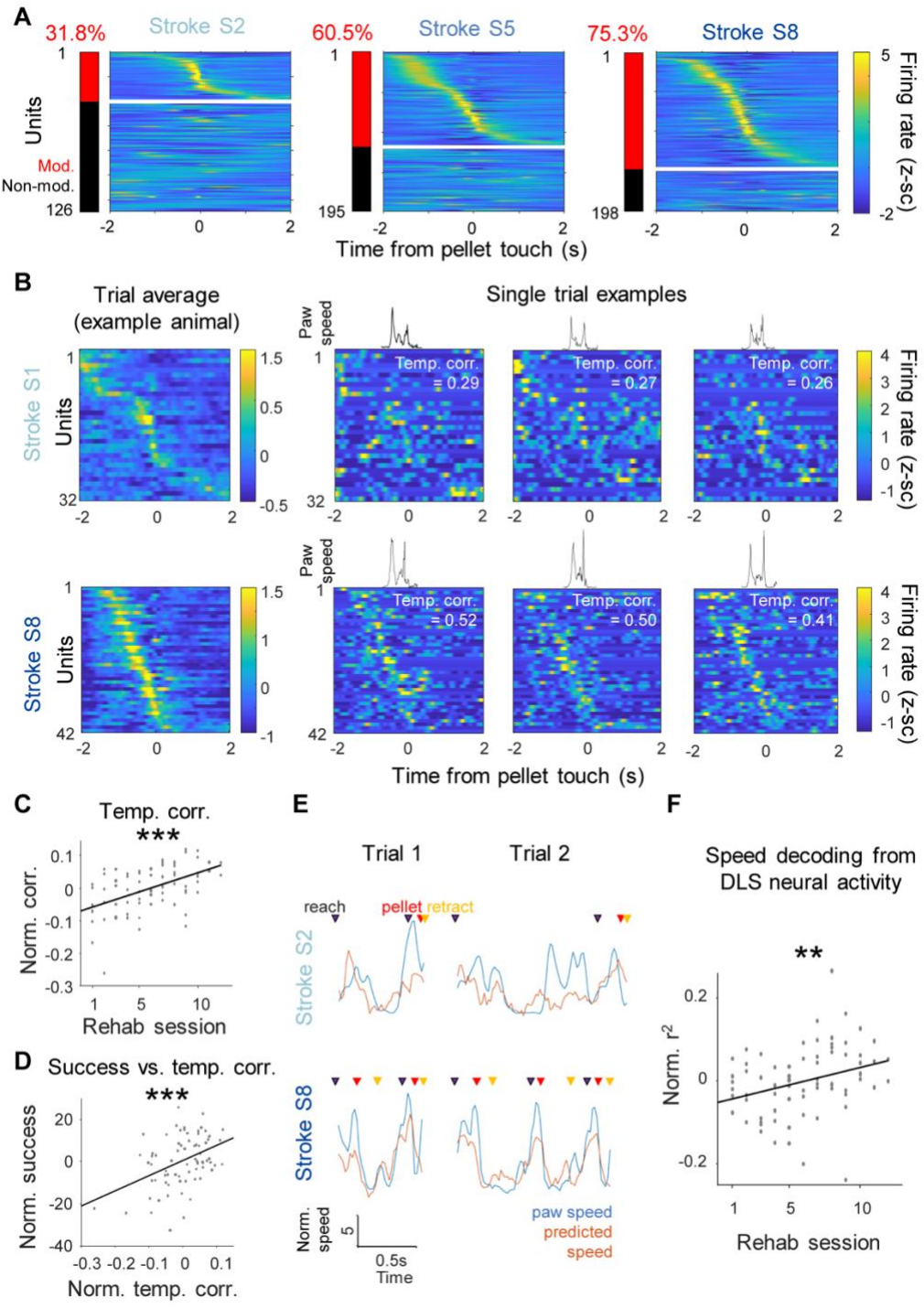

Figure 3.3: DLS neural dynamics reorganized during rehabilitation

(**A**) Peri-event time histograms (PETH) for all DLS units from 8 rats during rehabilitation sessions 2, 5 and 8. (**B**) Left: average PETH for an example rat. Right: single trial PETH examples. Black lines on top show paw speed for the single trials. (**C**) Single trial correlation with the session template across rehabilitation

sessions. Each dot represents the normalized (by mean subtraction within rat) correlation for one session of one rat. Black line is best fit line based on linear mixed effects model. (**D**) Correlation between normalized success rate and normalized template correlation. Success rate was normalized by mean subtraction across sessions of each rat. Same labeling conventions as in (C). (**E**) Example paw speed and predicted speed using DLS neural activity for an example rat. (**F**) Speed decoding r^2 across rehabilitation. Each dot represents the normalized (by mean subtraction within sessions of a rat) r^2 for one session of one rat. Black line is best fit line. **p<0.01, ***p<0.001. P-values are for the regression coefficient, obtained using linear mixed effects model, with session or template correlation as fixed effect and rat identity as random effect.

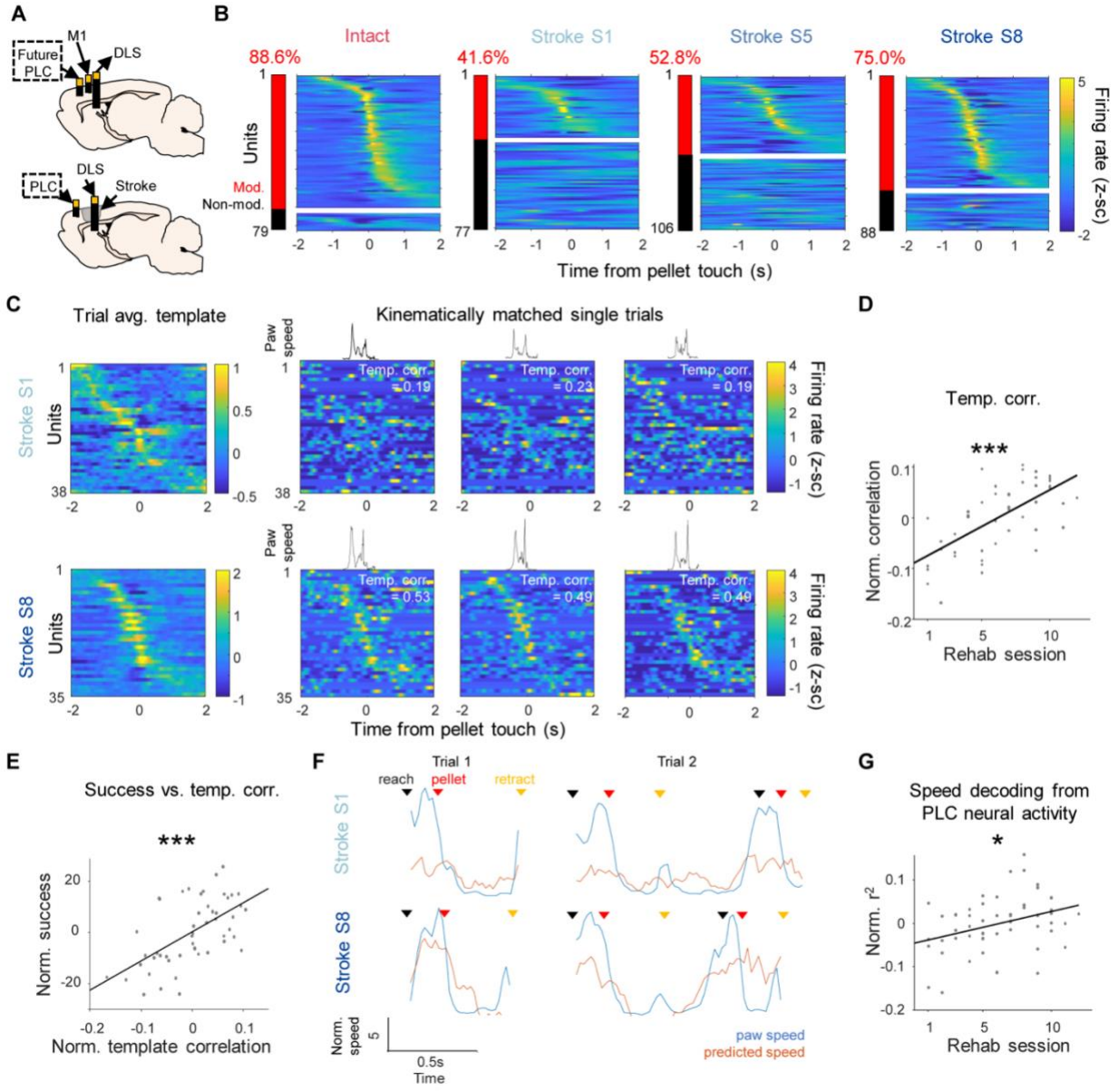

Figure 3.4: Changes in PLC activity paralleled changes in DLS

(**A**) Electrode locations for intact and stroke rats. (**B**) PETH of all PLC units from intact rats (n=3) and sessions 1, 5 and 8 of stroke rats (n=6). (**C**) Left: trial averaged PETH for all units in an example rat. Right: single trial PETH examples. Black lines on top show paw speed for the single trials. (**D**) Single trial to session template correlation across rehabilitation. Each dot represents the normalized (by mean subtraction across sessions of individual rats) correlation for one session of one rat. Black line is best fit line. (**E**) Correlation between normalized success rate and normalized template correlation. Success rate was normalized by mean subtraction across sessions of individual rats. Same labeling conventions as in (D). (**F**) Examples trials from a rat, showing actual paw speed and predicted speed using PLC neural activity. (**G**) R^2 of speed decoding using PLC activity over rehabilitation. Each dot represents the normalized r^2 for one

session of one rat. The r^2 values were normalized by mean subtraction across sessions of each rat. Black line is best fit line. *p<0.05, ***p<0.001. P-values are for the regression coefficient, obtained using linear mixed effects model, with session or template correlation as fixed effect and rat identity as random effect.

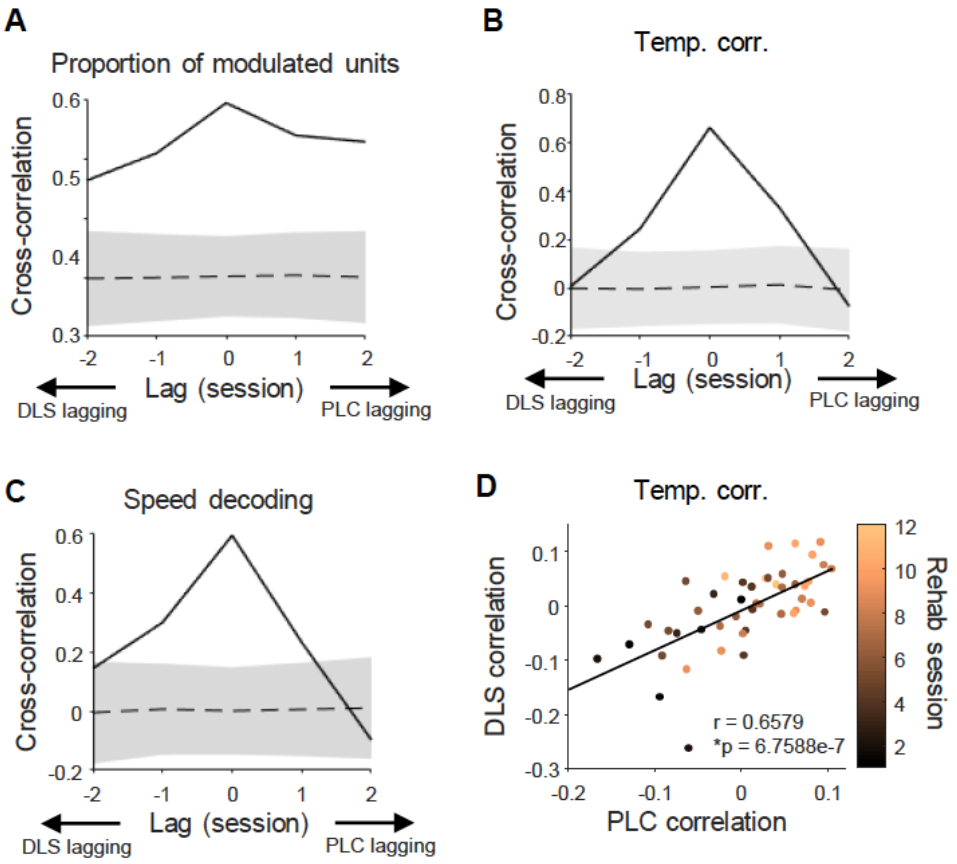

Figure 3.5: Neural changes in PLC and DLS occurred simultaneously across rehabilitation sessions

(**A**) Solid black line shows correlation between the proportion of modulated units in PLC and DLS at different time-lags. Dotted black line shows mean and grey shaded area indicates standard deviation of shuffled distribution. (**B**) Correlation between PLC and DLS template correlation at different time lags. Same labeling conventions as (A). (**C**) Correlation between speed decoding r^2 of PLC and DLS at different time lags. Same labeling conventions as (A). (**D**) Correlation between PLC and DLS template correlation, across animals and rehabilitation sessions, at zero time lag. Each dot represents the normalized template correlation for one session of a rat, colored by rehabilitation session. Black line is best fit line.

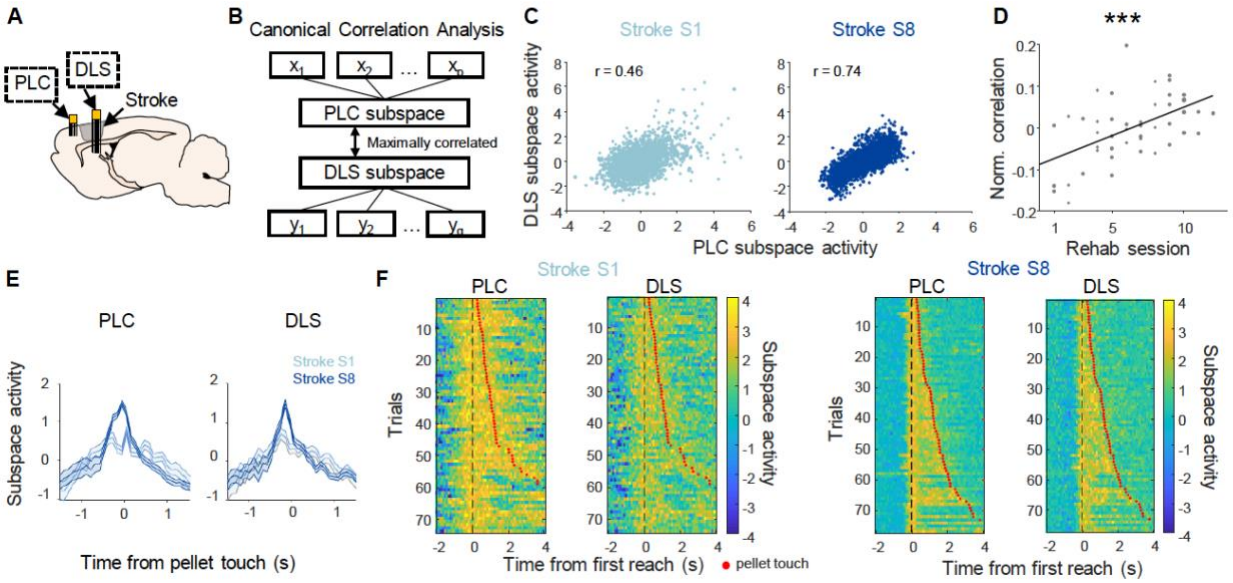

Figure 3.6: Fine-timescale coordination between PLC and DLS increased after rehabilitation

(**A**) Simultaneous electrophysiology recording from PLC and DLS. (**B**) Description of canonical correlation analysis (CCA). CCA finds linear combinations of PLC units (x_1, x_2, … x_p) and DLS units (y_1, y_2, … , y_q) that maximizes the correlation between PLC and DLS. (**C**) DLS vs. PLC subspace activity (from the first canonical component) during movement (-1.5 to 1.5s around pellet touch) for example sessions from a rat. Each dot represents one time bin of a trial from the session. (**D**) PLC-DLS canonical correlation of top component during movement across rehabilitation. Each dot represents the normalized (by mean subtraction across sessions of individual rats) correlation for one session of one rat. Black line is fitted regression line. ***p<0.001. P-value is for the regression coefficient, obtained using linear mixed effects model, with session as fixed effect and rat identity as random effect. (**E**) PLC and DLS subspace activity against movement time across all trials for an example rat. Solid lines represent mean and shaded area denotes SEM. (**F**) PLC and DLS subspace activity from single trials sorted by first reach to pellet touch duration.

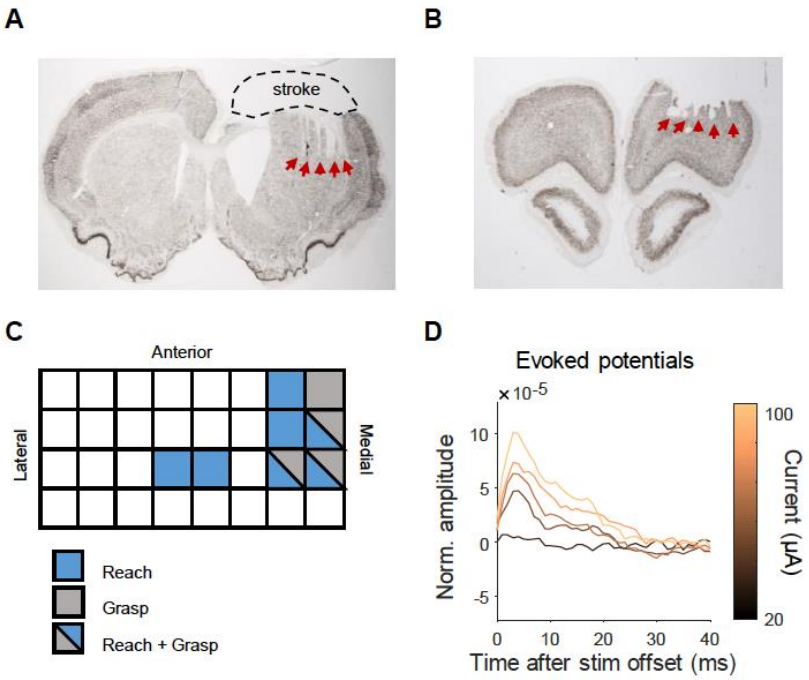

Figure 3.S1: Electrode localization

(**A**) Histology image with NeuN staining showing location of stroke and DLS electrodes (red arrows) for an example stroke rat. (**B**) Histology image with NeuN staining showing location of PLC electrodes (red arrows) for an example stroke rat. (**C**) Grid represents the channels in the multi-electrode array used for PLC recording and color indicates channels where stimulation evoked reach, grasp or other forelimb movement. PLC array was centered at 4mm anterior and 2mm lateral to bregma. Dimensions are not to scale. (**D**) Short-latency evoked potentials in DLS from a single biphasic stimulation pulse in the PLC of a stroke rat. Colored lines indicate increasing current pulses from 20μA (black) to 100μA (yellow).

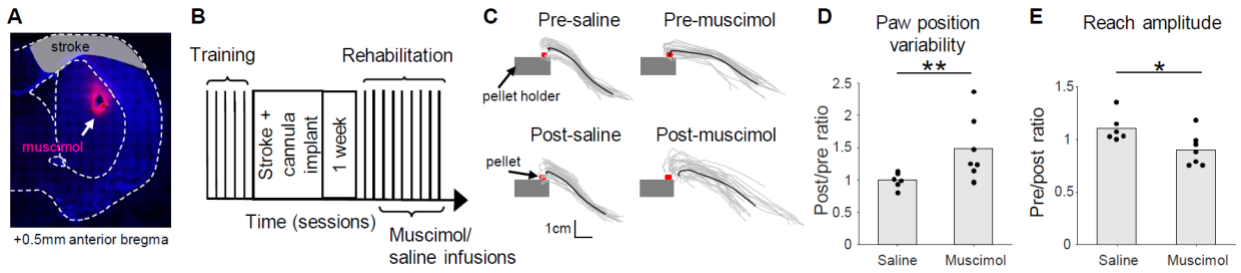

Figure 3.S2: DLS is necessary for consistent and high amplitude movement after stroke

(**A**) Fluorescent histology image showing stroke and muscimol injection (shown in pink) location. Blue represents DAPI staining. (**B**) Muscimol experimental paradigm. (**C**) Example paw trajectories before and after saline or muscimol infusion, from two example rats. (**D**) Post/pre ratio of paw position variability, the Euclidean distance between paw positions of single trials and the mean position across trials. Each dot represents one session from one rat (total of 7 musicmol and 6 saline sessions from 4 rats). Bar represents mean across sessions. (**E**) Post/pre-infusion ratio of reach amplitude, the farthest distance the paw reaches beyond the slot. *p<0.05, **p<0.01, based on linear mixed effects model.

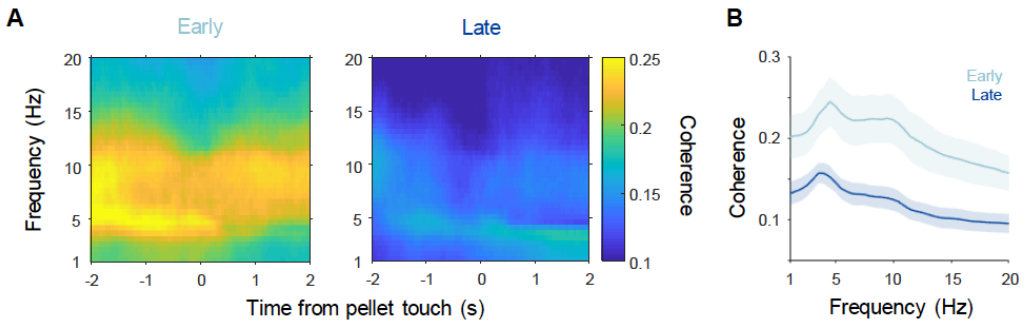

Figure 3.S3: PLC-DLS LFP coherence decreased after rehabilitation

(**A**) Spectrogram of the average PLC-DLS LFP coherence across rats (n=6) in early (first recorded session post-stroke) and late (last recorded session) rehabilitation. (**B**) PLC-DLS coherence spectrums from -0.75s to 0.25s around pellet touch. Solid line shows mean across rats and shaded area indicates S.E.M.

Table 3.S1. Number of rats used for experiments

Experiment	Figures	Behavioral training	Stroke	No. of rats
Simultaneous PLC-DLS recordings	3.1A-C, E-F; 3.2B-F; 3.3; 3.4; 3.5; 3.6, 3.S1D	Yes	Yes	8
Viral tracing	3.1D	No	Yes	3
Simultaneous PLC-DLS recordings in intact rats	3.2A, C; 3.4A-B	Yes	No	3
DLS recording in intact rats	3.2A, C	Yes	No	4
ICMS mapping	3.S1C	No	No	1
Muscimol	3.S2	Yes	Yes	4

References

1. Whishaw, I. Q., O'Connor, W. T. & Dunnett, S. B. The Contributions of Motor Cortex, Nigrostriatal Dopamine and Caudate-Putamen To Skilled Forelimb Use in the Rat. *Brain* **109**, 805–843 (1986).

2. Houk, J. C. & Wise, S. P. Feature Article: Distributed Modular Architectures Linking Basal Ganglia, Cerebellum, and Cerebral Cortex: Their Role in Planning and Controlling Action. *Cereb. Cortex* **5**, 95–110 (1995).

3. Lemke, S. M., Ramanathan, D. S., Guo, L., Won, S. J. & Ganguly, K. Emergent modular neural control drives coordinated motor actions. *Nat. Neurosci.* **22**, 1122–1131 (2019).

4. Sauerbrei, B. A. *et al.* Cortical pattern generation during dexterous movement is input-driven. *Nature* **577**, 386–391 (2020).

5. Costa, R. M., Cohen, D. & Nicolelis, M. A. L. Differential Corticostriatal Plasticity during Fast and Slow Motor Skill Learning in Mice. *Curr. Biol.* **14**, 1124–1134 (2004).

6. Yin, H. H. *et al.* Dynamic reorganization of striatal circuits during the acquisition and consolidation of a skill. *Nat. Neurosci.* **12**, 333–341 (2009).

7. Wagner, M. J. *et al.* Shared Cortex-Cerebellum Dynamics in the Execution and Learning of a Motor Task. *Cell* **177**, 1–14 (2019).

8. Doyon, J. & Benali, H. Reorganization and plasticity in the adult brain during learning of motor skills. *Curr. Opin. Neurobiol.* **15**, 161–167 (2005).

9. Nudo, R. J. & Milliken, G. W. Reorganization of movement representations in primary motor

cortex following focal ischemic infarcts in adult squirrel monkeys. *J. Neurophysiol.* **75**, 2144–2149 (1996).

10. Ramanathan, D., Conner, J. M. & Tuszynski, M. H. A form of motor cortical plasticity that correlates with recovery of function after brain injury. *Proc. Natl. Acad. Sci. U. S. A.* **103**, 11370–5 (2006).

11. Castro-Alamancos, M. A. & Borrell, J. Functional recovery of forelimb response capacity after forelimb primary motor cortex damage in the rat is due to the reorganization of adjacent areas of cortex. *Neuroscience* **68**, 793–805 (1995).

12. Ramanathan, D. S. *et al.* Low-frequency cortical activity is a neuromodulatory target that tracks recovery after stroke. *Nat. Med.* **24**, 1257–1267 (2018).

13. Nudo, R. J., Wise, B. M., SiFuentes, F. & Milliken, G. W. Neural Substrates for the Effects of Rehabilitative Training on Motor Recovery After Ischemic Infarct. *Science (80-.).* **272**, 1791–1794 (1996).

14. von Monakow, C. *Lokalisation im Gehirn und Funktionelle Sta'rungen Induziert Durch Kortikale Läsionen.* (Bergmann JF, 1914).

15. Carrera, E. & Tononi, G. Diaschisis: past, present, future. *Brain* **137**, 2408–2422 (2014).

16. Collins, K. C., Kennedy, N. C., Clark, A. & Pomeroy, V. M. Kinematic Components of the Reach-to-Target Movement After Stroke for Focused Rehabilitation Interventions: Systematic Review and Meta-Analysis. *Front. Neurol.* **9**, 472 (2018).

17. Lai, S. *et al.* Quantitative Kinematic Characterization of Reaching Impairments in Mice After a Stroke. *Neurorehabil. Neural Repair* **29**, 382–392 (2015).

18. Jin, X., Tecuapetla, F. & Costa, R. M. Basal ganglia subcircuits distinctively encode the parsing and concatenation of action sequences. *Nat. Neurosci.* **17**, 423–430 (2014).

19. Markowitz, J. E. *et al.* The Striatum Organizes 3D Behavior via Moment-to-Moment Action Selection. *Cell* **174**, 44-49.e17 (2018).

20. Thura, D. & Cisek, P. The Basal Ganglia Do Not Select Reach Targets but Control the Urgency of Commitment. *Neuron* **95**, 1160–1170 (2017).

21. Shmuelof, L. & Krakauer, J. W. Are we ready for a natural history of motor learning? *Neuron* **72**, 469–476 (2011).

22. Hardwick, R. M., Rajan, V. A., Bastian, A. J., Krakauer, J. W. & Celnik, P. A. Motor Learning in Stroke: Trained Patients Are Not Equal to Untrained Patients With Less Impairment. *Neurorehabil. Neural Repair* **31**, 178–189 (2017).

23. Yin, H. H. The sensorimotor striatum is necessary for serial order learning. *J Neurosci* **30**, 14719–14723 (2010).

24. Dhawale, A. K., Wolff, S. B. E., Ko, R. & Ölveczky, B. P. The basal ganglia can control learned motor sequences independently of motor cortex. *bioRxiv* 827261 (2019) doi:10.1101/827261.

25. Wolff, S. B. E., Ko, R. & Ölveczky, B. P. Distinct roles for motor cortical and thalamic inputs to striatum during motor learning and execution. *bioRxiv* 825810 (2019) doi:10.1101/825810.

26. Musall, S., Kaufman, M. T., Juavinett, A. L., Gluf, S. & Churchland, A. K. Single-trial neural dynamics are dominated by richly varied movements. *Nat. Neurosci.* **22**, 1677–1686 (2019).

27. Wong, C. C., Ramanathan, D. S., Gulati, T., Won, S. J. & Ganguly, K. An automated behavioral

box to assess forelimb function in rats. *J. Neurosci. Methods* **246**, 30–7 (2015).

28. Guo, J. Z. *et al.* Cortex commands the performance of skilled movement. *Elife* **4**, 1–18 (2015).

29. Morandell, K. & Huber, D. The role of forelimb motor cortex areas in goal directed action in mice. *Sci. Rep.* 1–14 (2017) doi:10.1038/s41598-017-15835-2.

30. Yttri, E. A. & Dudman, J. T. A Proposed Circuit Computation in Basal Ganglia: History-Dependent Gain. *Mov. Disord.* **33**, 704–716 (2018).

31. Dudman, J. T. & Krakauer, J. W. The basal ganglia: From motor commands to the control of vigor. *Curr. Opin. Neurobiol.* **37**, 158–166 (2016).

32. Gharbawie, O. A., Karl, J. M. & Whishaw, I. Q. Recovery of skilled reaching following motor cortex stroke: Do residual corticofugal fibers mediate compensatory recovery? *Eur. J. Neurosci.* **26**, 3309–3327 (2007).

33. Koralek, A. C., Costa, R. M. & Carmena, J. M. Temporally Precise Cell-Specific Coherence Develops in Corticostriatal Networks during Learning. *Neuron* **79**, 865–872 (2013).

34. Semedo, J. D., Zandvakili, A., Machens, C. K., Yu, B. M. & Kohn, A. Cortical Areas Interact through a Communication Subspace. *Neuron* **102**, 1–11 (2019).

35. Veuthey, T. L., Derosier, K., Kondapavulur, S. & Ganguly, K. Single-trial cross-area neural population dynamics during long-term skill learning. *Nat. Commun.* **11**, 4057 (2020).

36. Gallego, J. A. *et al.* Cortical population activity within a preserved neural manifold underlies multiple motor behaviors. *Nat. Commun.* **9**, 4233 (2018).

37. Sussillo, D., Churchland, M. M., Kaufman, M. T. & Shenoy, K. V. A neural network that finds a naturalistic solution for the production of muscle activity. *Nat. Neurosci.* **18**, 1025–1033 (2015).

38. Cheng, H. W. *et al.* Differential spine loss and regrowth of striatal neurons following multiple forms of deafferentation: a Golgi study. *Exp. Neurol.* **147**, 287–298 (1997).

39. Carmichael, S. T. & Chesselet, M.-F. Synchronous neuronal activity is a signal for axonal sprouting after cortical lesions in the adult. *J. Neurosci.* **22**, 6062–6070 (2002).

40. Dancause, N. Extensive Cortical Rewiring after Brain Injury. *J. Neurosci.* **25**, 10167–10179 (2005).

41. Ishida, A. *et al.* Dynamic Interaction between Cortico-Brainstem Pathways during Training-Induced Recovery in Stroke Model Rats. *J. Neurosci.* **39**, 7306–7320 (2019).

42. Murray, J. M. & Escola, G. S. Learning multiple variable-speed sequences in striatum via cortical tutoring. *Elife* **6**, (2017).

43. Lerner, T. N. & Kreitzer, A. C. Neuromodulatory control of striatal plasticity and behavior. *Curr. Opin. Neurobiol.* **21**, 322–327 (2011).

44. Peters, A. J., Chen, S. X. & Komiyama, T. Emergence of reproducible spatiotemporal activity during motor learning. *Nature* **510**, 263–7 (2014).

45. Hyland, B. Neural activity related to reaching and grasping in rostral and caudal regions of rat motor cortex. *Behav. Brain Res.* **94**, 255–269 (1998).

46. Brown, a. R. & Teskey, G. C. Motor Cortex Is Functionally Organized as a Set of Spatially Distinct Representations for Complex Movements. *J. Neurosci.* **34**, 13574–13585 (2014).

47. Esposito, M. S., Capelli, P. & Arber, S. Brainstem nucleus MdV mediates skilled forelimb motor tasks. *Nature* **508**, 351–356 (2014).

48. Isa, T. Dexterous Hand Movements and Their Recovery After Central Nervous System Injury. *Annu. Rev. Neurosci.* **42**, 315–335 (2019).

49. Kawai, R. *et al.* Motor Cortex Is Required for Learning but Not for Executing a Motor Skill. *Neuron* **86**, 800–812 (2015).

50. Perlmutter, J. S. & Mink, J. W. Deep Brain Stimulation. *Annu. Rev. Neurosci.* **29**, 229–257 (2006).

51. Cramer, S. C. Drugs to Enhance Motor Recovery After Stroke. *Stroke* **46**, 2998–3005 (2015).

52. Wallstrom, G., Liebner, J. & Kass, R. E. An Implementation of Bayesian Adaptive Regression Splines (BARS) in C with S and R Wrappers. *J. Stat. Softw.* **26**, 1–21 (2008).

CHAPTER 4 : DICUSSION

Summary and implications

Measuring and characterizing neural activity during behavior is the first step to understanding the mechanisms that produce that behavior, and in this case, mechanisms that underlie motor recovery after stroke. Here, we used chronic in vivo electrophysiology to track spiking and local field potential (LFP) activity during rehabilitation training sessions after stroke. Chapter 2 focused on the activity in the perilesional cortex (PLC). We found that low frequency oscillations (LFOs), in both spiking and LFP activity, was diminished after stroke and tracked motor recovery. Epidural electrical stimulation increased the amplitude of LFOs and improved motor function in chronic stroke animals. These results show that LFOs can be used as a biomarker for motor recovery and for testing and development of neuromodulatory therapies. Chapter 3 focused on the single-trial neural activity in PLC and dorsolateral striatum (DLS), and the interactions between them. We found that movement-related neural activity in both PLC and DLS reorganized simultaneously during stroke recovery. Specifically, motor improvements were correlated with more consistent trial to trial spiking activity and a more reliable relationship between neural activity and instantaneous movement speed. Spiking activity in PLC and DLS during movement also became more coordinated with recovery.

Across both chapters, we found that synchronous and reliable bursts of activity in neurons within and between motor areas were crucial for the execution of fast, accurate and consistent movements after stroke. The LFOs described in Chapter 2 were a measure of synchronized spiking activity in motor cortex that was precisely locked to the low frequency LFP. Such synchronized oscillatory spiking may be needed to effectively activate downstream areas[1–3] and hence drive skilled motor actions. While LFOs were not an explicit focus in Chapter 3, we did observe a similar increase in LFOs in DLS during recovery in stroke animals. Increases in LFO amplitude also occur in both M1 and DLS during motor learning in intact

animals[4]. These results indicate that synchronized oscillatory activity in DLS is also a feature of skilled motor actions and suggest that LFO activity across the entire motor network may be important for recovery. In Chapter 3, we focused on spiking activity and assessing neural variability on a finer timescale. This extends work in Chapter 2 by showing that the synchronized bursts of neural activity that emerge with recovery were also more reliable and consistent from trial to trial and to motor behavior. This is similar to the increases in reliability of neural activity patterns during motor learning in intact animals[5,6]. Altogether, we showed that movement-related neural dynamics in both PLC and DLS reorganized after stroke by becoming more synchronized and reliable.

Furthermore, we found that neural dynamics in both PLC and DLS reorganized at the same time and became more coordinated during recovery, suggesting that both structures may be contributing to recovery. This highlights the importance of studying multiple motor areas and the interactions among them. The brain is a network and damage or reorganization in one area affects other connected areas[7]. Consideration of the entire network is needed to gain a holistic view of stroke recovery.

The finding that synchronous and reliable bursts of activity across motor areas emerge during rehabilitation suggests that interventions that increase coordinated bursting may enhance recovery. Electrical stimulation is one easily translatable way of modulating neural dynamics. Past studies have shown that cortical electrical stimulation, especially when combined with rehabilitation training, could induce plasticity and improve motor function post-stroke[8–13]. However, these studies did not explicitly target movement-related neural dynamics and the stimulation appear to be effective only when applied soon after stroke[8,10]. In Chapter 2, we found that epidural electrical stimulation applied during movement could increase the amplitude of LFOs and improve motor function even in the chronic phase post-stroke. Although the exact mechanism by which electrical stimulation aids motor function is to be determined, it is possible that stimulation modifies the baseline excitability of neurons[14,15], lowering the threshold for action potential initiation and hence promotes synchronous and reliable neural activity needed for skilled

motor actions. This work demonstrates that it is possible to enhance motor function even in the chronic phase, shows that modulating ongoing neural dynamics during movement is feasible and paves the way for future exploration of stimulation paradigms that target neural dynamics. Given our finding that DLS is also reorganized during motor recovery in a coordinated manner with PLC, future studies could experiment with DLS as well as paired PLC-DLS stimulation.

Overall, this thesis advanced the field by: (1) identifying synchronous and reliable movement-related neural dynamics as markers of recovered motor function post-stroke, (2) developing and validating electrical stimulation paradigms to modulate ongoing neural dynamics and improve motor function, (3) highlighting the importance of remote areas, specifically the dorsolateral striatum, and the multi-area interactions in motor recovery.

Limitations and future directions

Although we observed changes in neural activity patterns that were associated with motor function post-stroke, the casual contributions of these activity patterns were not determined. LFOs could be an epiphenomena or correlate of some other neural processes that underlie stroke recovery, such as axonal sprouting and changes in synaptic plasticity[16,17]. The increase in reliability and consistency of neural activity could also be a result rather than cause of motor recovery. Experiments that directly disrupt or enhance these activity patterns, for example by applying stimulation at particular phases of the ongoing LFO[18,19], would be needed to assess their causal role. Future studies could also measure neural activity during movement together with molecular and cellular plasticity changes after stroke to better understand how they relate to each other.

Similarly, the exact causal contribution of DLS and the coordination between PLC and DLS to recovery was difficult to determine. While we showed in Chapter 3 that DLS was necessary for consistent

and high amplitude movements post-stroke, it was difficult to disentangle its role in motor execution from recovery. Any manipulation that disrupts motor execution will inevitably affect learning and rehabilitation as subjects will no longer be able to perform the task as well. Instead of suppressing DLS activity, future studies could disrupt plasticity[20], for instance by blocking NMDA receptors with AP5[21,22], to assess the necessity of DLS plasticity for motor recovery. To assess the causal role of corticostriatal projections, targeted optogenetics delivered by viruses could be used to selectively manipulate corticostriatal projections.

We found in Chapter 3 that PLC and DLS became more coordinated with each other during recovery, but we could not determine if this was due to strengthening of the monosynaptic connection between them or to a third area driving both of them. We found that LFP coherence between PLC and DLS decreased but spiking coordination, as measured by canonical correlation analysis, during movement increased with recovery. This suggests that PLC and DLS may only be transiently coordinated during movement, perhaps by a third area, rather than more strongly coupled in general. Although we found evidence of preserved monosynaptic structural and functional connectivity between PLC and DLS, we did not study the changes over rehabilitation. This can be done in future studies by measuring the amplitude of short-latency evoked potentials in DLS from optogenetic or electrical stimulation in PLC throughout rehabilitation training. Virally targeted calcium imaging[23,24] can also be conducted to track the movement related activity of corticostriatal neurons specifically, and differentiate their activity from that of PLC and DLS neurons in general. Future work that measure activity from other motor areas, such as the motor thalamus, cerebellum and brain stem motor areas, will also be important to assess the roles of the entire motor network in motor recovery.

We demonstrated in this thesis that epidural electrical stimulation can alter ongoing neural dynamics and enhance motor function. However, the mechanisms of electrical stimulation were unclear. Electrical stimulation causes artifacts during electrophysiology recordings, making it difficult to measure

its exact effects on individual neurons. Optical imaging, for example fiber photometry, is less affected by electrical artifacts and can be used in future studies to study how neural activity during movement is affected by electrical stimulation.

The experiments in this thesis were mostly conducted in rodents and more work has to be done to assess generalizability to human stroke patients. The corticospinal tract in rodents and primates are organized differently[25,26] and motor recovery might manifest in distinct ways. Rodent models of stroke, while more controlled, also do not always mimic human stroke[27]. We attempted to evaluate the relevance of LFOs in humans in Chapter 2 by analyzing electrocorticography activity from a human stroke patient during reaching. We found that low frequency power in the stroke patient was reduced compared to intact subjects. A subsequent electroencephalography study in human stroke patients also found reduced LFOs[28], supporting the generalizability of LFOs. Future studies should assess this in a larger cohort in human stroke patients or with non-human primate stroke models, and also measure activity from the striatum to investigate if the striatum also reorganizes similarly after stroke in primates.

In our rehabilitation training sessions, we did not make a clear distinction between true recovery (regaining lost function) and compensation (using alternative strategies to perform a task). It is likely that there is a mixture of both in the experiments we conducted[29]. The reorganization and stimulation effects we observed could be partially associated with compensation and it is important to clearly identify and target neural dynamics that are linked to true recovery. Future studies should employ more detailed kinematic analysis to distinguish between the two[30,31].

This work provided a framework for exploration of movement-related neural dynamics in the motor network during stroke recovery. Further work investigating the causal and mechanistic role of these neural dynamics and multi-area interactions will greatly improve our understanding of motor recovery and lead to new therapies.

References

1. van Wijk, B. C. M., Beek, P. J. & Daffertshofer, A. Neural synchrony within the motor system: what have we learned so far? *Front. Hum. Neurosci.* **6**, 1–15 (2012).

2. Fries, P. Rhythms for Cognition: Communication through Coherence. *Neuron* **88**, 220–235 (2015).

3. Fries, P. A mechanism for cognitive dynamics: Neuronal communication through neuronal coherence. *Trends Cogn. Sci.* **9**, 474–480 (2005).

4. Lemke, S. M., Ramanathan, D. S., Guo, L., Won, S. J. & Ganguly, K. Emergent modular neural control drives coordinated motor actions. *Nat. Neurosci.* **22**, 1122–1131 (2019).

5. Peters, A. J., Chen, S. X. & Komiyama, T. Emergence of reproducible spatiotemporal activity during motor learning. *Nature* **510**, 263–7 (2014).

6. Makino, H. *et al.* Transformation of Cortex-wide Emergent Properties during Motor Learning. *Neuron* **94**, 880-890.e8 (2017).

7. Carrera, E. & Tononi, G. Diaschisis: past, present, future. *Brain* **137**, 2408–2422 (2014).

8. O'Bryant, A. J. *et al.* Enduring Poststroke Motor Functional Improvements by a Well – Timed Combination of Motor Rehabilitative Training and Cortical Stimulation in Rats. *Neurorehabil. Neural Repair* 1–12 (2014) doi:10.1177/1545968314562112.

9. Boychuk, J. a *et al.* Enhanced Motor Recovery After Stroke With Combined Cortical Stimulation and Rehabilitative Training Is Dependent on Infarct Location. *Neurorehabil. Neural Repair* 1545968315624979- (2015) doi:10.1177/1545968315624979.

10. Jones, T. A. & Adkins, D. L. Motor System Reorganization After Stroke: Stimulating and Training Toward Perfection. *Physiology (Bethesda).* **30**, 358–70 (2015).

11. Adkins, D. L. *et al.* Epidural cortical stimulation enhances motor function after sensorimotor cortical infarcts in rats. *Exp. Neurol.* **200**, 356–370 (2006).

12. Allman, C. *et al.* Ipsilesional anodal tDCS enhances the functional benefits of rehabilitation in patients after stroke. *Sci. Transl. Med.* **8**, (2016).

13. Levy, R. M. *et al.* Epidural Electrical Stimulation for Stroke Rehabilitation: Results of the Prospective, Multicenter, Randomized, Single-Blinded Everest Trial. *Neurorehabil. Neural Repair* **30**, 107–19 (2016).

14. Nitsche, M. A. & Paulus, W. Sustained excitability elevations induced by transcranial DC motor cortex stimulation in humans. *Neurology* **57**, 1899–1901 (2001).

15. Reato, D., Rahman, A., Bikson, M. & Parra, L. C. Low-intensity electrical stimulation affects network dynamics by modulating population rate and spike timing. *J. Neurosci.* **30**, 15067–15079 (2010).

16. Carmichael, S. T. Cellular and molecular mechanisms of neural repair after stroke: Making waves. *Ann. Neurol.* **59**, 735–742 (2006).

17. Carmichael, S. T. Plasticity of cortical projections after stroke. *Neurosci.* **9**, 64–75 (2003).

18. Gulati, T., Guo, L., Ramanathan, D. S., Bodepudi, A. & Ganguly, K. Neural reactivations during sleep determine network credit assignment. *Nat. Neurosci.* **20**, 3–5 (2017).

19. Cardin, J. A. *et al.* Driving fast-spiking cells induces gamma rhythm and controls sensory

responses. *Nature* **459**, 663–7 (2009).

20. Koralek, A. C., Jin, X., Long II, J. D., Costa, R. M. & Carmena, J. M. Corticostriatal plasticity is necessary for learning intentional neuroprosthetic skills. *Nature* **483**, 331–335 (2012).

21. Goodman, J., Ressler, R. L. & Packard, M. G. Enhancing and impairing extinction of habit memory through modulation of NMDA receptors in the dorsolateral striatum. *Neuroscience* **352**, 216–225 (2017).

22. Pauli, W. M., Clark, A. D., Guenther, H. J., O'Reilly, R. C. & Rudy, J. W. Inhibiting PKMζ reveals dorsal lateral and dorsal medial striatum store the different memories needed to support adaptive behavior. *Learn. Mem.* **19**, 307–314 (2012).

23. Nelson, A., Abdelmesih, B. & Costa, R. M. Corticospinal neurons encode complex motor signals that are broadcast to dichotomous striatal circuits. *bioRxiv* (2020) doi:https://doi.org/10.1101/637447.

24. Kupferschmidt, D. A., Juczewski, K., Cui, G., Johnson, K. A. & Lovinger, D. M. Parallel, but Dissociable, Processing in Discrete Corticostriatal Inputs Encodes Skill Learning. *Neuron* **96**, 476-489.e5 (2017).

25. Lemon, R. N. Descending Pathways in Motor Control. *Annu. Rev. Neurosci.* **31**, 195–218 (2008).

26. Lemon, R. Recent advances in our understanding of the primate corticospinal system. *F1000Research* **8**, 274 (2019).

27. Carmichael, S. T. Rodent models of focal stroke: Size, mechanism, and purpose. *NeuroRX* **2**, 396–409 (2005).

28. Bönstrup, M. *et al.* Low-Frequency Brain Oscillations Track Motor Recovery in Human Stroke. *Ann. Neurol.* **86**, 853–865 (2019).

29. Moon, S. K., Alaverdashvili, M., Cross, A. R. & Whishaw, I. Q. Both compensation and recovery of skilled reaching following small photothrombotic stroke to motor cortex in the rat. *Exp. Neurol.* **218**, 145–153 (2009).

30. Jones, T. A. Motor compensation and its effects on neural reorganization after stroke. *Nat. Rev. Neurosci.* **18**, 267–280 (2017).

31. Alaverdashvili, M. & Whishaw, I. Q. Motor cortex stroke impairs individual digit movement in skilled reaching by the rat. *Eur. J. Neurosci.* **28**, 311–322 (2008).

Publishing Agreement

It is the policy of the University to encourage open access and broad distribution of all theses, dissertations, and manuscripts. The Graduate Division will facilitate the distribution of UCSF theses, dissertations, and manuscripts to the UCSF Library for open access and distribution. UCSF will make such theses, dissertations, and manuscripts accessible to the public and will take reasonable steps to preserve these works in perpetuity.

I hereby grant the non-exclusive, perpetual right to The Regents of the University of California to reproduce, publicly display, distribute, preserve, and publish copies of my thesis, dissertation, or manuscript in any form or media, now existing or later derived, including access online for teaching, research, and public service purposes.

DocuSigned by:
Ling Guo
E458D4E574CB442...
Author Signature

12/9/2020
Date